Optical Properties of Iridium(III) Cyclometalates: Excited State Interaction with Small Molecules and Dynamics of Light-Harvesting Materials

A DISSERTATION
SUBMITTED TO THE FACULTY OF THE GRADUATE SCHOOL
OF THE UNIVERSITY OF MINNESOTA
BY

Kyle Robert Schwartz

IN PARTIAL FULFILLMENT OF THE REQUIREMENTS
FOR THE DEGREE OF
DOCTOR OF PHILOSOPHY

Professor Kent R. Mann

August 2012

Acknowledgements

For me the Mann Lab has been an ever changing environment since the day I arrived. Survival has taken a distinct sort of resilience to weather its many phases. The players have functioned to facilitate, and, at times, to impede, each uniquely assisting in progression and development, whether immediate or delayed, contributions that cannot be discounted in either capacity. Of those involved, I must point to the lasting impact of then postdoctoral research assistant, now assistant professor of chemistry, Raghu Chitta. Never have I learned so much from one person about so many things, both in and out of the laboratory. My gratitude towards his generosity is profound. Another senior labmate, Kari McGee, was perhaps unaware, or maybe in full realization, of the seed she planted in my brain as a fledgling inorganic chemist. A compulsion of self abuse from which there is no respite, only the desire to pursue further the mysteries yet uncovered in iridium coordination chemistry. The remainder of my Mann lab contemporaries all taught me something different about playing the game. You've got to be lucky, get your hands dirty, keep the details straight, and blow the doors open.

My collaborators in the Gladfelter lab are recognized for providing many opportunities to discuss science and other fine topics following our joint group meetings. I am also indebted to Pere Miró, my postdoctoral collaborator from the Cramer group, for his computational expertise without which a significant portion of my research would be incomplete. Numerous thanks also go to everyone who makes this department function.

As for Kent, the Mann of a thousand analogies, he taught me that the heart of science is in the data and the interpretation is … just that… up for interpretation. A set of data is worth a thousand words and Kent could glean more from one figure than anyone. Although I admit, I was never as adept a beaker style chemist as he; his off the cuff chemistry style values experimentation over rumination. This mentality embodies all that is great about being a scientist, the ability to get in the lab and try out your wildest idea.

There really isn't too much else to say. It has been a great ride the events of which shaped me scientifically and a personally. Finally, special thanks must of course go to my wife, whose patience during my ordeal has been unrivaled, only she has the real story.

Abstract

The research presented in this thesis concerns the use and understanding of luminescent Ir(III) cyclometalates. Areas of research involve the design, synthesis, and characterization of novel luminescent Ir(III) cyclometalates, including photophysical investigation of their phosphorescent excited states using steady-state and time resolved absorption/luminescence spectroscopies. This broad research description may be further separated into two subareas: study of excited state interaction with small molecules and excited-state dynamics of metal-organic light harvesting dyads.

The first chapter of this thesis examines the interaction of Ir(III) cyclometalates with the small molecule carbon dioxide (CO_2). It has been the goal of investigators to develop methods for direct optical detection of CO_2. This has been difficult as CO_2 is considered chemically inert and there are few luminescent probes directly sensitive to CO_2. Most optical detection schemes previously developed for CO_2 use indirect detection methods, which rely upon measuring changes in pH brought about by hydrolysis of CO_2. Research efforts to design a reliable method for the direct optical detection of CO_2 were accomplished through development of a system where hydrazine, a simple amino ligand, when coupled into the coordination sphere of an Ir(III) cyclometalate reacts with CO_2. The result of this reaction provides a significant shift in the luminescence λ_{max} of the phosphorescent probe, a previously unobserved optical response for the direct detection of CO_2.

The second chapter investigates phosphorescent excited states and their ability to function as triplet sensitizers for the generation of singlet oxygen ($^1O_2$) and luminescent

probes for molecular oxygen (O_2) concentration. Interaction of phosphorescent excited states with O_2 results in energy transfer from the luminescent probe to O_2, quenching the phosphorescent excited state. Energy transfer also generates the reactive oxygen species (ROS) $^1O_2$. We have used this duality to develop an analytical methodology to follow the serendipitously discovered photoreactivity of $^1O_2$ with common organic solvent dimethyl sulfoxide (DMSO) using the luminescence profile of Ir(III) and Ru(II) phosphors. Reaction of the triplet sensitized $^1O_2$ with a photooxygenation substrate results in the consumption of O_2 from the system and an increase in the observed luminescence intensity. Detailed kinetic investigations of the luminescence recovery and O_2 depletion were preformed on air-saturated closed cell systems. Determinations of the quantum efficiencies for the photooxygenation system were performed and differences in choice of triplet sensitizer discussed. Study of $^1O_2$ reactivity with substrates of biological and environmental relevance using this methodology should provide an additional tool to understand better oxidative damage induced by $^1O_2$ within these systems.

In chapter three a detailed study involving the design, synthesis, and characterization of the electrochemical and phototophysical properties of Ir(III) cyclometalates with pendant terthiophenes as secondary organic chromophores is presented. The interplay of the excited states between each chromophore represents an interesting photoredox active system for energy-to-light or light-to-energy devices. Greater knowledge of the primary photophysical events within these complexes will provide a better understanding of how energy moves in these hybrid systems after light absorption, leading to increased device efficiency.

Table of Contents

Acknowledgements **i**

Abstract **ii**

Table of Contents **iv**

List of Tables **vi**

List of Figures **vii**

List of Schemes **ix**

List of Symbols and Abbreviations **x**

Chapter One Optical Response of a Cyclometalated Ir(III) Hydrazino Complex to Carbon Dioxide: Generation of a Strongly Luminescent Ir(III) Carbazate **1**

Overview **2**

Introduction **3**

Experimental Details **6**

Results and Discussion **12**

Conclusions **31**

Chapter Two Triplet-Sensitized Photooxygenation of Dimethyl Sulfoxide to Dimethyl Sulfone Monitored by Luminescence Spectroscopy **33**

Overview **34**

Introduction **35**

Experimental Details **39**

Results and Discussion **43**

Conclusions **70**

Chapter Three Effect of Axially Projected Oligothiophene Pendants and Nitro-Functionalized Diimine Ligands on the Lowest Excited State in Cationic Ir(III) bis-Cyclometalates. **73**

Overview **74**

Introduction **75**

Experimental Details **79**

Results and Discussion **90**

Conclusions **114**

Bibliography **116**

Appendix A Structural Discussion of C, N Ring Flip In Single Crystal X-ray Crystallography. **131**

Appendix B Obtaining the Implicit and Explicit forms of the Integrated Rate Law for O_2 Consumption. **132**

List of Tables

Chapter One

Table 1. Crystallographic Data and Refinement Parameters for the Ir(III) Hydrazino (**2a**) and Carbazate (**3**) Complexes **18**

Table 2. Selected Bond Lengths and Angles for Ir(III) Hydrazino **2a** and Carbazate **3** Complexes **19**

Table 3. Photophysical Properties of Ir(III) Hydrazino (**2a**) and Carbazate (**3**) Complexes **20**

Chapter Two

Table 1. Values for two point K_{sv} determination for Ir(III) and Ru (II) sensitizers in DMSO **50**

Table 2. Fitting Parameters for Ir(III) and Ru(II)/DMSO Photooxygenation Systems **59**

Table 3. Contribution of Kinetic Terms for Ir(III) and Ru(II) Sensitizers **63**

Table 4. Fitting Parmeters and Determination of Quantum Efficiency for Ir(III)/DMSO Photooxygenation System **65**

Table 5. Fitting Parameters and Determination of Quantum Efficiency for Ru(II)/TME/MeOH Photooxygenation System **68**

Chapter Three

Table 1. Crystallographic Data and Refinement Parameters for $[Ir(ppy)_2(4–NO_2–bpy)]PF_6$ **93**

Table 2. Selected Bond Lengths and Angles for $[Ir(ppy)_2(4–NO_2–bpy)]PF_6$ (**10**) **94**

Table 3. Photophysical and Electrochemical Properties of 3T Oligomer (**6**) and Cationic Ir(III) Complexes (**9** – **12**) **98**

Table 4. TD-DFT Predicted Energies and Transitions for the Three Lowest Singlet and Triplet Excited States of 3T-Pendant Complexes **11** and **12** **105**

List of Figures

Chapter One

Figure 1. ^{1}H NMR of **2a** and **3** in DMSO-d_6 **14**

Figure 2. ^{1}H NMR of **2c** in *o*-dichlorobenzene-d_4 **14**

Figure 3. Thermal ellipsoid plots for single crystal structures of **2a** and **3** **17**

Figure 4. Absorption and Luminescence spectra of **2a** and **3** in DMSO **21**

Figure 5. Lifetime plot of luminescence decay for **2a** and **3** in DMSO **21**

Figure 6. Luminescence spectra at of **2a** before and after exposure to CO_2 in DMSO, DMF, MeOH, ACN **23**

Figure 7. ^{1}H NMR of **2a** before and after addition of TFA and **4** in DMSO-d_6 **25**

Figure 8. Optical response upon exposure of **2a** to CO_2 in DMSO monitored at wavelengths: 500, 522, and 550 nm **29**

Chapter Two

Figure 1. No-D ^{1}H NMR of, neat DMSO, neat DMSO spiked with 0.1% $DMSO_2$, and neat DMSO with $Ir(ppy)_2(cbz)$ or Methylene Blue after 5 h of irradiation under O_2 atmosphere **45**

Figure 2. Luminescence recovery of air-saturated DMSO sensitizer solutions monitored at 524 nm for $Ir(ppy)_2(cbz)$, and 620 nm for $[Ru(bpy)_3]Cl_2$ **57**

Figure 3. $[O_2]$ profiles for air-saturated DMSO sensitizer solutions of $Ir(ppy)_2(cbz)$ and $[Ru(bpy)_3]Cl_2$ during photooxygenation **58**

Figure 4. Linearized luminescence recovery data for air-saturated DMSO sensitizer solutions of $Ir(ppy)_2(cbz)$ and $[Ru(bpy)_3]Cl_2$ **60**

Figure 5. Stern-Volmer plots for air-saturated DMSO sensitizer solutions of $Ir(ppy)_2(cbz)$ and $[Ru(bpy)_3]Cl_2$ using corrected PL intensity and luminescence lifetimes. **62**

Figure 6. Profiles of kinetic terms for air-saturated DMSO sensitizer solutions of $Ir(ppy)_2(cbz)$ and $[Ru(bpy)_3]Cl_2$ during photooxygenation **64**

Figure 7. Luminescence recovery at 620 nm for $[Ru(bpy)_3]Cl_2$/TME/MeOH photooxygenation system **67**

Figure 8. $[O_2]$ profile for $[Ru(bpy)_3]Cl_2$/TME/MeOH photooxygenation system **67**

Chapter Three

Figure 1. Molecular structures of cationic Ir(III) bis-cyclometalates **9**,**10** (control complexes), and **11**, **12** (3T–pendant complexes) **78**

Figure 2. Thermal ellipsoid plot for single crystal structure of $[Ir(ppy)_2(4–NO_2–bpy)]PF_6$ **95**

Figure 3. Contour plots of frontier orbitals for control complexes (**9**–**10**) and 3T–pendant complexes (**11**–**12**) in the ground state **97**

Figure 4. Cyclic voltammograms for control complexes (**9**–**10**) and 3T–pendant complexes (**11**–**12**) in ACN **99**

Figure 5. UV-vis absorption spectra of for control complexes (**9**–**10**), 3T Oligomer (**6**), and 3T–pendant complexes (**11**–**12**) in ACN **103**

Figure 6. Energy level diagram for the lowest excited states in the 3T–pendant complexes (**11**–**12**) **104**

Figure 7. Luminescence spectra of 3T oligomer (**6)** and control complexes control complexes (**9**–**10**) in ACN **109**

List of Schemes

Chapter One

Scheme 1. Synthesis of Ir(III) Hydrazino and Carbazate Complexes **13**

Scheme 2. Competitive Pathways to *N*-Carboxylation in the Ir(III) Hydrazine System **27**

Chapter Two

Scheme 1. Physical and chemical processes pertaining to the photooxygenation reaction **52**

Chapter Three

Scheme 1. Synthesis of 3T Oligomer and cationic Ir(III) bis-Cyclometalates **91**

List of Symbols and Abbreviations

(aq)	aqueous
(g)	gas
$[O_2]_0$	initial O_2 concentration
$[O_2]_{air}$	concentration of O_2 in air
$[O_2]_t$	time dependent O_2 concentration
°	measure of angle in degrees
°C	measure of temperature in degree Celsius
^{13}C	Carbon 13 isotope of the carbon nuclei
$^1A^*$	triplet sensitizer in the singlet excited state
^1H	proton, the most abundant isotope of the hydrogen nuclei
^1LC	ligand centered
^1LLCT	singlet ligand-to-ligand charge-transfer
$^1O_2$	singlet excited state of molecular oxygen
$^1\pi \rightarrow \pi^*$	singlet π to π* absorption
$^1\pi$–π^*	singlet π / π * state
$^3A^*$ or A^*	triplet sensitizer in the triplet excited state
^3LC	triplet ligand centered excited state
^3LLCT	triplet ligand-to-ligand charge-transfer
3T	terthiophene
$^3\pi$–π^*	triplet pi / pi* state
Å	Ångström
A	triplet sensitizer in the ground state
a.u.	arbitrary units
atm	atmospheres
B	photooxygenation substrate
base	experimental PL intensity correction term
bpy	2,2′-bipyridine
br	broad
C	photoproduct
C^N	cyclometalating ligand
C_2	point group of twofold rotation about the principle axis
calcd	calculated
cbz	carbazate anion ($H_2NNHCOO^-$)
CCD	charge coupled device
cm	centimeter
cm^{-1}	wavenumbers
CSD	Cambridge Structural Database
d	doublet
dd	doublet of doublets
ddd	doublet of doublet of doublets
DFT	density functional theory
DMS	dimethyl sulfide

$DMSO_2$	dimethyl sulfone
DOM	dissolved organic matter
DSSC	dye-sensitized solar cell
dπ	metal pi bonding orbital
$d\pi_{Ir(III)} \rightarrow \pi^*_{C\text{^}N}$	metal π to cyclometalating ligand π* absorption
$d\pi_{Ir(III)} \rightarrow \pi^*_{N\text{^}N}$	metal π to diimine ligand π* absorption
$d\pi_{Pt(II)} \rightarrow \pi^*_{N\text{^}N}$	metal π to diimine ligand π* absorption
$E^{\circ\prime}$	standard potential of redox couple
$E_{1/2(ox)}$	half-wave potential for oxidation
$E_{1/2(red)}$	half-wave potential for reduction
E_{caldd}	calculated energy of absorption
EI	electron impact
EPR	electron paramagnetic resonance
eV	electronvolts
f^{-1}	inverse mathematic function
f	mathematic function
g	gram
GC-MS	gas chromatography-mass spectrometry
GOF	goodness of fit
h	hours
HOMO	highest occupied molecular orbital
HRESI	high resolution electrospray ionization
HRMS	high resolution mass spectrometery
Hz	hertz
hν	photon
I	PL intensity in the presence of quencher
I_{450}	source intensity
I_0	PL intensity in the absence of quencher
I_{air}	initial PL intensity of air saturated solution
Int	proposed reaction intermediate
i-pr	iso-propyl
I_t	time dependent PL intensity
J	proton coupling constant in hertz
K	measurement of temperature in kelvin
k_1	rate constant for deactivation of $^1O_2$ by photooxygenation substrate
k_{1O2}	rate constant for deactivation of $^1O_2$ by radiative and nonradiative decay (sum of k_{rO2} and k_{nrO2})
k_2	rate constant for proposed rate determining step for reaction of $^1O_2$ with photooxygenation substrate to generate "Int"
k_3	rate constant for reaction of "Int" with photooxygenation substrate to form photoproduct
k_{abs}	rate constant for absorption process of A

k_{et}	rate constant for energy transfer resulting in production of $^1O_2$ and PL quenching via dynamic quenching
k_{isc}	rate constant for intersystem crossing
$k_{no\ et}$	rate constant for PL quenching without generation of $^1O_2$ via dynamic quenching
$k_{nr\ 1A*}$	nonradiative rate constant for excite state decay of $^1A*$
k_{nr}	nonradiative rate constant for excited state decay of A*
k_{nrO2}	nonradiative rate constant for excited state decay of $^1O_2$
k_{obs}	observed rate constant for photooxygenation system
k_q	bimolecular rate constant for the quenching of A* by O_2 (sum of k_{et} and $k_{no\ et}$)
k_r	radiative rate constant for excited state decay of A*
k_{rO2}	radiative rate constant for excited state decay of $^1O_2$
K_{sv}	Stern-Volmer dynamic quenching constant
L	neutral monodentate ancillary ligand
L^X	anionic bidentate ancillary ligand
LEC	light-emitting electrochemical cell
LED	light-emitting diode
LUMO	lowest unoccupied molecular orbital
M	molar
m	multiplet
M^+ or $[M]^+$, $[M\cdot]^+$	parent ion
MALDI	matrix assisted laser desorption ionization
Mes	mesityl substituent
MHz	megahertz
min	minutes
mL	milliliters
mm	millimeter
mm	millimeter
mmol	millimoles
MO	molecular orbital
MoKα	emitted Kα X-ray wavelength from molybdenum target
mol	moles
MS	mass spectrometry
mV	millivolts
N	Avagadro's number
N^N	diimine ligand
n-Bu	normal butyl group
NIR	near-infrared
nm	nanometers
NMR	nuclear magnetic resonance
No-D	no-deuterium
o	ortho ring position
$O_2\cdot^-$	superoxide anion

OLED	organic light-emitting diode
OTf^-	triflate anion ($CF_3SO_3^-$)
P	pressure
PDT	photodynamic therapy
PET	photo induced electron transfer
Ph	phenyl substituent
$Ph^-_{C\wedge N}$	anionic phenyl moiety of cyclometalating ligand
pH	measure of hydrogen ion concentration quantifying acidity
PL	photoluminescence
PMT	photo-multiplier tube
ppm	parts per million
ppy	2-phenylpyridine
PTFE	polytetrafluoroethylene
PtOEP	platinum(II) octaethylporphyrin
Q	quencher
r.t.	room temperature
ROS	reactive oxygen species
s	seconds (time)
s	singlet (^{1}H NMR)
$S_{\#}$	singlet excited state (# = 1,2,3)
S_0	singlet ground state
SD	standard deviation
SDD	Stuttgart/Dresden basis set
SMD	Spartan Molecular Database
t	time
t	triplet (^{1}H NMR)
$T_{\#}$	triplet excited state (# = 1,2,3)
t_0	initial time
$TBAPF_6$	teratbutylammonium hexafluorophosphate
TD-DFT	time-dependent density functional theory
TME	tetramethylethylene
TOF	time of flight
UV	ultraviolet
V	volts
V	volume of unit cell
v/v	volume to volume ratio
vis	visible
V_{soln}	volume of air-saturated sensitizer solution in reaction cell
W	Watt
W(x)	Lambert W function
wt %	weight percent
Z	number of formula units per unit cell
β	molecular interaction term of $^1O_2$ and DMSO(k_{1O2} / $k_2 + k_3$)
δ	chemical shift in parts per million

ε	molar absorptivity
θ	degrees of data collection
λ	wavelength
λ_{450}	cutoff wavelength 450 nm
λ_{calcd}	calculated absorption wavelength
λ_{em}	emission wavelength
λ_{ex}	excitation wavelength
λ_{max}	absorption maximum wavelength
μ	signifies a group that bridges two or more coordination centers
μL	microliters
μs	microseconds
π	pi bonding orbital
π^*	pi antibonding orbital
$\pi_{ph} \rightarrow \pi^*_{N\text{^}N}$	cyclometalating Ph π to diimine ligand π^* absorption
τ	luminescence lifetime in the presence of quencher
τ_0	luminescence lifetime in the absence of quencher
τ_{em}	luminescence lifetime
ω	axis of goniometer platform rotation
ϕ_{em}	quantum efficiency of emission
ϕ_{et}	quantum efficiency of energy transfer
ϕ_{isc}	quantum efficiency of intersystem crossing
ϕ'_{obs}	observed quantum efficiency for photooxygenation system adjusted for O_2-saturated solutions
ϕ_{obs}	observed quantum efficiency for photooxygenation system using air-saturated solutions
ϕ_{rxn}	quantum efficiency of photoreaction between $^1O_2$ and DMSO

─ Chapter One ─

Optical Response of a Cyclometalated Ir(III) Hydrazino Complex to Carbon Dioxide: Generation of a Strongly Luminescent Ir(III) Carbazate

Overview. A system pairing the luminescent core of $[Ir(ppy)_2L_2]^+$ (ppy = 2-phenylpyridine) with simple hydrazino ancillary ligands (L = N_2H_4) has been prepared for the direct optical detection of carbon dioxide (CO_2). Silver-assisted and silver-free techniques were used for successful introduction of N_2H_4 into the $[Ir(ppy)_2Cl]_2$ coordination sphere at room temperature to give the corresponding bis-cyclometalated Ir(III) hydrazino species as either a $CF_3SO_3^-$ (OTf^-, **2a**) or Cl^- (**2b**) salt. The silver-free route was accomplished by direct replacement of the ligated Cl^- using a slight excess of hydrazine. The luminescence profile of the cationic Ir(III) hydrazino complex **2a** (λ_{em} = 501 nm) undergoes a red shift (λ_{em} = 524 nm), accompanied by a change in peak shape during exposure to CO_2 in solution. Spectral changes observed are attributed to formation of the corresponding neutral carbazate species $Ir(ppy)_2(H_2NNHCOO)$ (**3**) and are not consistent with protonation of the ligated hydrazine. Conversion of the hydrazino to the carbazate species is solvent-dependent and irreversible. The hydrazino and carbazate species have been structurally characterized by single crystal X-ray diffraction. Both compounds exhibit long-lived and intense room-temperature luminescence in solution with τ_{em} = 1.56 and 1.80 μs and ϕ_{em} = 0.42 and 0.45, respectively.

Introduction. The interaction of small molecules with transition metals complexes is a topic of wide interest and diversity and holds importance for many facets of scientific research. The use of O_2 in photodynamic therapy[1], NO in biological messaging[2], N_2 as an industrial feedstock[3], and H_2O for production of H_2 as fuel[4] represents a few of the most notable examples. Increased attention towards the level of greenhouse gases such as carbon dioxide (CO_2) in the atmosphere has revived interest in the small molecule as a target of activation[5], sequestration[6], and, of particular appeal to our research group, optical detection using colorimetric[7] or luminescent[8] sensing motifs. The relatively inert nature of CO_2 has proven these to be difficult objectives. Most optical detection schemes previously developed for CO_2 use indirect detection methods that rely primarily upon the acidic properties of CO_2 to cause a subsequently detected change in pH. In principle, the few pH indicators that have been used to sense CO_2 are subject to much interference; additionally, the requisite buffers, and reference fluorophores add a level of unwanted complexity to the sensing scheme that could be eliminated via direct detection of CO_2. Efforts to develop a direct method of optical detection for CO_2 have made use of amines appended to organic fluorophores.[9] Fluorophores such as substituted pyrenes exhibit an observable increase in fluorescence due to a decrease in the photoinduced electron transfer (PET) quenching as a result of the reaction between the amino functionality and CO_2, forming a carbamic acid or carbamate. The amine/CO_2/carbamate equilibrium can be reversed by removal of the dissolved CO_2 by purging solutions with an inert gas.

In practice the effects of CO_2 exposure to organic fluorophores containing pendant alkyl amines are complicated and solvent dependent. Previous work has shown

that highly basic polar aprotic solvents such as dimethyl sulfoxide (DMSO), *N*,*N*-dimethylformamide (DMF), and pyridine (Py) are required for complete conversion of arylalkylamines to their corresponding carbamic acids.[9c] Less basic solvents react with a different stoichiometry to give unwanted ammonium carbamate salts. Decreased PET quenching has also been observed in organic and transition metal luminophores with appended amines upon protonation.[10] The dual reactivity of the amino functionality complicates interpretation of the sensing mechanism as changes in the luminescence profile initiated by protonation or *N*-carboxylation would be indistinguishable from one another, and in the case of the ammonium carbamate ion pair, both outcomes would be observed.

Application of a sensing motif that allows for differentiation between *N*-carboxylation and protonation is desired. In principle, producing a spectral shift should allow this complication to be deconvoluted from the overall optical response. A spectral shift may be achieved through alteration of the coordination sphere of a transition metal luminophore upon exposure to an analyte. Utilizing simple amines both as ligands and sites for CO_2 binding presents the opportunity for stabilization of the *N*-carboxylated species and a spectral shift through ligation. The simple amine hydrazine and its *N*-carboxylate, carbazate ($H_2NNHCOO^-$), have been known for quite sometime to undergo complexation with a large variety of transition metal ions.[11] Study of this well defined carbamate formation to detect CO_2 by a luminescent shift is the primary focus of this effort.

We report herein the synthesis, characterization, and photophysical properties, of the cationic $[Ir(ppy)_2(N_2H_4)_2]X$ [ppy = 2-phenylpyridine, $X^- = CF_3SO_3^-$, OTf^- (**2a**), Cl^-

(**2b**)] and neutral $Ir(ppy)_2(H_2NNHCOO)$ (**3**) Ir(III) bis-cyclometalates. The bis-hydrazino species can be obtained from the parent μ-chloro-bridged dimer using conventional silver reagents for Cl^- abstraction (**2a**) or through direct replacement in the presence of a slight excess of N_2H_4 (**2b**), yielding a synthetically useful silver-free Cl^- abstraction. Exposure of the ligated hydrazine to CO_2 results in a previously unreported luminescent optical response for CO_2. The presence of CO_2 is detected by a red shift in the observed luminescence λ_{em} accompanied by a change in peak shape. Crystallographic and ^1H NMR data have confirmed the mechanism of response to involve transformation of a neutral monodentate hydrazino ligand to the anionic bidentate carbazate ligand when exposed to CO_2 in solution.

Experimental Details.

General Considerations. NMR spectra were recorded on a Varian Unity or Varian Inova 300 MHz instrument. High-resolution mass spectrometry was performed on a Bruker BioTOF II mass spectrometer. All spectra were recorded in commercially available solvents (Sigma-Aldrich, Fischer, Mallinkrodt Chemical), which were used as is. The gases CO_2 (99.98 % from Minneapolis Oxygen) and N_2 (high purity grade from Airgas), used as is, were introduced to the samples with a needle in a cell closed with a needle a septum. The cyclometalated Ir(III) μ-chloro-bridged dimer, $[Ir(ppy)_2Cl]_2$, was prepared using the method of Watts from $IrCl_3 \cdot 3H_2O$ (Johnson Matthey) in a refluxing mixture of 3:1 2-methoxyethanol and water.[12] The acetonitrile solvento complex $[Ir(ppy)_2(NCCH_3)_2]OTf$ (**1**) was prepared as previously described from $[Ir(ppy)_2Cl]_2$ in acetonitrile using AgOTf in the place of $AgPF_6$.[13]

$[Ir(ppy)_2(N_2H_4)_2]OTf$ (2a): $[Ir(ppy)_2(NCCH_3)_2]OTf$ (0.100 g, 0.1367 mmol) was dissolved in 5 mL of methanol. Excess hydrazine monohydrate 99 % ($N_2H_4 \cdot H_2O$, 25 μL) was added to the solution yielding a green-brown murky reaction mixture. The solution was allowed to stir for 30 min at r.t., which upon settling gave a black precipitate. The solution was run through a Celite pad giving a clear, bright yellow solution. Solvent was removed via rotary evaporation giving the product **2a** as a glassy yellow powder (0.0922 g, 95 %). X-ray quality crystals were grown from the slow evaporation of a CH_2Cl_2/heptane solution. ^{1}H NMR (300 MHz, DMSO-d_6): δ 9.20 (d, 2H, J = 5.1 Hz), 8.19 (d, 2H, J = 7.5 Hz), 8.01 (t, 2H, J = 7.5 Hz), 7.73 (d, 2H, J = 6.9 Hz), 7.48 (t, 2H, J = 7.2 Hz), 6.83 (t, 2H, J = 6.9 Hz), 6.68 (t, 2H, J = 7.5 Hz), 6.06 (d, 2H, J = 7.5 Hz), 5.77

(d br, 2H, J = 10.5 Hz), 5.61 (d br, 2H, J = 10.5 Hz). HRESIMS (M^+): calcd for $C_{22}H_{24}IrN_6$, 565.1686, found, 565.1687.

$[Ir(ppy)_2(N_2H_4)_2]Cl$ (2b): $[Ir(ppy)_2Cl]_2$ (0.0700g, 0.0653 mmol) was dissolved in a 2:1 mixture of CH_2Cl_2/MeOH and placed under an Ar atmosphere. Once the solid had dissolved hydrazine monohydrate 99 % ($N_2H_4 \cdot H_2O$, 25 μL, 0.515 mmol) was added to the reaction mixture and allowed to stir at r.t. for 3 h. Solvent was removed via rotary evaporation giving the product as a yellow residue**.** The residue was redissolved in MeOH and precipitated from solution upon addition of diethyl ether. The resulting yellow solid was filtered on a fritted glass funnel and dried in vacuo to give 0.0726g **2b** (93 %). ^{1}H NMR (300 MHz, DMSO-d_6): δ 9.23 (d, 2H, J = 6.0, 1.2 Hz), 8.19 (d, 2H, J = 7.8 Hz), 8.01 (ddd, 2H, J = 7.6, 7.6, 1.2 Hz), 7.73 (dd, 2H, J = 7.8, 1.2 Hz), 7.47 (ddd, 2H, J = 7.2, 5.7, 1.2 Hz), 6.82 (ddd, 2H, J = 7.6, 7.6, 1.2 Hz), 6.68 (ddd, 2H, J = 7.6, 7.6, 1.2 Hz), 6.06 (dd, 2H, J = 7.6, 1.2 Hz), 5.86 (d br, 2H, J = 10.5 Hz), 5.64 (d br, 2H, J = 10.5 Hz). HRESIMS (M^+): calcd for $C_{22}H_{24}IrN_6$, 565.1686, found, 565.1698. Resonances for the distal N-H protons were not observed in DMSO-d_6 for either the OTf^- (**2a**) or Cl^- (**2b**) due to rapid exchange with residual H_2O. See preparation and characterization of **2c**.

$[Ir(ppy)_2(N_2H_4)_2]PF_6$ (2c): A fresh solution of compound **2b** (0.1116 g, 0.187 mmol) in 2:1 mixture of CH_2Cl_2/MeOH was prepared as described in the main text. The solution was concentrated to ~1.5 mL, treated with $NaPF_6$ (0.2507 g, 1.49 mmol) and allowed to stir for 30 min. Diethyl ether was added to induce precipitation followed by filtration. The bright yellow solid was washed with cold H_2O and diethyl ether then dried in vacuo to give $[Ir(ppy)_2(N_2H_4)_2]PF_6$. Yield: 78 % ^{1}H NMR (300 MHz, DMSO-d_6): δ 9.39 (d, 2H, J = 5.4 Hz), 7.82 (d, 2H, J = 8.1 Hz), 7.72 (dd, 2H, J = 1.2, 8.4 Hz), 7.58 (d,

2H, J = 7.5 Hz), 7.23 (dd, 2H, J = 1.2, 7.2 Hz), 6.99 (dd, 2H, J = 1.2, 7.5 Hz), 6.85 (dd, 2H, J = 1.2, 7.5 Hz), 6.47 (d, 2H, J = 7.5 Hz), 5.33 (d br, 2H, J = 10.5 Hz), 4.75 (d br, 2H, J = 10.5 Hz) 3.43 (s br, 4H).

Ir(ppy)$_2$(H$_2$NNHCOO) (3): The neutral carbazate species **3** was obtained by two methods that are described below as method 3a and method 3b.

Method 3a. A fresh solution of compound **2a** (0.0250 g, 0.0342 mmol) in methanol was prepared as described above. The solution was concentrated to ~1 mL and bubbled with CO_2 (g) for 30 min at r.t. resulting in a yellow microcrystalline precipitate. The yellow solid was collected on a fritted glass filter removing excess methanol solution. Solid was dried in vacuo to give 0.0182 g of pure compound **3** (92 %). See below for characterization.

Method 3b. The direct synthesis of **3** starting from the μ-chloro-bridged dimer [Ir(ppy)$_2$Cl]$_2$ was accomplished by redissolving the residue obtained from synthesis of **2b** in MeOH. The MeOH solution of **2b** was then bubbled with gaseous carbon dioxide (CO_2(g)) generated from dry ice for 30 min at r.t. to give a yellow precipitate. The yellow solid was collected on a fritted glass funnel removing excess methanol solution and washed with water and diethyl ether. The solid was dried in vacuo to give 0.0677 g of pure compound **3** (90 %). X-ray quality crystals were grown from slow evaporation of an acetone/acetonitrile solution. ^{1}H NMR (300 MHz, DMSO-d_6): δ 9.04 (d, 1 H, J = 5.1 Hz), 8.71 (dd, 1 H, J = 5.7, 0.9 Hz), 8.14 (d, 2 H, J = 8.1 Hz), 7.95 (t, 2 H, J = 7.5 Hz), 7.68 (t, 2 H, J = 6.6 Hz), 7.47 (ddd, 1 H, J = 6.9, 5.7, 1.2 Hz), 7.40 (ddd, 1 H, J = 7.2, 5.7, 1.5 Hz), 7.22 (s br, 1 H), 6.94 (d br, 1 H, J = 8.7 Hz), 6.76 (ddd, 1 H, J = 8.7, 7.5, 1.2 Hz), 6.73 (ddd, 1 H, J = 9.0, 7.8, 1.5 Hz), 6.60 (ddd, 1 H, J = 7.5, 6.6, 1.5 Hz), 6.57

(ddd, 1 H, J = 7.2, 6.0, 1.2 Hz), 6.41 (d br, 1 H, J = 8.7 Hz), 6.20 (dd, 1 H, J = 7.8, 1.2 Hz), 5.94 (dd, 1 H, J = 7.8, 1.2 Hz). HRESIMS (M + Na^+): calcd for $C_{23}H_{19}IrN_4NaO_2$, 599.1029, found, 599.1045.

X-ray Structural Determination. The data for the structural determination were collected in the X-ray Crystallographic Lab in the LeClair-Dow Instrumentation Facility (Department of Chemistry, University of Minnesota). Single crystals of compounds **2a** and **3** were placed onto a glass capillary and mounted on a Bruker SMART platform CCD diffractometer for **2a**, while **3** was mounted on a Siemens SMART platform CCD diffractometer for a data collection at 173(2) K using a graphite monochromator and Mo Kα radiation (λ = 0.71073 Å). An initial set of cell constants was calculated from reflections harvested from three sets of 20 frames such that orthogonal wedges of reciprocal space were surveyed. Final cell constants were determined from a minimum of 2595 strong reflections from the actual data collection. Data were collected to the extent of 1.5 hemispheres to a resolution of 0.77 Å for **2a**, and 0.84 Å for **3**. Four major sections of frames were collected with 0.30º steps in ω. The intensity data were corrected for absorption and decay using *SADABS*.[14] The space groups $P2_1/c$ (**2a**) and $P\bar{1}$ (**3**) were determined based on systematic absences and intensity statistics. Direct-methods solutions provided the positions of most nonhydrogen atoms. Full-matrix least squares/difference Fourier cycles were performed to locate the remaining nonhydrogen atoms. All nonhydrogen atoms were refined with anisotropic displacement parameters, and all hydrogen atoms were placed in ideal positions and refined as riding atoms with relative isotropic displacement parameters. All calculations were performed using the

SHELXTL suite of programs.[15] Further discussion of the cyclometalating ppy ligands ring assignment can be found in Appendix A.

Optical Spectroscopy and Luminescence Lifetimes. Absorption spectra of the Ir(III) bis-cyclometalates were collected in DMSO solution using a 1 cm pathlength on a Cary 14 spectrophotometer running the *OLIS globalworks* software suite. Photoluminescence experiments used to obtain luminescence quantum yields were obtained with an excitation wavelength of 400 nm in DMSO using a front face geometry, with optical densities of solutions >2.0. Data were collected on a Spex Fluorolog 1680 0.2 m double spectrofluorimeter, equipped with a Hamamatsu R928 photomultiplier tube (PMT), running *Datamax* software. Solutions of the Ir(III) bis-cyclometalates were deaerated ≥ 60 minutes prior to collection using an argon purge. All spectra were corrected for the wavelength dependence of the detector. Luminescence quantum yields (ϕ_{em}) were measured relative to *fac*-Ir(ppy)$_3$ in deaerated toluene ($\phi_{em} = 0.40$)[16], estimated absolute uncertainties in ϕ_{em} measurements are ± 20 %; the precision is much better. The luminescence spectra used to monitor the CO_2 gas exposure experiments were obtained using a light-emitting diode (LED) as the source of excitation (λ_{ex} = 405 nm) and a bifurcated fiber optic with front-face detection. Data were collected using an Ocean Optics Inc. CCD spectrophotometer connected to a computer running the *OOIBase32* software suite (v. 2.0.6.5). In this case the spectra displayed were not corrected for detector response.

Luminescence lifetimes were obtained in solution with an in-house constructed circuit that pulses a 405 nm LED for excitation of the sample. The light was conducted through one leg of a bifurcated fiber optic probe to a cuvette that contained a DMSO

solution of either **2a** or **3**. The cuvette was deaerated by sparging the solution with nitrogen. The luminescence decay and scattered light were collected by the other fiber optic leg, filtered through a cut off filter to remove the scattered excitation light and conducted to a Hamamatzu R928 PMT. The PMT signal was digitized by a sampling digital oscilloscope (Phillips PM 3323) interfaced to a computer running a *LabView* program. More details concerning the lifetime data acquisition and processing have been presented previously.[17]

Results and Discussion

Synthesis. The Ir(III) hydrazino complexes $[Ir(ppy)_2(N_2H_4)_2]X$ [X = OTf^-, (**2a**), X = Cl^-, (**2b**)] were synthesized in near quantitative yield from either the bis-acetonitrile solvento complex (**1**)[13] or directly from the parent μ-chloro-bridged dimer, $[Ir(ppy)_2Cl]_2$ at room temperature[12] (Scheme 1). The direct substitution of ligated Cl^- for a neutral monodentate ligand is unique to the N_2H_4 molecule and is attributed to its electron rich character. Previous examples of direct Cl^- substitution have only been observed in the preparation of anionic $[Ir(C^N)(L)_2]^-$ (C^N = cyclometalating ligand) species where L = CN^- NCS^- or NCO^-.[18] Attempts to directly obtain analogous cationic $[Ir(ppy)_2(L_2)]^+$ species where L = alkyl primary amine (*i*-$PrNH_2$) or imine (Py) were unsuccessful. Our results and work by Chin et al. indicate the use of silver reagents would be required for efficient chloride abstraction.[19] Compounds **2a** and **2b** display nearly identical ^1H NMR spectra. Introduction of two hydrazino ligands into the coordination sphere of the metal was confirmed by ^1H NMR as evidenced by the observation of two broad doublets at 5.61 and 5.77 ppm corresponding to the pair of diastereotopic protons located on the Ir(III)-ligated N atoms of the hydrazino moeity (Figure 1a, species **2a** only). This assignment was further supported by the presence of eight ppy ligand ^1H signals present from 6.0 to 9.5 ppm indicative of a symmetric coordination sphere. The absence of a ^1H resonance for the distal N-H protons of the hydrazine ligand in **2a** is hypothesized to be the result of intermolecular exchange with protons from residual water in DMSO-d_6. To confirm this hypothesis the ^1H NMR spectrum was obtained in *o*-dichlorobenzene-d_4, a solvent with much lower residual water content. Due to poor solubility of either the OTf^- or the Cl^- salts in *o*-dichlorobenzene-d_4 the Cl^- was

Scheme 1. Synthesis of Ir(III) Hydrazino and Carbazate Complexes

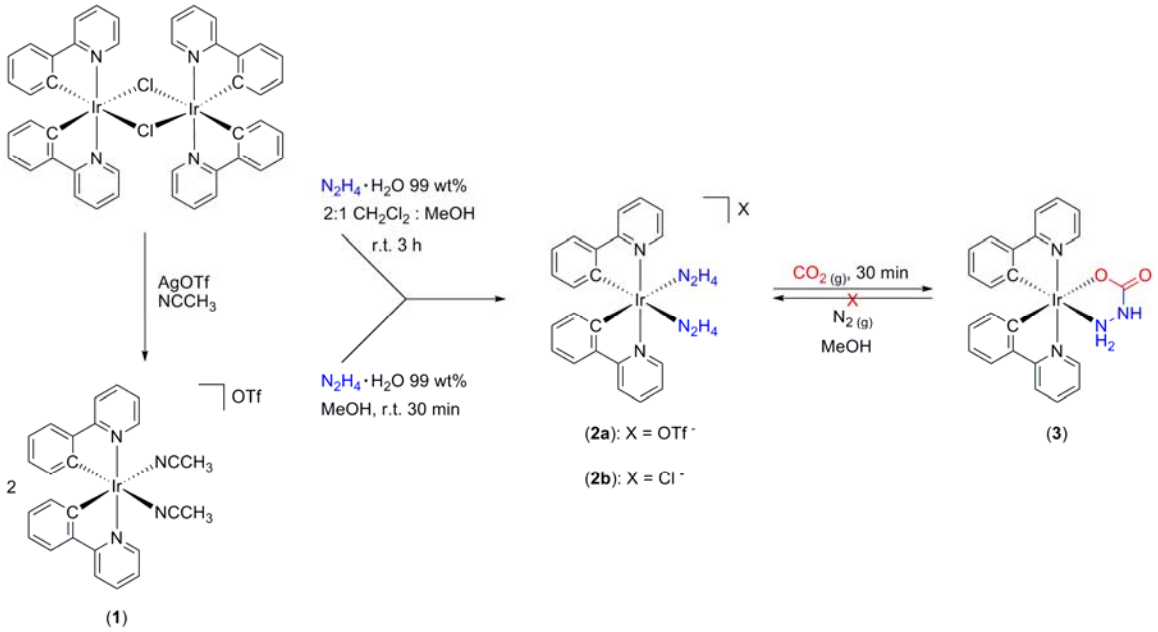

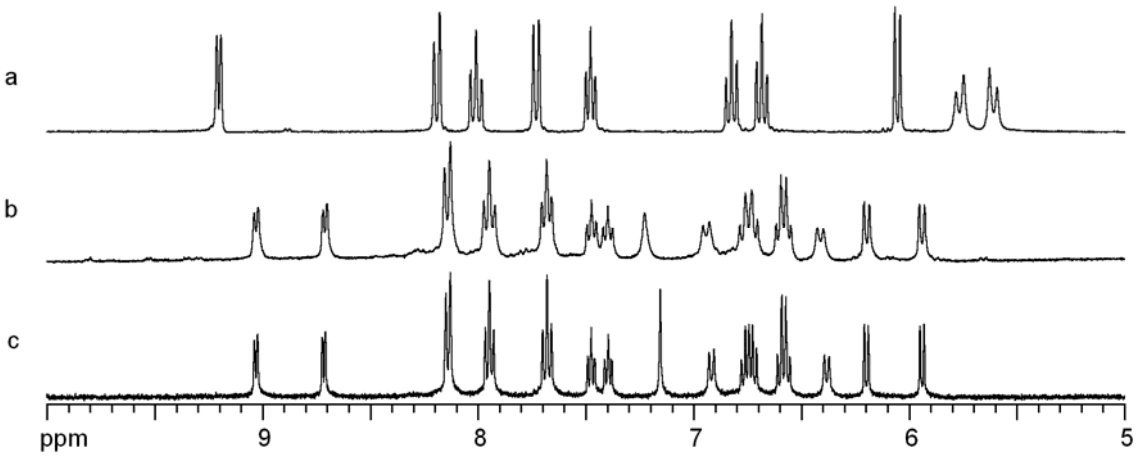

Figure 1. ^{1}H NMR DMSO-d_6 of (a) **2a**, (b) **3** generated in situ, (c) **3** synthetic preparation.

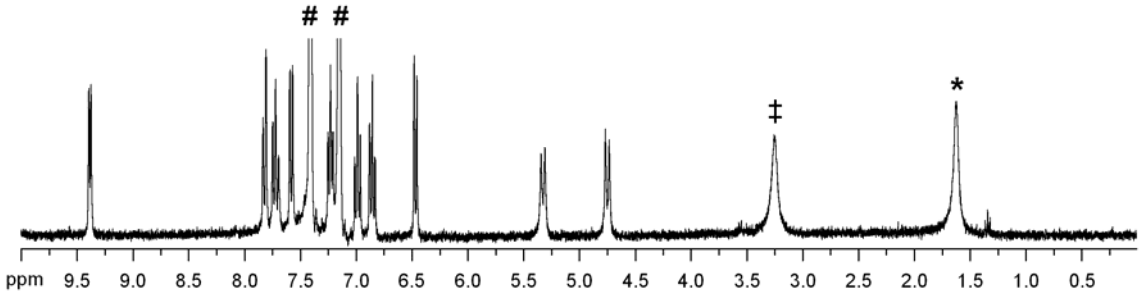

Figure 2. ^{1}H NMR of **2c** in *o*-dichlorobenzene-d_4 (#), distal N-H ^{1}H signal (‡), H_2O solvent impurity (*).

metathesized to the PF_6^- salt **2c**. The distal N-H ^{1}H resonances were observed as a broad singlet at 3.43 ppm for **2c** in *o*-dichlorobenzene-d_4 (Figure 2).

Complete conversion of the hydrazino complex **2a** to the carbazate complex **3** takes place by reaction of **2a** with CO_2 in solution. The result of bubbling CO_2 through a sample of **2a** in DMSO-d_6 for 60 min gives the in situ conversion of **2a** to **3** and the ^{1}H NMR spectrum shown in Figure 1b. Comparison of the ^{1}H NMR spectra for **2a** and **3** reveals an increase in the number of ^{1}H signals from 10 to 14, as expected upon converting from a symmetric ($\sim C_2$) to an asymmetric coordination sphere (Figure 1). The most telling peak in the spectrum of **3** is the appearance of a broad singlet between 7.15 and 7.23 ppm corresponding to the presence of an amide, indicating *N*-carboxylation of the ligated hydrazine has occurred. Chelation of the *N*-carboxylate moiety results in loss of the second hydrazino ligand,[20] leading to the formation of a bidentate carbazate ligand. The newly formed **3** is a neutral Ir(III) tris-chelate as opposed to its monocationic parent **2a**. Attempts to reverse the reaction of **2a** with CO_2 by bubbling solutions of the newly formed solution of **3** with N_2 gave no reaction. Compound **3** was also isolated on a preparative scale from the two different pathways outlined in Scheme 1. The first involves bubbling CO_2 through a concentrated solution of **2a** in MeOH to afford **3** as a yellow microcrystalline precipitate. The second generates **3** directly from the μ-chloro-bridged dimer $[Ir(ppy)_2Cl]_2$ after exposure to a slight excess of hydrazine at room temperature to generate the intermediate **2b** followed by exposure to CO_2. Comparison of the ^{1}H NMR spectra in DMSO-d_6 of the products obtained by both methods to the spectrum of the species generated in situ revealed them to be **3** in each case (Figure 1).

X-ray Crystallography. Single crystals of X-ray quality were grown for compounds **2a** and **3** by slow evaporation from mixtures of CH_2Cl_2/heptane and acetone/acetonitrile respectively. Relevant crystallographic information for **2a** and **3** is shown in Table 1, and a list of selected bond lengths and angles can be found in Table 2. Compounds **2a** and **3** are the first bis-cyclometalated Ir(III) species containing a monodentate hydrazine and an unsubstituted carbazate ligand, respectively, to be characterized crystallographically. The structures obtained for compounds **2a** and **3** display two ppy ligands in the *mer* or C,C-*cis*/N,N-*trans* arrangement about a pseudooctahedral Ir(III) center (Figure 2). A set of monodentate N_2H_4 ligands (**2a**) and a bidentate N,O-bound anionic $H_2NNHCOO^-$ ligand (**3**) occupy the remaining two coordination sites in the structures, with both ancillary ligand sets *trans* to the metalated ppy carbon atoms.

Although compound **2a** is the first bis-cyclometalated Ir(III) species containing a monodentate hydrazine to be characterized crystallographically a relevant Ir(III) sulfido cluster containing two monodentate hydrazino ligands has also been structurally characterized.[21] The N-N bond lengths found in **2a** are 1.461(7) and 1.454(8) Å for atoms N3-N4 and N5-N6 respectively. A direct comparison of the N-N bond lengths for the Ir(III) sulfido species shows one typical distance of 1.46(3) and one short distance of 1.38(4) Å. An average N-N bond length of 1.445 Å, obtained from a large sample of transition metal hydrazino complexes found in the CSD[22], is nearly the same as that of free hydrazine, N-N (1.45 Å).[23] All Ir(III) hydrazino ligands observed, including the short N-N distance (1.38(4) Å) are within the calculated average based on reported standard uncertainties.

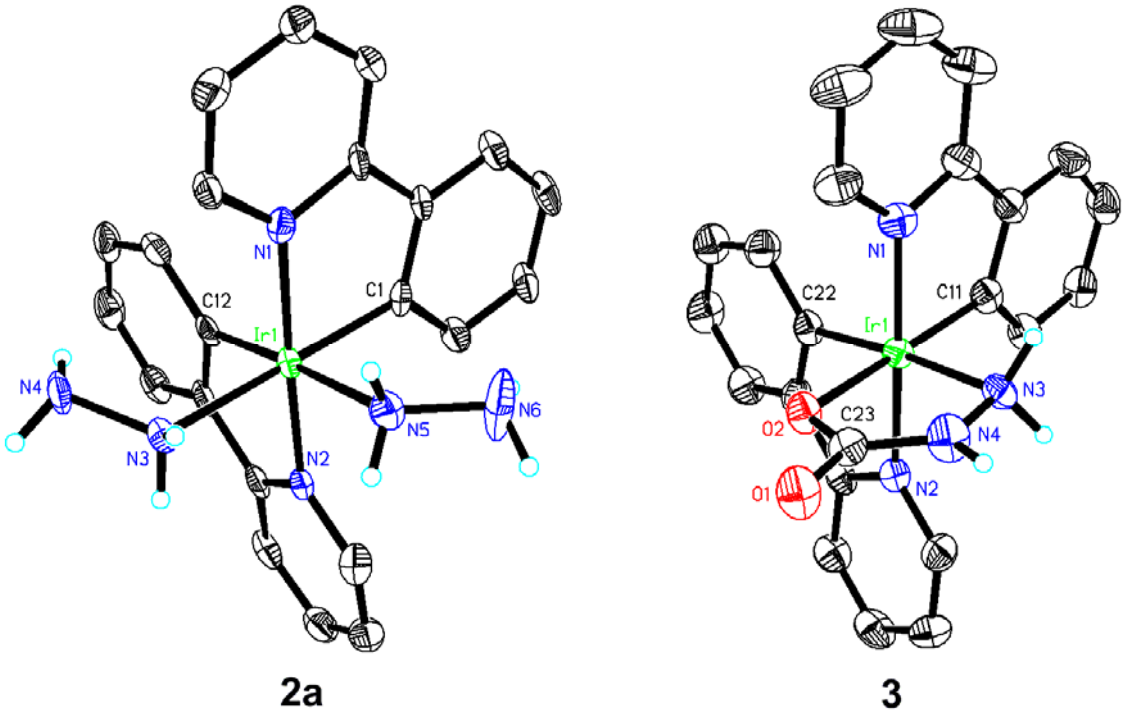

Figure 3. Thermal ellipsoid plots representing 50 % probability of **2a** and **3**, with ppy H atoms, molecules of solvation, and the OTf^- counter ion (**2a**) omitted for clarity.

Table 1. Crystallographic Data and Refinement Parameters for the Ir(III) Hydrazino (**2a**) and Carbazate (**3**) Complexes

Compound	$[Ir(ppy)_2(N_2H_4)_2]OTf$ (**2a**)	$Ir(ppy)_2(H_2NNHCOO)$ (**3**)
empirical formula	$C_{23}\ H_{26}\ F_3\ Ir\ N_6\ O_4\ S$	$C_{25}\ H_{26}\ Ir\ N_5\ O_4$
crystal color, morphology	Yellow, needle	yellow, plate
crystal system	Monoclinic	Triclinic
space group	$P2_1/c$	$P\bar{1}$
a, Å	15.024(3)	8.7740(6)
b, Å	9.7170(19)	9.4310(7)
c, Å	18.813(4)	16.2130(12)
α, deg	90	98.9020(10)
β, deg	109.883(3)	92.7260(10)
γ, deg	90	109.0090(10)
Volume (*V*), $Å^3$	2582.8(9)	1246.24(16)
Z	4	2
formula weight, g mol^{-1}	731.76	652.71
density (calculated), g cm^{-3}	1.882	1.739
temperature, K	173(2)	173(2)
absorption coefficient (μ), mm^{-1}	5.314	5.397
F(000)	1432	640
θ range, deg	1.44 to 27.57	1.44 to 27.57
Index ranges	$-18 \le h \le 19$	$-10 \le h \le 10$
	$-12 \le k \le 12$	$-11 \le k \le 11$
	$-24 \le l \le 24$	$-19 \le l \le 19$
reflections collected	26779	12462
independent reflections	5858 [R_{int} = 0.0652]	4412 [R_{int} = 0.0375]
weighting factors,[a] *a, b*	0.0688, 2.8073	0.0283, 1.3791
max, min transmission	0.7770, 0.1764	0.8905, 0.3831
data/restraints/parameters	5858/0/343	4412/3/316
R_1, wR_2 [$I > 2\sigma(I)$]	0.0412, 0.1011	0.0270, 0.0617
R_1, wR_2 (all data)	0.0683, 0.1164	0.0354, 0.0656
GOF	1.068	1.091
largest diff. peak, hole e$Å^{-3}$	3.137, -3.129	1.191, -0.956

[a] $w = [\sigma^2(F_o^2) + (aP)^2 + (bP)]^{-1}$, where $P = (F_o^2 + 2F_c^2)/3$.

Complex **3** is the first Ir(III) species containing an unsubstituted carbazate to be characterized crystallographically. A search of the CSD[22] yields only one Ir(III) structure containing the methyl ester derivative of carbazate. The neutral methyl ester is found in both the monodentate-N and bidentate-N,O coordination modes, with N-N bond lengths of 1.412(18) and 1.409(14) Å respectively.[24] An average N-N bond length of 1.413 Å tabulated from a sampling of the transition metal carbazate complexes found in the CSD.[22] The N-N bond length found for atoms N3 and N4 in the structure of **3** is 1.424(6) Å.

Table 2. Selected Bond Lengths and Angles for Ir(III) Hydrazino **2a** and Carbazate **3** Complexes

Compound	Atoms	Bond Length (Å)	Atoms	Bond Angle (°)
2a	Ir1 – N1	2.039(5)	N1 – Ir1 – C1	81.0(2)
	Ir1 – N2	2.033(5)	N2 – Ir1 – C12	79.9(3)
	Ir1 – C1	2.032(6)	N3 – Ir1 – N5	85.1(2)
	Ir1 – C12	2.004(6)	Ir1 – N3 – N4	118.4(4)
	Ir1 – N3	2.213(5)	Ir1 – N5 – N6	119.7(4)
	Ir1 – N5	2.192(6)		
	N3 – N4	1.461(7)		
	N5 – N6	1.454(8)		
3	Ir1 – N1	2.025(4)	N1 – Ir1 – C11	80.45(19)
	Ir1 – N2	2.037(4)	N2 – Ir1 – C22	80.0418)
	Ir1 – C11	1.985(5)	N3 – Ir1 – O2	76.96(14)
	Ir1 – C22	2.004(5)	Ir1 – N3 – N4	108.5(3)
	Ir1 – N3	2.176(4)		
	Ir1 – O2	2.173(3)		
	N3 – N4	1.424(6)		
	N4 – C23	1.339(7)		
	O1 – C23	1.261(6)		
	O2 – C23	1.297(6)		

Electronic Spectroscopy. The absorption and luminescence spectra collected for the Ir(III) hydrazino (**2a**) and carbazate (**3**) species are shown in Figure 4. The corresponding spectral data are summarized in Table 3. Both **2a** and **3** display an intense high energy band at ~ 265 nm (not displayed in Figure 4) and a series of moderate to weak absorption shoulders from ~ 340 - 500 nm as expected for bis-cyclometalated Ir(III) species.[18, 25] The high energy transitions have are typically assigned as the allowed $^1\pi \rightarrow \pi^*$ transitions centered on the cyclometalating ppy ligands. The remaining moderately intense absorption shoulders and weak absorption tails are labeled as either singlet metal-to-ligand charge-transfer (^{1}MLCT) or triplet metal-to-ligand charge-transfer (^{3}MLCT) transitions ($d\pi_{Ir(III)} \rightarrow \pi^*_{C^N}$) because of the absence or noninvolvement of the ancillary ligand (L = neutral monodentate, hydrazino or L^X = anionic bidentate, carbazate) π-system with the frontier orbitals. The electronic differences imparted on the Ir(III) center by the ancillary hydrazino (L) and carbazate (L^X) ligands in the cationic **2a** and neutral **3** result in a 26 nm (1314 cm^{-1}) shift in the lowest energy ^{1}MLCT transition from 432 (**2a**) to 458 (**3**) nm.

Table 3. Photophysical Properties[a] of Ir(III) Hydrazino (**2a**) and Carbazate (**3**) Complexes

Compound	λ_{abs}, nm (ε, x10^4 M^{-1} cm^{-1})	λ_{em}, nm[b]	ϕ_{em}[c, d]	τ_{em}, μs[e]
2a	264 (3.13), 350 (0.49), 393 (0.34), 432 (0.22), 480 (0.03)	501	0.42	1.56(1)
3	267 (2.63), 338 (0.49), 365 (0.36),408 (0.27), 458 (0.21), 490 (0.07)	524	0.45	1.80(1)

[a]All spectra recorded in deaerated DMSO solutions at 298 K. [b]λ_{ex} = 400 nm. [c] Determined relative to *fac*-Ir(ppy)$_3$ in toluene (ϕ_{em} = 0.40).[16] [d]Considered accurate to ± 20 %. [e]λ_{ex} = 405 nm.

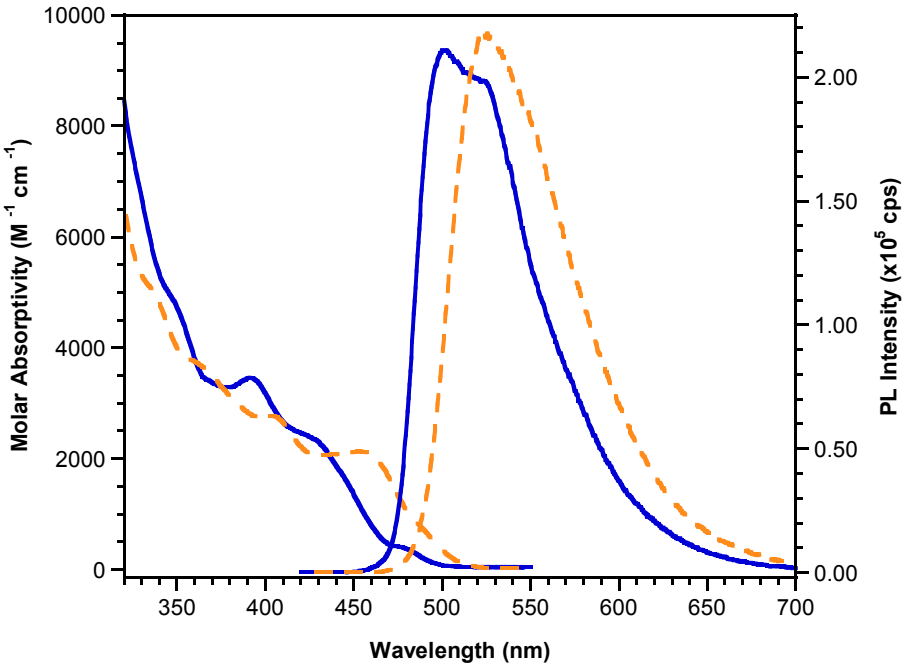

Figure 4. Absorption and Luminescence spectra of (—) **2a** and (- - -) **3** in deaerated DMSO at 298 K. λ_{ex} = 400 nm.

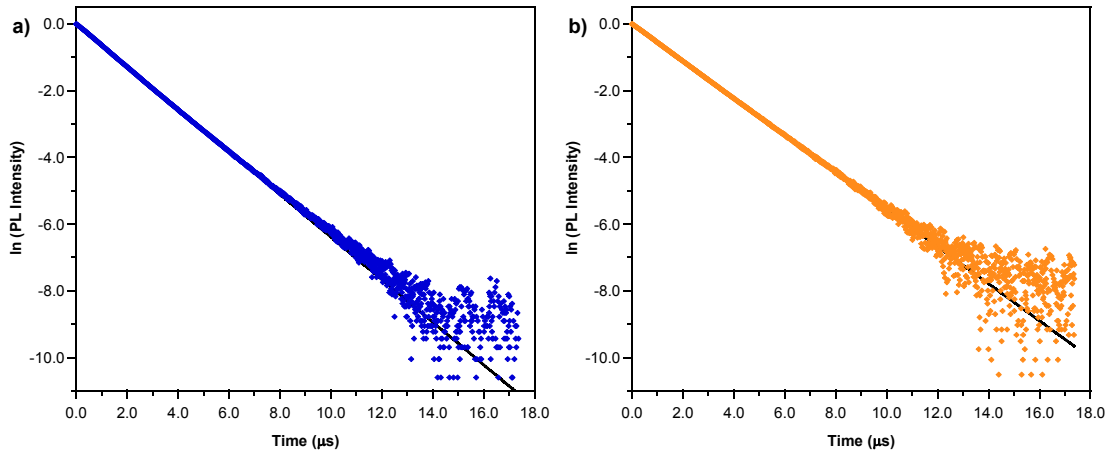

Figure 5. Lifetime plot of luminescence decay in deaerated DMSO solutions for (a) **2a**, (b) **3**. Experimental data (blue and orange squares) and the least squares fit to a single exponential (solid line) are shown. The line was fit only to data after the cessation of the light pulse at zero time. Lifetimes were 1.56(1) µs and 1.80(1) µs for **2a** and **3** respectively. λ_{ex} = 400 nm.

The Ir(III) hydrazino (**2a**) and carbazate (**3**) species both display strong luminescence in deaerated DMSO solutions at room temperature (Figure 4) and were found to have similar phosphorescence lifetimes (τ_{em} = 1.56 and 1.80 μs, Figure 5) and luminescence quantum yields (ϕ_{em} = 0.42 and 0.45, respectively). As observed for the absorption spectra, a 23 nm (876.11 cm^{-1}) red shift in the luminescence λ_{max} between **2a** and **3** highlights the differences in the electronic structure at the Ir(III) center. Also apparent is the loss of band structure in the luminescence profile of the carbazate species **3**. Of particular interest are the photophysical properties of the Ir(III) cabazate species **3**, which represents a new addition to the family of luminescent Ir(III) bis-cyclometalates of the type $Ir(C^N)_2(L^X)$. Phosphorescence lifetime and quantum yield measurements are similar to those of the related $Ir(ppy)_2(acac)$ (acac = acetylacetonate) species (τ_{em} = 1.6 μs, and ϕ_{em} = 0.34)[25d] and indicate the potential use of **3** as a triplet sensitizer or phosphorescent dopant in electroluminescent devices.

Optical Response to CO_2. The successful conversion of amine bearing fluorophores to carbamic acids by exposure to CO_2 has been shown to be highly solvent dependent.[9a, 9c] Solvents found suitable by previous investigators are DMSO, DMF, and Py while ACN, $CHCl_3$, 2-propanol, CH_3OH, benzene, dioxane and tetrahydrofuran were those named as unsuitable. The luminescence of **2a** was monitored in DMSO, DMF, CH_3OH, ACN, and $CHCl_3$ solutions under steady streams of both N_2 and CO_2 gas. No change was observed for solutions of **2a** under N_2 gas, with the exception of $CHCl_3$ where the solution darkened over time, leading to decomposition. Exposure of the remaining solutions to CO_2 showed a red shift in λ_{em}

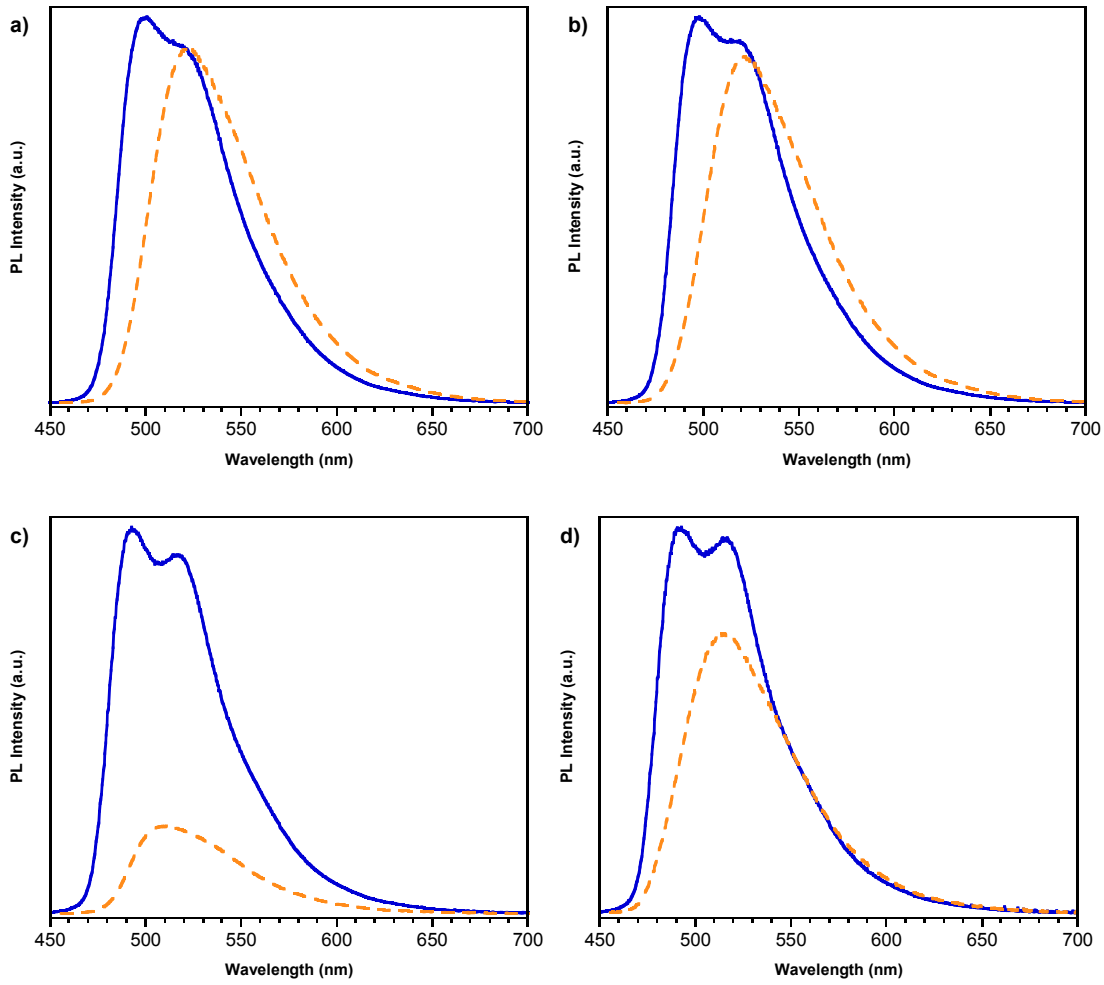

Figure 6. Uncorrected luminescence spectra at 298 K (λ_{ex} = 405 nm) of (—) **2a** before and (- - -) after exposure to CO_2 in (a) DMSO (60 min), (b) DMF (50 min), (c) MeOH (7 h), (d) ACN (14 h). For each solvent, the spectra are normalized to the initial intensity of **2a** prior to CO_2 exposure.

of **2a** upon conversion to the luminescent carbazate species **3** (Figure 6). Completion times for the conversion of **2a** to **3** were solvent dependent, with the fastest in DMSO, DMF and the slowest in MeOH and ACN.

As far as we know optical responses from motifs employing the amine/carbamate equilibrium to CO_2 have been limited to intensity changes. A novel optical sensing scheme using carbonate (from CO_2) to modulate the luminescence of a solvatochromic probe by altering the probes local environment has been reported.[8a] The sensing response, based on changes in polarity rather than pH, is formally a method of indirect detection. Observation of a spectral shift in λ_{em} as the optical response within the amine/carbamate motif has not yet been reported. The optical response of the Ir(III)-hydrazine system described here is due to the direct involvement of the amine/carbamate conversion with the coordination sphere of the transition metal chromophore. The conversion of **2a** to **3** results in changes to the Ir(III) coordination sphere shifting the relative energies of the lowest lying excited states. These shifts likely contribute significant ^{3}MLCT character into the lowest energy excited state, which is a mixture of triplet ligand centered (^{3}LC) and ^{3}MLCT states, resulting in loss of the vibrational structure observed in the luminescence profile.[26]

Two competitive pathways to *N*-carboxylation have been outlined for amine/carbamate systems.[9] The first results from an initial reaction of the amine with CO_2, followed by H^+ transfer to a second amine to form an ammonium carbamate ion pair [RR′NCOO$^-$] [RR′NH$_2^+$]. The second involves direct protonation of the amine via formation of carbonic acid in situ, forming an ammonium bicarbonate ion pair [HCO_3^-] [RR′NH$_2^+$]. In an effort to understand which of the two previously observed pathways

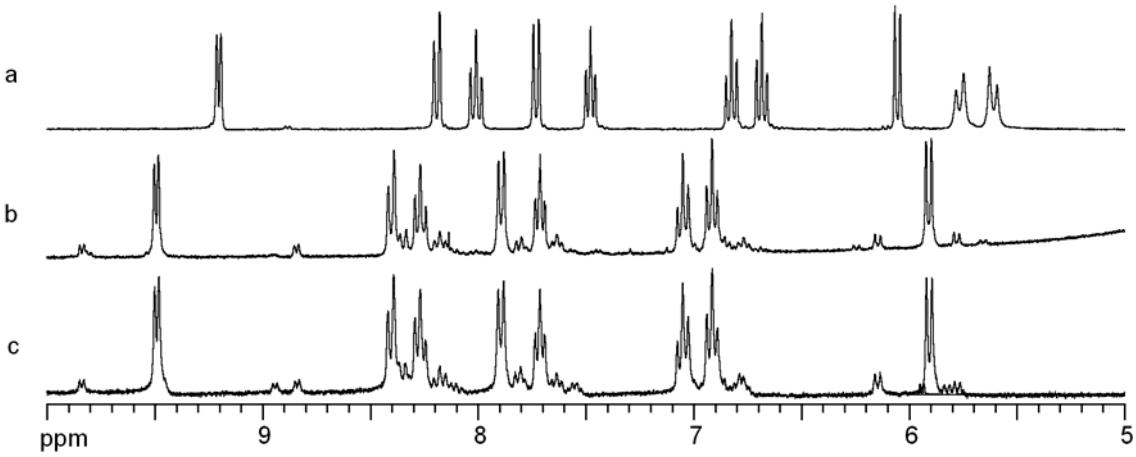

Figure 7. ^{1}H NMR DMSO-d_6 of (a) **2a**, (b) **4** after the addition of TFA to **2a**, (c) **4** prepared by dissolving **1** in DMSO-d_6.

may be operative in the Ir(III) hydrazine system described here, 2 equiv of trifluoroacetic acid (TFA) were added to a NMR tube of **2a** in DMSO-d_6. A deaerated sample of **2a** in DMSO-d_6 is intensely luminescent and gives the ^{1}H NMR spectrum shown in Figure 7a. It was found that addition of acid resulted in a dramatic decrease of the luminescence of the sample and gives the ^{1}H NMR spectrum shown in Figure 7b. Loss of both hydrazino ligands is evidenced by the absence of Ir-NH_2 proton signals at 5.61 and 5.77 ppm (Figure 7b).

These results suggest that protonation of the hydrazino ligands, to give coordinated $H_2NNH_3^+$, sufficiently weakens the Ir-N bond to cause subsequent displacement of $H_2NNH_3^+$ by the surrounding solvent forming the DMSO bis-solvento complex $[Ir(ppy)_2(DMSO)_2]^+$ (**4,** Scheme 2b). The identity of this species was confirmed as **4** after comparison of the ^{1}H NMR spectrum shown in Figure 7b with 7c, which contains **4** generated by addition of **1** to DMSO-d_6. The extremely weak luminescence of **4** has also been observed for similar solvento complexes including **1** and further supports this assignment.[13b]

Because conversion of **2a** to **3** during CO_2 exposure experiments does not yield the immediate near total loss of luminescence observed for protonation, we propose that the primary event that occurs during CO_2 exposure is *N*-carboxylation and not protonation (Scheme 2). This result also eliminates the uncertainty of quenching originating from protonation or *N*-carboxylation. Formation of an ammonium carbonate ion pair followed by the loss of $H_2NNH_3^+$ in sequence for both hydrazino ligands is expected to provide a result similar to that observed for addition of TFA, namely, the formation of the bis-solvento complex rather than the carbazate complex **3**.

Scheme 2. Competitive Pathways to *N*-Carboxylation in the Ir(III) Hydrazine System: (a) *N*-Carboxylation Followed by Proton Transfer (b) Direct Protonation

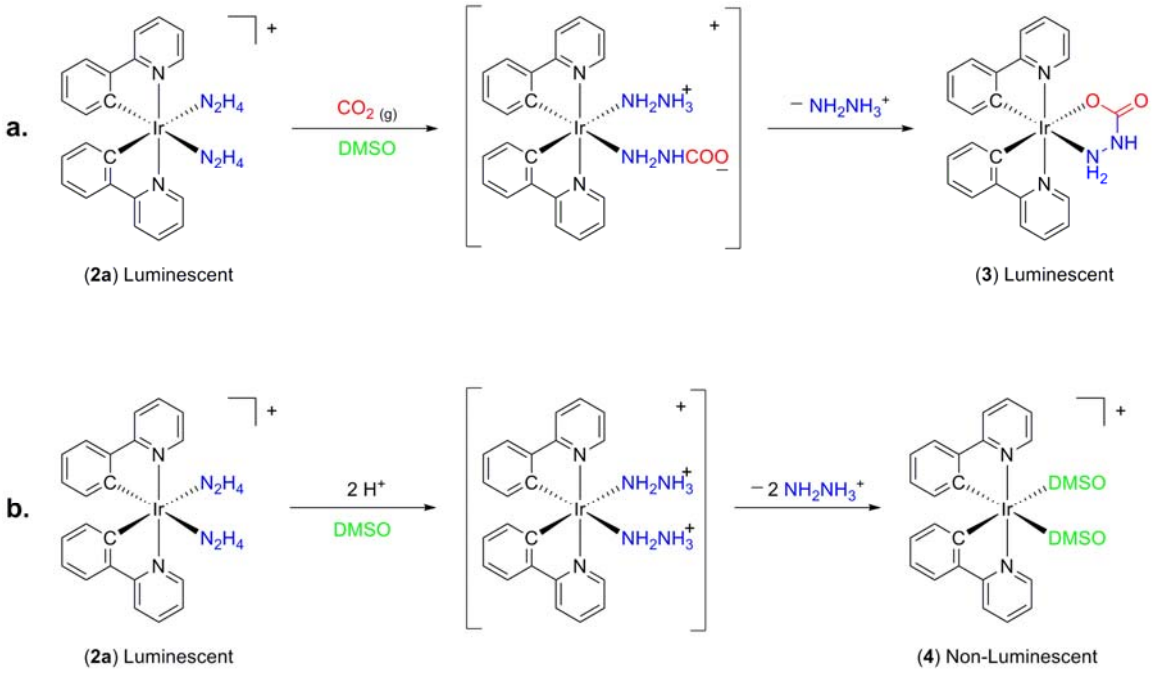

Elimination of the direct protonation pathway suggests that formation of an ammonium carbamate ion pair (Scheme 2a) is the more likely scenario. The Ir(III) hydrazine system here contains two potential CO_2 binding sites, one for each of the hydrazino ligands. After *N*-carboxylation of one hydrazino ligand occurs, proton transfer to the second is possible, leading to the formation of a "backside" metal-coordinated ammonium carbamate ion pair $M(NH_2NHCOO^-)(NH_2NH_3^+)$. This outcome should lead to the loss of a single hydrazino ligand as $H_2NNH_3^+$, followed by immediate chelation of the bidentate carbazate moiety to form the neutral Ir(III) carbazate species **3**.

Several preliminary kinetic runs using luminescence spectroscopy to follow the conversion of the bis-hydrazino species to the resulting carbazate were made to further investigate the optical response observed upon exposure of **2a** to CO_2. Data were obtained by collecting full-frequency steady-state emission spectra versus time during exposure of **2a** to CO_2 in DMSO solutions at room temperature. From these data, three wavelengths (500, 522, and 550 nm) that exhibited significant variation in the observed emission intensity during CO_2 exposure were selected. The intensity versus time data for the selected wavelengths were simultaneously fit to an irreversible, consecutive first-order reaction kinetic scheme. Three independent runs resulted in similar response functions and gave $k_1 = 0.02(1)\ s^{-1}$ and $k_2 = 0.0015(3)\ s^{-1}$ which indicated variation in the values for the rapid first process (k_1), while the values for the second process (k_2) were more consistent (Figure 8).

Analysis of these data suggests the fast, irreversible formation of an intermediate species upon exposure of **2a** to CO_2 in DMSO represented by k_1, followed by the comparatively slower irreversible conversion to the carbazate species **3** represented by k_2.

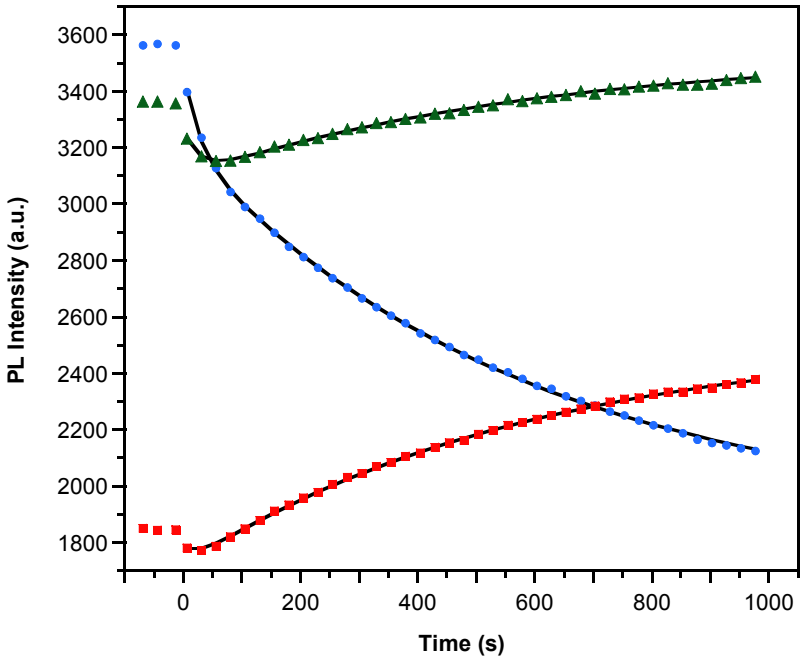

Figure 8. Optical response upon exposure of **2a** to CO_2 in DMSO monitored at wavelengths: (●) 500 nm, (▲) 522 nm, and (■) 550 nm. Intensity data for each wavelength was fit to the irreversible, consecutive reaction kinetic model(solid line) k_1 = 0.037, k_2 = 0.0017. Data points at negative times represent PL intensity at each wavelength before introduction of CO_2. λ_{ex} = 405 nm.

These results are seemingly consistent with the pathway depicted in Scheme 2a, which involves an initial rapid binding of CO_2 by **2a**, to form a monodentate carbazate intermediate, and the slower replacement of the second hydrazino ligand to form the final bidentate carbazate species **3**. Results obtained from these preliminary kinetic runs support the primary event to be *N*-carboxylation. It is unclear what the exact composition of the intermediate is, and the possibility of a doubly *N*-carboxylated intermediate cannot be ruled out at this time. The second process involves loss of hydrazine from the coordination sphere and replacement by the *N*-carboxylated terminus of the remaining monodentate carbazate ligand. It is unclear whether this is a stepwise or concerted process. Although this system shows desired reactivity, it demonstrates limited utility because of solvent dependence and lack of reversibility. Collection of the standard analytical chemistry metrics and more detailed kinetic studies that could fully characterize a working sensor scheme will need to await a faster and reversible system.

Conclusions. We have prepared novel hydrazino and carbazate transition metal species through coupling of a luminescent bis-cyclometalated Ir(III) core with the well defined chemistry between hydrazine and CO_2. Incorporation of hydrazine into the synthetic pathway was found to be an attractive and simple means for chloride abstraction. Treatment of the bis-hydrazino species with a stoichiometric portion of a proton source has been found to be an alternative means of preparing the labile Cl^--free bis-solvento species. Alternatively, exposure of the bis-hydrazino species to CO_2, thereby generating the corresponding neutral carbazates, provides a new synthetic strategy for the preparation of a family of neutral luminescent $Ir(C^N)_2(L^X)$ type complexes. This system has been well characterized and the products of CO_2 exposure determined by ^1H NMR and X-ray crystallography, demonstrating the suitability of ligated N_2H_4 as a site for CO_2 binding.

The attractive photophysical properties of this system were exploited to develop a scheme for the direct optical detection of CO_2 based on the hydrazine/carbazate conversion. The excited states of both the hydrazino and the carbazate complexes have long lifetimes (~ 1.5 μs) and high emission quantum yields (~ 0.4) in room temperature DMSO solutions. Reaction of the hydrazino complex with CO_2 affords the first instance of a spectroscopic shift λ_{em} as the optical response to CO_2 exposure within the amine/carbamate motif. Carbamic acids are known to be unstable, preferring the unprotonated anionic carbamate form, requiring a basic site for proton transfer. The Ir(III) hydrazine system developed here benefits from having two available sites for either *N*-carboxylation or protonation within the same luminophore. The 2:1 amine/CO_2 stoichiometry separates protonation from *N*-carboxylation through loss of the protonated

hydrazine while retaining the *N*-carboxylated moiety. Stabilization of the *N*-carboxylated hydrazino ligand through coordination provides the unique optical response of a 23 nm red shift in λ_{em}. Although the Ir(III) hydrazine system exhibits slow reaction times, unwanted solvent dependence, and irreversible binding of CO_2, this work is a first step toward achieving a reliable method for the direct optical detection of CO_2.

─ Chapter Two ─

Triplet-Sensitized Photooxygenation of Dimethyl Sulfoxide to Dimethyl Sulfone Monitored by Luminescence Spectroscopy

Overview. Photoreaction of triplet-sensitized singlet oxygen ($^1O_2$), a reactive oxygen species, with dimethyl sulfoxide (DMSO) leads to clean formation of dimethyl sulfone ($DMSO_2$) as the photoproduct. The identity of $DMSO_2$ as the photoproduct has been confirmed through ^1H NMR spectroscopy and significant conversions of DMSO to $DMSO_2$ were accomplished with both phosphorescent and dark triplet-sensitizers. Irradiation of air-saturated DMSO solutions containing phosphorescent sensitizers such as $Ir(ppy)_2(cbz)$ or $[Ru(bpy)_3]Cl_2$ is accompanied by an increase of the measured luminescence intensity. The luminescence increase is a direct result of O_2 depletion via the triplet-sensitized photoreaction of $^1O_2$ with the solvent. This provides the opportunity for phosphorescent excited states to serve as both sensitizer for production $^1O_2$, and probe for $^1O_2$ photoreactivity. This unusual luminescence recovery was monitored in depth using steady-state luminescence spectroscopy during irradiation of sealed sensitizer/substrate/solvent systems. Kinetic analysis of the luminescence recovery displayed for sensitizer solutions was performed using a model based on a proposed photooxygenation scheme and observed quantum efficiencies were determined. Excellent correlation of the experimental luminescence recovery data to the kinetic model was obtained. Extension of the method to a number of sensitizer/substrate/solvent combinations demonstrates the scope and utility of the method as a useful means to analyze relative reactivity of photooxygenation substrates.

Introduction. The diverse chemistry of molecular oxygen (O_2) and its ability to behave as both a vital[1] and detrimental[2] substance has interested scientist across many fields of research. In particular, the destructive qualities associated with O_2 involve chemistry of the excited state species known as singlet oxygen ($^1O_2$), and the reduced species known as superoxide anion ($O_2^{\cdot -}$). Both the excited state and the reduced species show increased reactivity over the neutral triplet ground state, O_2, and are classified as reactive oxygen species (ROS). The excited-state species can be most readily generated through energy transfer upon interaction of O_2 with an excited-state triplet sensitizer, such as Rose Bengal, Methylene Blue, platinum(II) octaethylporphyrin (PtOEP), or ruthenium(II) tris-bipyridyl ($[Ru(bpy)_3]Cl_2$]).[3]

Due to its light induced reactivity $^1O_2$ has been found particularly useful for organic phototransformations.[4] As a therapeutic reagent, the ROS can be generated in vivo to treat some forms of cancer using a process known as photodynamic therapy (PDT).[5] Dissolved organic matter (DOM) and humic substances have also been shown to sensitize the generation of $^1O_2$, a process which plays a critical role in remediation of environmental pollutants found in natural waters.[6] Understanding and controlling the reactivity of $^1O_2$ is of particular importance for the exploitation of $^1O_2$ as a remedial or therapeutic reagent,[7] and much effort has gone into the study of this ROS with substrates of biological and environmental relevance in these fields.

The increased reactivity of $^1O_2$ is attributed to its electrophilic character, reacting readily with electron-rich substrates, such as those with C=C bonds[8] or sulfur heteroatoms,[9] whose reactivity with $^1O_2$ has been a subject of intense investigation. Techniques used most commonly to study $^1O_2$ and its reactivity include analysis of the

oxygenated product[10] and uptake of O_2 gas[11] in conjunction with measurement of the luminescence intensity/decay of the excited state species for a given solvent system and substrate concentration.[12] Following the photoreactivity of $^1O_2$ using its phosphorescence spectral signature is attractive and allows for the direct measurement of [$^1O_2$] using optical spectroscopy, but presents two significant challenges for the experimenter. First, the phosphorescence signal of $^1O_2$ is observed in the infrared at 1270 nm,[3c] requiring detection equipment not routinely used for spectroscopic studies.[12a, 13] Second, difficulties in generating a significant excited state population of the ROS arise due to deactivation through bond-resonance energy transfer with the C-H and O-H bonds present in most organic solvents and water.[3c] This leads to a short-lived excited state and extremely weak phosphorescent signal.

Another technique utilizing an optical signature, used primarily for the determination of [O_2], is measurement of luminescence quenching.[14] Luminescence quenching is a decrease in the observed luminescence intensity arising from an energy transfer event between O_2 and phosphorescent triplet sensitizers. This unique relationship between phosphorescent excited states, as is the case for luminescent transition metal complexes, and O_2 has been a focus of our own research group in the development of porous crystalline materials for optical detection of small molecules, such as O_2.[15]

As one can imagine the generation of $^1O_2$ in these systems is not always innocent, leading to potential photoreactivity. The two outcomes of energy transfer, luminescence quenching and $^1O_2$ sensitization, could be exploited to monitor O_2 consumption over the course of a photoreaction, although, we have not found a description of luminescence quenching employed for this purpose. This connection was drawn in our own research lab

after observing peculiar behavior among a class of luminescent materials known as Ir(III) bis-cyclometalates when dissolved in aerated solutions of the common organic solvent dimethyl sulfoxide (DMSO). Undisturbed air-equilibrated DMSO solutions containing luminescent Ir(III) species displayed a rapid luminescence increase upon excitation of the solution. Quenching of the luminescence could be induced by agitation of the solution through stirring or mixing with a pipette. When agitation had ceased the luminescence was observed to increase as described above. This cycle could be consistently repeated.

In this report we establish the source of this unusual behavior as the photoreaction of triplet-sensitized $^1O_2$ with the common organic solvent DMSO, a reaction that has been scarcely addressed in the chemical literature.[16] To monitor the described photoreactivity we have developed a spectroscopic analytical technique and corresponding kinetic model based on luminescence quenching of phosphorescent transition metal species in solution. The method allows the phosphor to serve as both sensitizer and probe. Details on the development of this convenient, sensitive, and reproducible analytical technique are provided here.

The observed luminescence response is most dramatic for phosphorescent materials with long-lived triplet excited states and large luminescence quantum yields, such as the Ir(III) bis-cyclometalate, $Ir(ppy)_2(cbz)$ (cbz = carbazate, $H_2NNHCOO^-$).[17] These photophysical properties provide tremendous sensitivity to the presence of dissolved O_2 in solution.[18] We further demonstrate the scope of the method, extending our study to the model substrate 2,3-dimethyl-2-butene (tetramethylethylene, TME) and triplet sensitizers such as the phosphorescent $[Ru(bpy)_3]Cl_2$ and the dark Methylene Blue. Results obtained from previous work on a $[Ru(bpy)_3]Cl_2$/TME/MeOH photoxygenation

system have also been confirmed using the method described in this report, providing validation of our model and data analysis.[19]

Experimental Details.

General Considerations. NMR spectra were recorded on a Varian Unity or Varian Inova 300 MHz instrument. All experiments were conducted in commercially available solvents, dimethyl sulfoxide (DMSO, Sigma-Aldrich, Anhydrous ≥ 99.9 % A.C.S. Reagent Grade), methanol (MeOH, Macron Chemicals, Anhydrous) and were used as is. Reagent grade 2,3-dimethyl-2-butene (TME, Sigma-Aldrich, ≥ 99.9 %) was stored under argon atmosphere at 0 °C. Compressed air and oxygen (Minneapolis Oxygen Company) were introduced to photolysis samples open to the air from a gas cylinder using a stainless steel needle. Neutral bis-cyclometalated Ir(III) sensitizer, $Ir(ppy)_2(cbz)$, was prepared using the procedure previously described by our research lab.[17] Dicationic Ru(II) sensitizer, $[Ru(bpy)_3]Cl_2 \cdot 6H_2O$ (Strem Chemicals, Inc), and organic sensitizer Methylene Blue (Acros Organics) were commercially available and used as received.

Optical Spectroscopy. Luminescence measurements were performed using a light emitting diode (LED) as the excitation source (λ_{ex} = 405 nm) and a 6 (collection) around 1 (source) bifurcated fiber optic in the front face geometry, with optical densities of solutions >2.0. Data were collected using an Ocean Optics Inc. CCD spectrophotometer connected to a computer running the *OOIBase32* software suite (v. 2.0.6.5) using the Time Acquisition feature. Spectral data were monitored at both the luminescence and excitation maxima, averaging a 50 pixel bandwidth about the defined maximal wavelengths, and were not corrected for detector response.

Sample cuvettes containing sensitizer solution were periodically removed from the photolysis beam for collection of luminescence decay at the intermediate oxygen

concentrations produced over the course of a typical photolysis experiment, including the initial air and final "nitrogen" conditions (see discussion). Luminescence lifetimes were obtained in solution with an in-house constructed circuit that pulses (typically 1 μsec) a 405 nm laser diode for excitation of the sample. The light was conducted through one leg of a bifurcated fiber optic probe to a cuvette that contained a stirred DMSO solution of either Ir(III) or Ru(II) sensitizer. The luminescence decay and scattered light were collected by the other fiber optic leg, filtered through a cut off filter to remove the scattered excitation light and conducted to a Hamamatzu R928 PMT. The PMT signal was digitized by a sampling digital oscilloscope (Phillips PM 3323) interfaced to a computer running a LabView program. Detailed information concerning acquisition and processing of lifetime data has been presented previously.[15c]

Quantum efficiency measurements were performed using the micro Hatchard and Parker procedure[20], using 0.012 M potassium ferrioxalate, $K_3[Fe(C_2O_4)_3]$[21], solution as the chemical actinometer.[22] Solutions containing actinometer were irradiated with a 405 nm LED (ϕ_{405} = 1.14) and the corresponding change in absorption at 510 nm monitored using Ocean Optics Inc. spectrophotometer/white light source (USB-ISS-VIS). The white light source was filtered with a No. 8 Kodak WRATTEN cut off (λ_{450}) filter. Absorption measurements made at the analysis wavelength were extremely stable and reproducible, showing no sign of further reaction. Actinometry measurements were periodically performed prior to photolysis experiments and values of flux from the LED source incident on the cell were typically 2.4 x 10^{-9} einstein s^{-1}.

NMR Scale Photolysis of DMSO Sensitizer Solutions analyzed by No-D ^{1}H NMR. Stock solutions of $Ir(ppy)_2(cbz)$ and Methylene Blue (1.74 x 10^{-3} M, 10 mL) were

prepared using anhydrous nondeuterated DMSO ≥ 99.9 % for NMR scale photolysis experiments and a 750 μL aliquot of each sensitizer solution was added to a standard NMR tube. A control sample was also prepared using 750 μL of neat DMSO and no sensitizer. All stock solutions and NMR samples were prepared and stored in the dark until used. Each NMR sample was analyzed by No-Deuterium (No-D) ^{1}H NMR[23] immediately after preparation. Samples were then stored in the dark for 20 h and analyzed again to assess the degree of dark reaction. Samples were then left under a purge of pure O_2 gas delivered to the tubes from a gas cylinder using a stainless steel needle inserted in the DMSO solutions. Once purging the $Ir(ppy)_2(cbz)$ and control samples were irradiated using a 365 nm hand held mineral lamp, while the Methylene Blue sample was irradiated using a standard 60 W incandescent light bulb. After 5 h of continuous irradiation under an O_2 purge, samples were again placed in the dark and taken for analysis by No-D ^{1}H NMR to assess the degree of photoreaction. Solvent loss after 5 h of purging was negligible due to the high boiling point of DMSO (189 °C). No attempt was made to control or measure the intensity of the illumination sources.

Photolysis of DMSO Sensitizer Solutions. Photolysis experiments used freshly prepared stock solutions (1.74×10^{-3} M, 10.0 mL) of triplet sensitizer $Ir(ppy)_2(cbz)$ in anhydrous DMSO ≥ 99.9 %, prepared under 630 nm light and stored in the dark prior to photolysis. Solutions were air-saturated prior to photolysis by purging 2.0 mL aliquots of stock solution with compressed air for two minutes prior to data collection. Air-saturated sensitizer solutions were then used to fill a 4 x 10 mm self masking low volume quartz cell (Starna Cells, Inc, 29B-Q-10) containing a 2 x 7 mm PTFE coated stir bar. Care was taken to ensure no head space was present, giving a final solution volume of 1.65 mL

with PTFE cap inserted. Sensitizer solutions were stirred during photolysis experiments using a magnetic stirring system (Ultrafast Systems) in a side stir configuration, dictated by cell geometry. The programmed Time Acquisition feature of *OOIBase32* software was activated while simultaneously placing the sensitizer solution in front of the photolysis beam. Due to limitations of detector response and the nature of the light dependant experiment initial PL intensity data points were taken on average three seconds after time zero. Values for PL intensity at time zero can be obtained by extrapolation using Equation 13 below. Data were collected every minute for the duration of the photolysis experiment and stopped after changes in measured luminescence intensity had ceased. A low volume cell was used to decrease the length of time required to reach the described end point for luminescence recovery. The collected data were then fit using nonlinear least squares analysis performed with *Wolfram Mathematica 8* software package. For alternative sensitizer/substrate/solvent systems an essentially identical procedure was followed for preparation of stock solutions and photolysis samples. Typical concentrations of Ru(II) sensitizer and TME used were 8.77×10^{-4} and 1.20×10^{-2} M respectively in either MeOH or DMSO solvents.

Results and Discussion.

Determination of the Photoxygenation Product in DMSO. It was observed that dissolution of the triplet emitting phosphor $Ir(ppy)_2(cbz)$ (ppy = 2-phenylpyridine, cbz = carbazate, $H_2NNHCOO^-$) in DMSO for routine luminescence measurements resulted in a dramatic increase of photoluminescence (PL) intensity upon excitation of the air-equilibrated sample. A similar luminescence recovery was recorded by Demas for unstirred MeOH solutions of triplet sensitizer $[Ru(bpy)_3]Cl_2$ and TME, a known $^1O_2$ substrate.[24] It is well known that triplet excited states are capable of undergoing energy transfer with the triplet ground state of molecular oxygen (O_2) through collisional quenching. The aforementioned energy transfer event results in the generation of $^1O_2$, a reactive oxygen species (ROS). If present, quenching of phosphorescence from the triplet excited state also occurs.

An increase in luminescence intensity is therefore associated with depletion of O_2 from the system, which strongly indicates an irreversible photoreaction between $^1O_2$ and substrate in solution. A likely substrate is DMSO and not $Ir(ppy)_2(cbz)$ as photodegradation via oxidative damage to the sensitizer would likely result in a luminescence decrease rather than an increase. The oxidation state of the central sulfur atom in DMSO is between that of dimethyl sulfide (DMS) and dimethyl sulfone ($DMSO_2$). So it is conceivable to oxidize the sulfoxide further to the fully oxidized sulfone. Photooxidation of the fully reduced DMS by $^1O_2$ to generate the intermediate DMSO has been studied previously and occurs quite readily.[9b, 9e, 25] The literature is somewhat unclear as to the possibility of further DMSO oxidation to generate the sulfone via photoreaction with $^1O_2$. Aside from a singular report describing significant

photosensitized conversions of DMSO to $DMSO_2$,[16b] the subject is addressed by a limited number of categorical statements.[25a, 26]

In order to investigate the proposed photoreaction between triplet-sensitized $^1O_2$ and DMSO we turned to ^1H NMR spectroscopy to assist in indentifying the photooxygenation product. Based on the reported purity of the commercially available solvent (DMSO, Sigma-Aldrich ≥ 99.9 % A.C.S. Reagent Grade) any impurity present should be in a concentration of ≤ 0.1 %. For this reason we have opted to investigate the starting materials and photooxygenation reaction products using the No-Deuterium (No-D) ^1H NMR technique, as this level of impurity would likely not be detected at DMSO concentrations routinely used for standard ^1H NMR experiments run in deuterated solvent. For a detailed description of the No-D method we point readers to a publication on the subject by Hoye and co-workers.[23]

The No-D ^1H NMR spectrum of neat DMSO (14.1 M, Figure 1a) was recorded to examine the possibility of a DMS impurity providing the observed photosensitized reactivity in DMSO. The ^1H chemical shift of DMS has been reported to appear in the range of 2.30 – 2.00 ppm, 2.12 in $CDCl_3$[27] and 2.27 in 0.1 M $CF_3SO_3H_{(aq)}$.[28] Aside from the dominant signal at 2.50 ppm for DMSO and a small signal at 3.29 ppm for H_2O there are no resonances present from 10.00 – 3.30 ppm or 2.00 – 0.00 ppm. Enhancing the 3.30 – 2.00 ppm spectral region reveals ^{13}C satellites symmetrically positioned about the major DMSO signal at 2.27 and 2.73 ppm. No additional resonances attributable to a DMS impurity were found between 3.30 – 2.00 ppm or the reported 2.30 – 2.00 ppm range. Interestingly, a minor impurity was found at 2.95 ppm, assigned to the presence of $DMSO_2$ in DMSO. Addition of 0.1 % (1.41×10^{-2} M) $DMSO_2$ to the DMSO resulted in

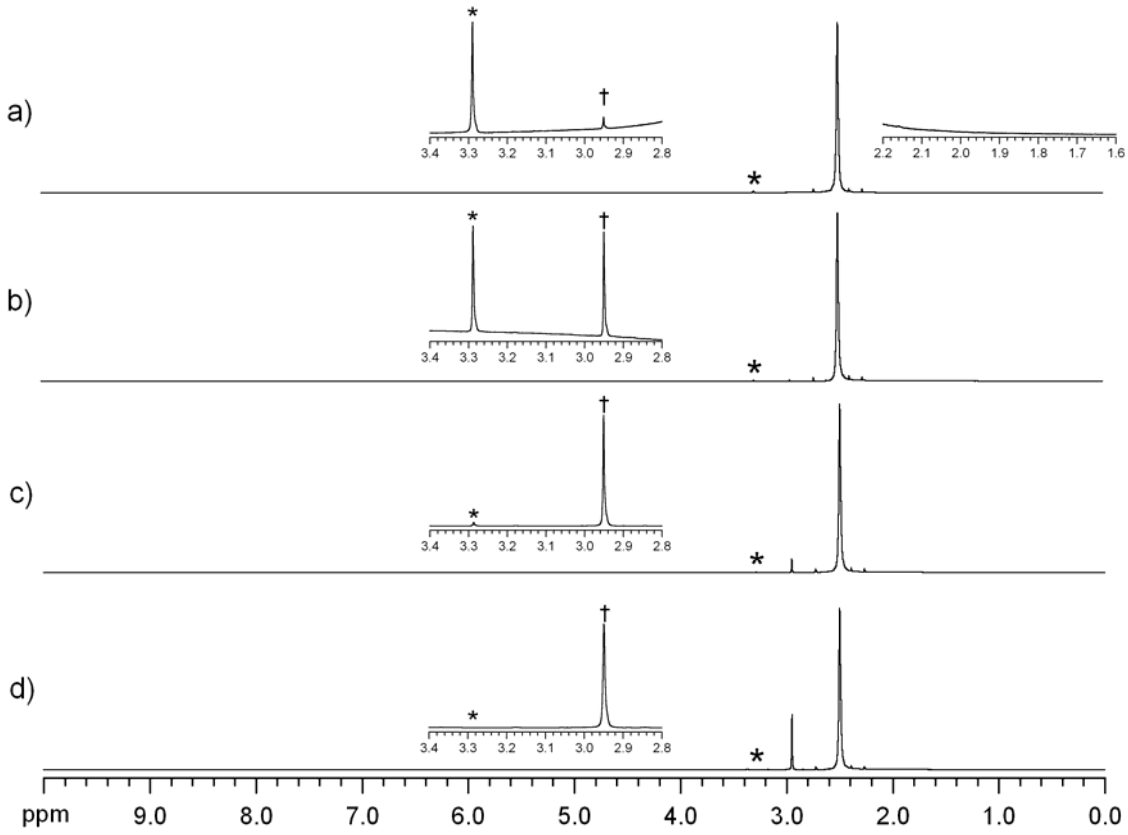

Figure 1. No-D ^{1}H NMR in DMSO (a) neat DMSO, (b) DMSO spiked with 0.1 % $DMSO_2$, (c) DMSO with $Ir(ppy)_2(cbz)$ after 5 h of irradiation under O_2 atmosphere, (d) DMSO with Methylene Blue after 5 h of irradiation under O_2 atmosphere. Insets (8x expansion) depict regions of interest for expected $DMSO_2$ and DMS chemical shifts. H_2O (*), $DMSO_2$ (†).

an increase of the signal at 2.95 ppm, confirming its identity as $DMSO_2$ (Figure 1b). Presence of a DMS impurity in the DMSO therefore does not appear to account for the observed photochemical reactivity. Observation of $DMSO_2$ in the commercially available solvent suggests that any $^1O_2$ generated in solution has already been scavenged by a once present DMS impurity, now fully converted, or the ubiquitous DMSO. In either case we believe DMS is likely to be absent from the DMSO, or below levels detectable by ^1H NMR spectroscopy.

Trace amounts of sulfone found in commercial DMSO indicate that formation of sulfone in situ appears to be reasonable, provided there is a source of $^1O_2$. Use of a triplet sensitizer can aid significantly in production of $^1O_2$ in solution, which in DMSO should then react to generate the sulfone if DMSO is a suitable substrate. To probe this hypothesis we again made use of the No-D NMR technique. Experimental conditions present during the original luminescence increase were reproduced, preparing 10 mL of a 1.74×10^{-3} M $Ir(ppy)_2(cbz)$ solution in DMSO, which was stored in the dark to prevent any photoreaction prior to collection of data. A 750 μL aliquot of the DMSO sensitizer solution was taken for No-D ^1H NMR. As for the neat DMSO solution, resonances for DMSO, H_2O, and the background level $DMSO_2$ were observed. No resonances for the triplet sensitizer were observed at this concentration. The sample of neat DMSO and DMSO sensitizer solution were then stored in the dark for 20 hours and the No-D spectrum recorded again. No changes were observed, verifying no dark reaction. Both samples were then continuously irradiated at 365 nm from a handheld mineral lamp while bubbled with a stream of O_2 gas for 5 h. Analysis of the sensitizer solution by No-D ^1H NMR depicted significant generation of $DMSO_2$ after irradiation for 5 h, with a large

resonance present at 2.95 ppm, the chemical shift observed previously for $DMSO_2$. Conversion of DMSO to $DMSO_2$ was clean, with no additional signals observed after irradiation of the sensitizer solution. The signal at 2.95 ppm corresponds to ~ 1.7 % conversion (60:1 DMSO:$DMSO_2$, Figure 1c) of the original DMSO concentration based on integration. For the neat DMSO solution no increase above the background was observed for the resonance at 2.95 ppm when irradiated in the absence of sensitizer. The same set of experiments was conducted using known triplet sensitizer Methylene Blue under irradiation from a household 60 W incandescent lamp, and similar results obtained. No dark reaction was observed, with the resonance at 2.95 ppm corresponding to ~ 10 % conversion (9:1 DMSO:$DMSO_2$, Figure 1d) of the original DMSO concentration after 5 hours based on integration. These experiments demonstrate the photoproduct can be obtained using multiple triplet sensitizers both phosphorescent and nonphosphorescent.

For both triplet sensitizers, conversions of DMSO to $DMSO_2$ under continuous irradiation and an oxygen atmosphere far exceed the maximal 0.1 % expected for any impurity responsible for the observed photochemical reactivity. The possibility of an undetectable catalytic amount of DMS is also not supported by previous literature, which reports the photooxygenation of sulfides by $^1O_2$ to be noncatalytic, with the exception of the cyclic substrate, thietane.[29] We also point out the volatile nature of DMS, evidenced by its low boiling point (38 °C) and appreciable vapor pressure (0.53 atm at 20 °C), further substantiates its absence from our O_2 purged solutions. Based on the results of our No-D ^1H NMR investigation and the physical properties of DMS, we argue $DMSO_2$ to be the photoproduct of the photoreaction between photosensitized $^1O_2$ and DMSO, not the result of a reaction mechanism that involves DMS.

Determination of K_{sv}. Confirmation of the proposed photoreaction between triplet-sensitized $^1O_2$ and DMSO has given cause to our in depth exploration of the luminescence recovery for air-saturated DMSO solutions containing triplet sensitizer. For this purpose, phosphorescent triplet sensitizers are the obvious choice, acting as both $^1O_2$ sensitizer and luminescent probe. This unique relationship between phosphorescent excited states and O_2 allows the photooxygenation to be monitored using steady-state luminescence spectroscopy. Organic triplet sensitizers such as Methylene Blue do not provide the necessary phosphorescent signature needed to monitor the photooxygenation in this way and are excluded from use for the remainder of this study.

Our choice of triplet sensitizer is the neutral bis-cyclometalated Ir(III) species mentioned above, $Ir(ppy)_2(cbz)$, whose synthesis, structural, and photophysical properties have been thoroughly studied in a previous report by our lab.[17] The long luminescence lifetime (τ_{em} = 1.8 μs) and large luminescence quantum yield (ϕ_{em} = 0.45) reported for the Ir(III) phosphor are photophysical properties desirable for investigation of photooxygenation using luminescence spectroscopy, providing excellent analytical signal and sensitivity. For comparison, photooxygenations were also carried out using the phosphorescent Ru(II) polypyridyl species, $[Ru(bpy)_3]Cl_2$, another well studied triplet sensitizer. The luminescence response displayed for each sensitizer during photooxygenation experiments is a concentration dependent phenomenon governed by the principles of luminescence quenching illustrated by the Stern-Volmer relationship (Eq. 1).

$$\frac{I_0}{I} = \frac{\tau_0}{\tau} = K_{sv}[Q] + 1 \qquad (1)$$

Expressed as either a ratio of luminescence intensities (I_0/I) or luminescence lifetimes (τ_0/τ) the most common representation of the Stern-Volmer relationship is shown in Equation 1. Variables I_0 and τ_0 are the PL intensity or lifetime of the triplet sensitizer in the absence of a quencher, I and τ are the PL intensity or lifetime in the presence of a known concentration of quencher, [Q] is the concentration of quencher (Q = O_2 from this point forward), and K_{sv} is the Stern-Volmer dynamic quenching constant. Solving Equation 1 for PL intensity (I) or lifetime (τ) clearly shows the inverse proportionality of the terms to $[O_2]$ where I_0, τ_0, and K_{sv} are constants (Eq. 2).

$$I = \frac{I_0}{K_{sv}[Q] + 1} \quad \text{or} \quad \tau = \frac{\tau_0}{K_{sv}[Q] + 1} \tag{2}$$

Further expansion of K_{sv} reveals its strong dependence on the photophysical properties of the triplet sensitizer, where k_r and k_{nr} are the radiative and nonradiative rate constants for relaxation of the phosphorescent excited state, and $1/k_r+k_{nr}$ represents τ_0 (Eq. 3).

$$K_{sv} = \frac{k_q}{k_r + k_{nr}} = k_q \tau_0 \tag{3}$$

Triplet sensitizers with long-lived phosphorescent excited states provide an increased probability for interaction with O_2 while in the excited state, resulting in enhanced luminescence quenching and larger values of K_{sv}. A reasonable estimate of the differences expected for the luminescence response of the Ir(III) and Ru(II) sensitizers can then be quantified by completing a Stern-Volmer determination to obtain a value for K_{sv}, a relative indicator of excited state sensitivity to the $[O_2]$.

Table 1. Values for two point K_{sv} determination for Ir(III) and Ru (II) sensitizers in DMSO[a]

Sensitizer	I_0	I_{air}	K_{sv} (atm^{-1})[b]	τ_0 (μs)	τ_{air} (μs)	K_{sv} (atm^{-1})[c]	k_q (atm^{-1} s^{-1})[d]
$Ir(ppy)_2(cbz)$	1221	135	38.5	1.80	0.19	40.7	22.0
$[Ru(bpy)_3]Cl_2$	52	20	7.5	0.96	0.36	8.0	8.1

[a]$[O_2]_{air}$ assumed to be 0.208 atm. [b]From intensity values. [c]From lifetime values. [d]Computed from average of values of K_{sv} obtained from intensity and lifetime data.

A preliminary two point Stern-Volmer determination for the Ir(III) and Ru(II) triplet sensitizers was carried out by measuring both the PL intensity and lifetime under N_2 and air in DMSO solutions. Clear differences in the photophysics of the Ir(III) and Ru(II) sensitizers can be seen in Table 1, leading to a large disparity in the values of K_{sv}. This preliminary determination provides a good prediction for the magnitude of the luminescence recovery expected during photooxygenation experiments for the respective sensitizers. Values of K_{sv} determined from the lifetime data are slightly higher than those determined from intensity data, and the true value of K_{sv} is expected to fall somewhere near this range of values, which are approximate at best using a simple two point determination.

It should also be mentioned at this time that there are some issues with providing an accurate value for the $[O_2]$ in air-saturated DMSO with which to determine the value of K_{sv} expressed in units of M^{-1}. A report from Franco et al. describes a photochemical determination of the $[O_2]$ for a number of air-saturated solutions.[30] The method involves monitoring the changes in absorption at 404 nm brought about by the triplet-sensitized 1:1 photooxygenation of 1,3-diphenylisobenzofuran by $^1O_2$. Measurements carried out in DMSO were reported to be in agreement with the lowest value (3.28×10^{-4} M) in a range

of $[O_2]$ previously determined for the air-saturated solvent ($3.23 \times 10^{-4} - 5.80 \times 10^{-4}$ M). The observation of an apparently low value for the photochemical determination of $[O_2]$ in air-saturated DMSO is consistent with our observation of a significant reaction between DMSO and triplet-sensitized $^1O_2$, which could lead to competition with the reaction of $^1O_2$ and 1,3-diphenylisobenzofuran in this system. Taking these factors into consideration we believe the method of determination described by reference 12 found in Franco's report provides the most accurate value of $[O_2]_{air} = 4.60 \times 10^{-4}$ M,[31] for the molar concentration of O_2 in air-saturated DMSO. For most situations we choose to represent the $[O_2]_{air}$ as 0.208 atm taken from the partial pressure of O_2 at 1.0 atm air, uncorrected for elevation or vapor pressure of DMSO (essentially negligible). Using atmospheric concentration units for $[O_2]$ provides values of K_{sv} with units of atm^{-1}. Conversion of $[O_2]$ to molar concentration units gives K_{sv} in units of M^{-1} and can be done by applying the appropriate Henry's law constant (4.52×10^2 atm M^{-1}).

Modeling the Photooxygenation. A typical photooxygenation scheme accounting for the notable physical and chemical processes can be found in Scheme 1, where A is the transition metal sensitizer in the ground state, $^1A^*$ and $^3A^*$ are the sensitizer in the excited singlet and triplet states respectively, O_2 is the triplet ground state of molecular oxygen, $^1O_2$ is the singlet excited state of molecular oxygen, B is the photoreaction substrate (DMSO), "Int" is a proposed reaction intermediate, and C the photoproduct ($DMSO_2$), with the respective rate constants displayed with each process. The photoreaction of $^1O_2$ with the substrate (B) to generate photoproduct (C) is described by Processes 10 and 11 of the photooxygenation scheme. Processes 10 and 11 result in the irreversible consumption of O_2 from the system, where a $^1O_2$ – substrate

Scheme 1. Physical and chemical processes pertaining to the photooxygenation reaction

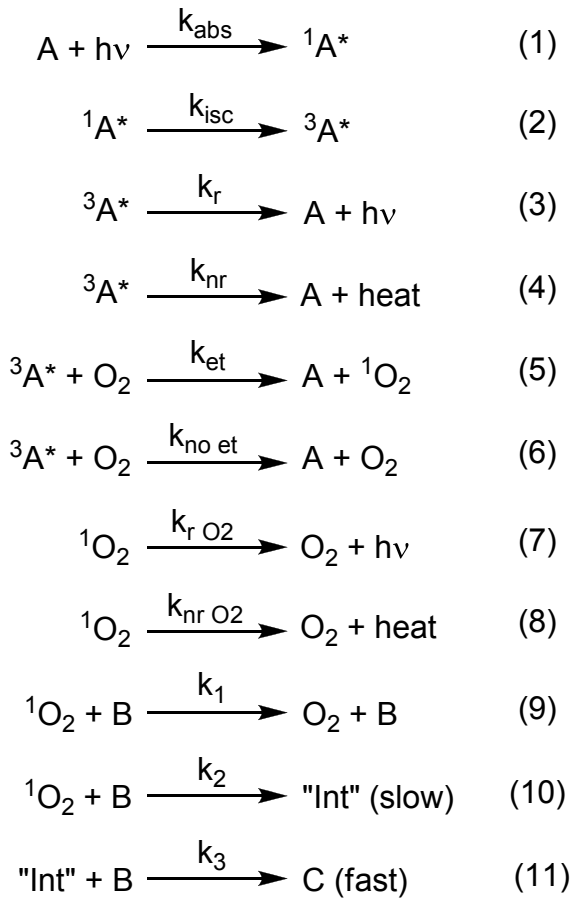

intermediate is formed during an initial slow process (rate determining step) followed by a second fast process to give the final photoproduct (C). Reaction of $^1O_2$ with substrate has been the targeted chemical process for the study of photooxygenation schemes. As mentioned above measurements involving analysis of the photooxygenated product are not instantaneous, and measuring $^1O_2$ phosphorescence (Process 6) can be challenging.

In the photooxygenation system described here the irreversible consumption of O_2 also results in an increase of the observed PL intensity from the triplet sensitizer, stabilizing at a maximal PL intensity once all of the O_2 has been depleted. Monitoring the luminescence recovery of air-saturated sensitizer solutions should provide a convenient means for monitoring the consumption of O_2 from the system. While it is true that the excited state species $^1O_2$ undergoes the photoreaction, it is the concentration of the ground state species that can be monitored by luminescence spectroscopy as outlined in Process 5 and 6 (quenching event) through their direct effect on Process 4 (^{3}A* phosphorescence, referred to as A* from this point forward). A kinetic model for the irreversible consumption of [O_2] from the system during irradiation of the air-saturated sensitizer solution is written in Equation 4.

$$\frac{d[O_2]}{dt} = -k_{et}[O_2][A^*] + k_{1O2}[^1O_2] + k_1[^1O_2][DMSO] \qquad (4)$$

The term k_{1O2} is the sum of the rate constants $k_{r\,O2}$ and $k_{nr\,O2}$ written for Process 7 and 8, which serve to deactivate the $^1O_2$ excited state. Rate constants k_{et} and $k_{no\ et}$ both induce quenching of A*, but only k_{et} results in generation of $^1O_2$. Therefore, $k_{no\ et}$ is excluded from our definition of the rate law. Photooxygenations were performed under continuous irradiation; we make the assumption that grow in of [A*] is rapid and the [A*] reaches a

very low steady-state value. We apply the steady-state approximation to $[^1A^*]_{ss}$, $[A^*]_{ss}$, and $[^1O_2]_{ss}$. Substitution of intermediate concentrations that result from the steady-state approximations and $k_q = K_{sv}(k_r + k_{nr})$ into Equation 4 provide the final expression for the rate law of $[O_2]$ consumption (Eq. 5) where k_{obs} is the composite term shown in Equation 6 with contributions from both sensitizer ($k_{nr1A^*} << k_{isc}$) and O_2 photophysics as well as the monochromatic source intensity (I_{405}). Inversion of Equation 5 followed by separation of the variables dt and $d[O_2]$ allows for direct integration to give Equation 7, the integrated rate law, which takes a linear form with the slope defined as k_{obs}.

$$\frac{d[O_2]}{dt} = -k_{obs}\frac{K_{sv}[O_2]}{K_{sv}[O_2]+1} \tag{5}$$

$$k_{obs} = I_{405}\,\Phi_{isc}\,\Phi_{et}\,\Phi_{rxn}\frac{[DMSO]}{\beta+[DMSO]} \tag{6}$$

$$\Phi_{isc} = \frac{k_{isc}}{k_{isc}+k_{nr1A^*}} = 1,\ \Phi_{et} = \frac{k_{et}}{k_{et}+k_{noet}},\ \Phi_{rxn} = \frac{k_2+k_3}{k_1+k_2+k_3},\ \beta = \frac{k_{1O2}}{k_2+k_3}$$

$$\frac{\ln\frac{[O_2]_0}{[O_2]_t}}{K_{sv}} + [O_2]_0 - [O_2]_t = k_{obs}(t-t_0) \tag{7}$$

Solving the integrated rate law for $[O_2]_t$ can be done by first rearranging Equation 7 to arrive at the form $x = f(y) = y\,e^y$, shown in Equation 8. Simple algebraic manipulation alone cannot be used to express Equation 8 in terms of $[O_2]$. To do so requires use of the Lambert W function (W), also known as the Omega function or the product log.[32] The Lambert W function, $W(x)$, can be described as the inverse function of the mathematical scenario in which $x = f(y) = y\,e^y$ whose inverse function is then $y = f^{-1}(x) = W(x)$. Application of the Lambert W function to Equation 8 provides the form $y = f$

$^{-1}$ (x) = W(x), as seen in Equation 9. This form of the integrated rate law can then be solved for time dependent O_2 concentration $[O_2]_t$ to provide Equation 10, or expressed

$$K_{sv}[O_2]_0 e^{K_{sv}([O_2]_0 - k_{obs}(t-t_0))} = K_{sv}[O_2]_t e^{K_{sv}[O_2]_t} \quad (8)$$

$$K_{sv}[O_2]_t = W(K_{sv}[O_2]_0 e^{K_{sv}([O_2]_0 - k_{obs}(t-t_0))}) \quad (9)$$

in terms of the experimentally measurable variable, the time dependent PL intensity I_t, by making a substitution for $[O_2]$ from the rearranged Stern-Volmer relationship (Eq. 11) and solving for I_t to obtain Equation 12

$$[O_2]_t = \frac{W(K_{sv}[O_2]_0 e^{K_{sv}([O_2]_0 - k_{obs}(t-t_0))})}{K_{sv}} \quad (10)$$

$$[O_2]_t = \frac{\frac{I_0}{I_t} - 1}{K_{sv}} \quad (11)$$

$$I_t = \frac{I_0}{W(K_{sv}[O_2]_0 e^{K_{sv}([O_2]_0 - k_{obs}(t-t_0))}) + 1} \quad (12)$$

Equations 10 and 12 represent the time dependent O_2 concentration and PL intensity at any given time (t) during the steady-state photooxygenation reaction, providing a kinetic model for analysis of the experimentally collected I_t data, that can be transformed into the associated $[O_2]_t$ data using Eq. 10 or 11.

Data analysis was conducted in *Wolfram Mathematica 8* using Equation 13, which contains an additional term "base" to correct measured PL intensity values for experimental artifacts, such as stray light. Experimental PL intensity data are fit to the model using a nonlinear least squares analysis in the *Mathematica* suite while allowing the parameters k_{obs}, K_{sv}, I_0, and "base" to be varied simultaneously. Initial estimates for

the fitting parameters were provided from the experimental data for I_0 and previously determined values of K_{sv}, while best guesses were made for k_{obs} and "base".

$$I_t = \frac{I_0 - \text{base}}{W(K_{sv}[O_2]_0 e^{K_{sv}([O_2]_0 - k_{obs}(t-t_0))}) + 1} + \text{base} \quad (13)$$

The corresponding $[O_2]_t$ data are obtained from corrected PL intensities using a modification of the Stern-Volmer relationship (Eq. 14) or the kinetic model (Eq. 10)

$$[O_2]_t = \frac{\frac{I_0 - \text{base}}{I_t - \text{base}} - 1}{K_{sv}} \quad (14)$$

Monitoring Photooxygenation. The triplet-sensitized photooxygenation of DMSO upon irradiation of air-saturated Ir(III) and Ru(II) sensitizer solutions was investigated using steady-state luminescence spectroscopy. Changes in PL intensity with time were followed at the sensitizer determined PL maximum (λ_{em}) and are shown in Figure 2. Beginning from a fully quenched PL intensity (I_{air}), the air-saturated sensitizer solutions displayed a recovery in PL intensity, which ceased to change after all O_2 had been consumed by the photoreaction. Upon stabilization of the PL intensity the solution is effectively considered "degassed", and the final value of PL intensity is representative of unquenched luminescence or the luminescence intensity in the absence of quencher, I_0.

Each data set was fit to the kinetic model shown in Equation 13 and the parameters fit are summarized in Table 2. A plot of the corresponding $[O_2]_t$ data is plotted in Figure 3. Photooxygenations carried out using the Ir(III) and Ru(II) sensitizers provide excellent correlation to the kinetic model for both I_t and $[O_2]_t$ despite the two very different luminescent responses. Notable comparisons of the obvious graphical differences in the luminescence recovery (Figure 1) are also evident in the parameters fit

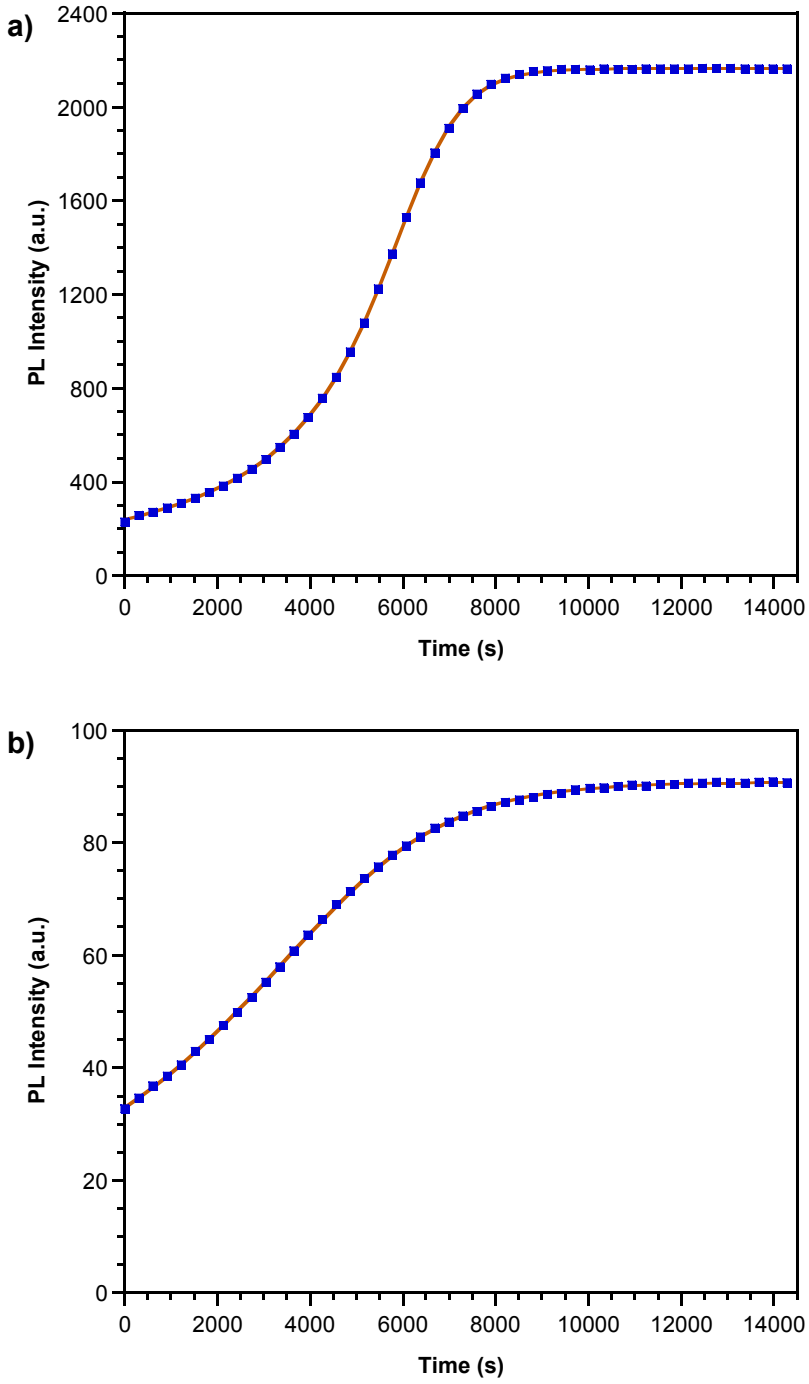

Figure 2. Luminescence recovery of air-saturated DMSO sensitizer solutions monitored at (a) 524 nm for $Ir(ppy)_2(cbz)$ (b) 620 nm for $[Ru(bpy)_3]Cl_2$, including data fit to Eq. 13 (solid line). Every 5th data point shown for clarity. λ_{ex} = 405 nm.

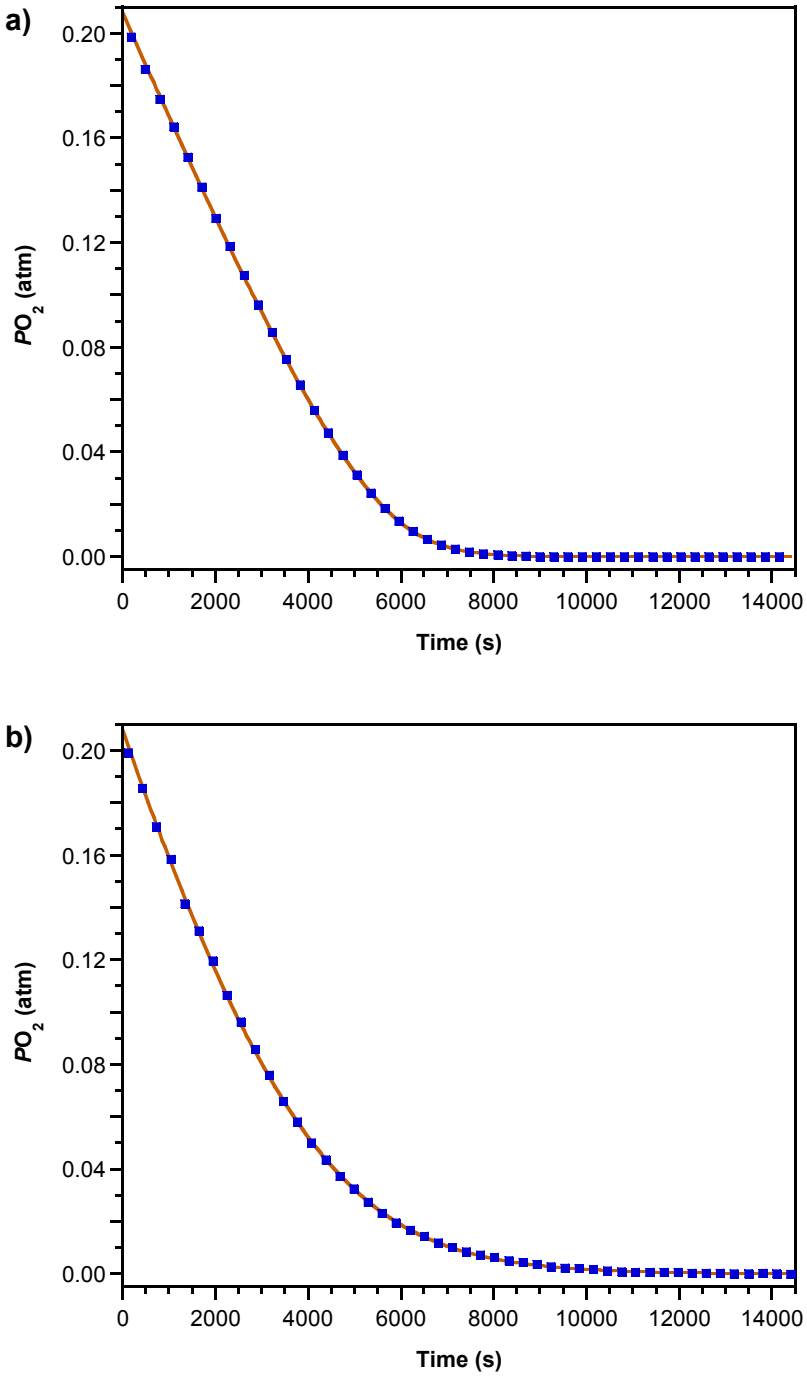

Figure 3. $[O_2]$ profiles for air-saturated DMSO sensitizer solutions during photooxygenation (a) $Ir(ppy)_2(cbz)$, (b) $[Ru(bpy)_3]Cl_2$, obtained from Eq. 14 (■), and Eq. 10 (solid line). Every 5th data point shown for clarity. λ_{ex} = 405 nm.

Table 2. Fitting Parameters for Ir(III) and Ru(II)/DMSO Photooxygenation Systems

Sensitizer	R^2	k_{obs} (atm s^{-1})	K_{sv} (atm^{-1})	I_0	base
$Ir(ppy)_2(cbz)$	0.999998	$4.600(1)x10^{-5}$	34.35(5)	2163.3(2)	-29.6(7)
$[Ru(bpy)_3]Cl_2$	0.999996	$8.457(19)x10^{-5}$	7.56(4)	90.80(2)	-4.0(3)

(Table 2). The Ru(II)/DMSO photooxygenation system displays an observed rate constants nearly a 2x greater than its Ir(III)/DMSO counterpart, clearly depicted in Figure 4 by plotting the corresponding $[O_2]_t$ data using the linearized form of the integrated rate law (Eq. 7) with the slope of the line representative of k_{obs}. Values of k_{obs} obtained from linear fits of the data plotted in Figure 4 are also nearly a factor of two different at 4.632 x 10^{-5} atm s^{-1} and 8.358 x 10^{-5} atm s^{-1} for Ir(III) and Ru(II) sensitizers respectively.

Despite sensitization of the same photooxygenaton reaction, differences in k_{obs} for the two systems are expected as k_{obs} is a composite term with contributions from both sensitizer and O_2 photophysics. A deconstruction of k_{obs} to its components suggests that the terms ϕ_{et} and β are the most likely sources for the differences in k_{obs} to arise, while the terms ϕ_{rxn}, ϕ_{isc}, and [DMSO] are constant for both photooxygenation systems. Although ϕ_{isc}, leading to the population of the triplet excited state, is taken to be unity for both the Ir(III) and the Ru(II) sensitizers, deactivation of their triplet excited states via interaction with O_2 is not. Luminescence lifetime data shows the $Ir(ppy)_2(cbz)$ to possesses a longer lived excited state than $[Ru(bpy)_3]Cl_2$. This difference in PL lifetime provides an increased probability for an excited state interaction of the sensitizer with O_2, increasing the magnitude of luminescence quenching, but does not necessarily increase

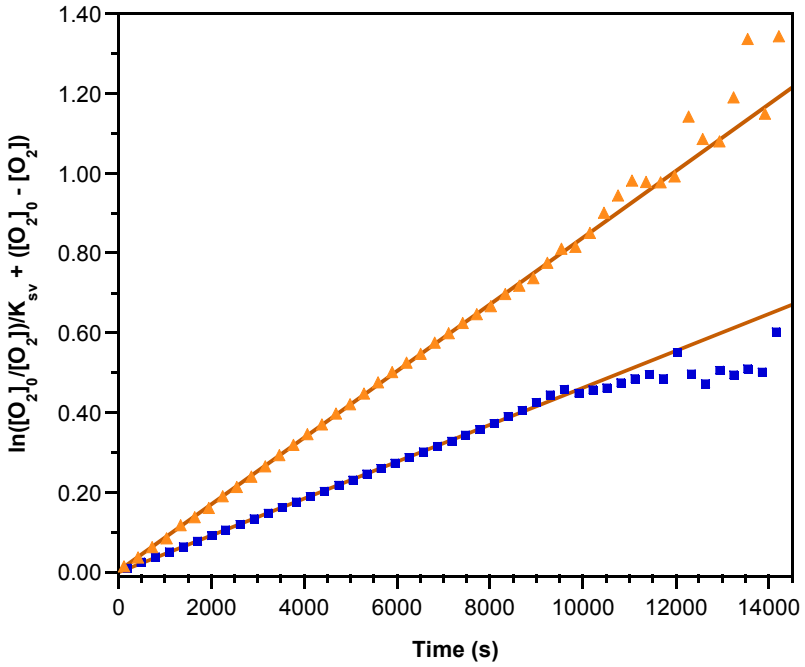

Figure 4. Linearized data for the luminescence recovery of air-saturated DMSO sensitizer solutions (■) $Ir(ppy)_2(cbz)$,(▲) $[Ru(bpy)_3]Cl_2$, including linear fits (solid line). Every 5th data point shown for clarity. λ_{ex} = 405 nm.

the quantum efficiency of $^1O_2$ production. The rate constant for $^1O_2$ decay (k_{1O2}) is found in the term β, a ratio of k_{1O2} to k_2. As both sensitizers may serve to deactivate the $^1O_2$ differently, dependence of k_{1O2} on sensitizer selection is also likely to contribute to differences in k_{obs}.

The values fit for the parameter K_{sv} are reflective of the disparity between the initial and final (I_0) PL intensities for the Ir(III) and Ru(II) sensitizers (Figure 1). Generation of a Stern-Volmer plot for the two sensitizers using the corrected PL intensities and the corresponding [O_2] data illustrates graphically the differences in [O_2] sensitivity between the two sensitizers with the slope of the line representative of K_{sv} (Figure 5). The values of K_{sv} obtained from the linear fit of the data plotted in Figure 5 are the same as those found in Table 2, and are based on 240 individual PL intensity ratios and [O_2] values. For comparison, photooxygenations were performed using the standard steady-state photolysis apparatus to irradiate the samples, which were then periodically removed from the setup to measure the increase in the luminescence lifetime as the [O_2] was depleted. A Stern-Volmer plot of the measured luminescence lifetimes and the corresponding values of [O_2] (obtained from fitting of the steady-state PL intensities) is shown in Figure 5. Values of K_{sv} were determined to be 38.93 atm^{-1} and 8.09 atm^{-1} for Ir(III) and Ru(II) sensitizers respectively. The two point (Table 1) and six point (lifetime data) K_{sv} determinations show good agreement with one another, while the 240 point determination obtained from the steady-state photolysis provides consistently lower values for K_{sv}. This is likely due to strong dependence of K_{sv} on the PL intensity values, which upon application of the "base" correction returns larger values of I and I_0 for the corrected PL intensities. This correction decreases the ratio of I_0/I and therefore

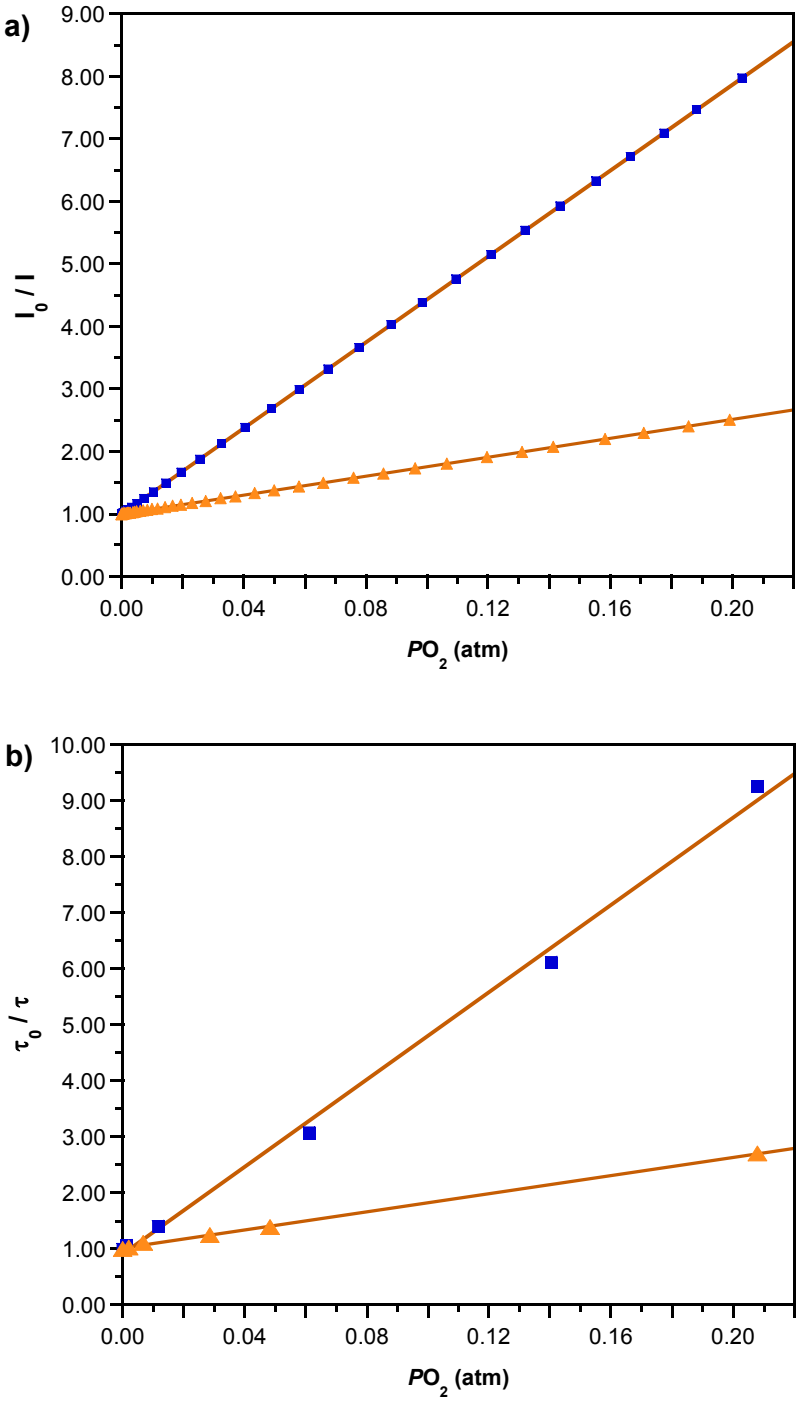

Figure 5. Stern-Volmer plots for air-saturated DMSO sensitizer solutions using (a) corrected PL intensity values, every 5th data point shown for clarity (b) luminescence lifetimes, (■) $Ir(ppy)_2(cbz)$, (▲) $[Ru(bpy)_3]Cl_2$, including linear fits (solid line). λ_{ex} = 405 nm.

the value of K_{sv}. Despite the strong dependence of K_{sv} on the value fit for "base" the rigorous 240 point determination is taken to be a more thorough determination over the two point and six point determinations.

Table 3. Contribution of Kinetic Terms for Ir(III) and Ru(II) Sensitizers

		$Ir(ppy)_2(cbz)$		$[Ru(bpy)_3]Cl_2$	
Time	% $[O_2]_0$	% linear	% ln	% linear	% ln
early	90	88	12	61	39
middle	50	85	15	53	47
late	1	62	38	25	75

Examination of the linear form of the integrated rate law (Eq. 7) shows a mixed-order kinetic term consisting of both a linear ($[O_2]_0 - [O_2]$) and a natural log ($\ln([O_2]_0 / [O_2]) / K_{sv}$) term. One may be tempted to simplify the kinetic model by treating the data at early or late times as either zero- or first-order using either the linear or natural log term respectively. Plotting the individual kinetic terms alongside the mixed-order kinetic term (their sum) versus time reveals the response of the individual kinetic terms over the course of a typical photooxygenation (Figure 6). Contributions of the linear and natural log terms to the mixed-order term vary over the course of the photooxygenation and are summarized in Table 3. It is clear from both Figure 6 and the contributions shown in Table 3 that a mixed-order term is needed to accurately describe the kinetics of the photooxygenation system as contribution to the mixed term from neither the linear, nor the ln term, is sufficiently large to allow for exclusion of the other. Simplification of the kinetic model results poor agreement with the model, leading to large errors in the parameters fit.

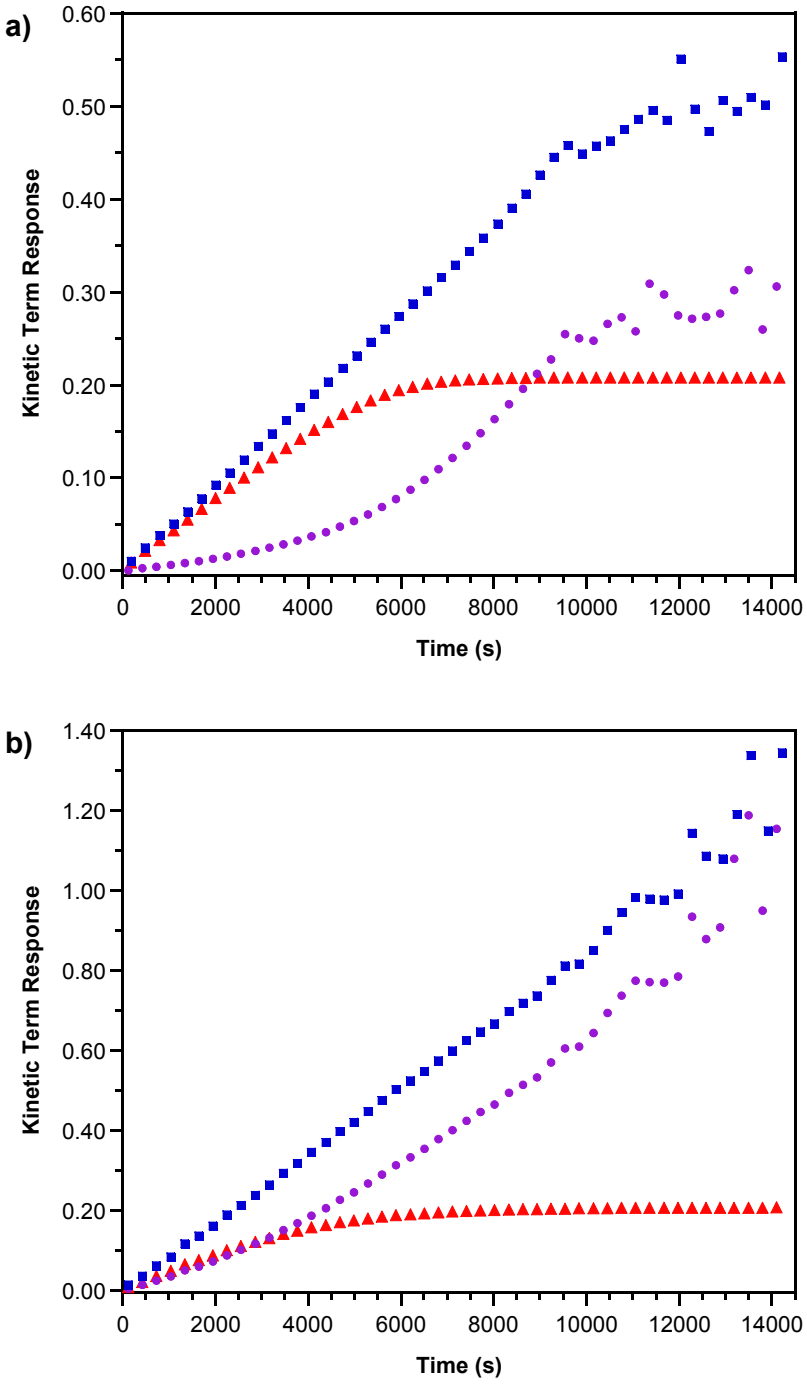

Figure 6. Profiles of kinetic terms for air-saturated DMSO sensitizer solutions during photooxygenation (a) $Ir(ppy)_2(cbz)$, (b) $[Ru(bpy)_3]Cl_2$, (■) mixed term, (▲) linear term, (●) ln term. Every 5th data point shown for clarity. λ_{ex} = 405 nm.

Determination of ϕ_{obs}. In order to determine the quantum efficiency observed (ϕ_{obs}), actinometry (Appendix C) was performed prior to collection of triplicate photooxygenation experiments using the Ir(III)/DMSO photooxygenation system. Each data set was fit to the kinetic model shown in Equation 13 using both 0.208 atm and 4.60 x 10^{-4} M values for $[O_2]_0$, with fitting parameters summarized in Table 4. Corresponding values of ϕ_{obs} were calculated using Equation 15 where V_{soln} is the volume of solution

Table 4. Fitting Parameters[a] and Determination or Quantum Efficiency for Ir(III)/DMSO Photooxygenation System

Run	R^2	k_{obs} (atm s^{-1})	K_{sv} (atm^{-1})	I_0	base	ϕ_{obs} (%)[b]
1	0.999997	3.959(1) x 10^{-5}	34.40(6)	1976.9(4)	-22.1(8)	4.17
2	0.999994	3.958(2) x 10^{-5}	35.97(8)	1980.8(5)	-26.4(10)	4.17
3	0.999995	4.016(2) x 10^{-5}	36.57(6)	1955.4(3)	-14.2(9)	4.17
Run	R^2	k_{obs} (M s^{-1})	K_{sv} (M^{-1})	I_0	base	ϕ_{obs} (%)
1	0.999997	8.756(2) x 10^{-8}	15528(19)	1976.9(4)	-22.4(6)	4.17
2	0.999994	8.754(3) x 10^{-8}	16267(26)	1980.0(5)	-26.3(8)	4.17
3	0.999995	8.882(3) x 10^{-8}	16539(24)	1955.4(3)	-14.2(8)	4.17

[a]Data were fit to Eq. 13 using both 0.208 atm and 4.60 x 10^{-4} M for initial values of O_2. [b]Average values calculated from six independent data collections (Appendix C). Values of k_{obs} varied with source intensity indicated while values of ~ 4.0% were consistently obtained for ϕ_{obs}.

irradiated and N hν / t is the moles of photons absorbed by the solution per unit time in seconds. The triplicate data collections were performed in direct succession of one

$$\Phi_{obs} = t \frac{k_{obs} V_{soln}}{N h\nu} \qquad (15)$$

another over the course of 12 hours and the values fit for both k_{obs} and K_{sv} are comparable across the three runs, and average values for k_{obs} (3.978(3) x 10^{-5} ± 0.8 % atm s^{-1}) and K_{sv} (35.65(12) ± 3 % atm^{-1}) have a variance less than 3 %. Quantum efficiencies of 4.0 % ± 4

% were consistently obtained for Ir(III)/DMSO photooxygenation system irradiated at 405 nm. The photooxygenation of sulfides is known to proceed rapidly in protic solvents with quantum efficiencies measured as high as 60% in ethanol:H_2O (95:5) mixtures.[33] Comparison of the large sulfide photooxygenation quantum efficiencies to the low values obtained for the DMSO photooxygenation system may account for its absence from discussion during the analysis of the DMS photooxygenation mechanism. The electron-rich DMS is a far better substrate for $^1O_2$ reactivity than the comparably electron-poor DMSO. Even when running the photooxygenation in neat DMSO quantum efficiencies are still quite low. Lifetimes of $^1O_2$ excited state are also shown to be strongly shortened when measured in DMSO,[34] which strongly deactivates the $^1O_2$ through bond-resonance energy transfer.

To demonstrate the scope of the method triplet-sensitized photooxygenation of model substrate TME (1.20×10^{-2} M) in MeOH upon irradiation of an air-saturated Ru(II) sensitizer solution was investigated using steady-state luminescence spectroscopy. This system has been thoroughly investigated by Demas et al. and the ϕ_{obs} reported to be 86 % (Standard Deviation of 2) for the photooxygenation of TME by irradiation of an O_2-saturated Ru(II) sensitizer solution in MeOH.[19] Changes in PL intensity with time were followed at the sensitizer determined PL maximum (λ_{em}) and a typical data collection is shown in Figure 7. Beginning from a fully quenched PL intensity (I_{air}), the air-saturated sensitizer solutions displayed a recovery in PL intensity, which ceased to change after all O_2 had been consumed by the photoreaction, as observed for the Ir(III) and Ru(II)/DMSO photooxygenation systems.

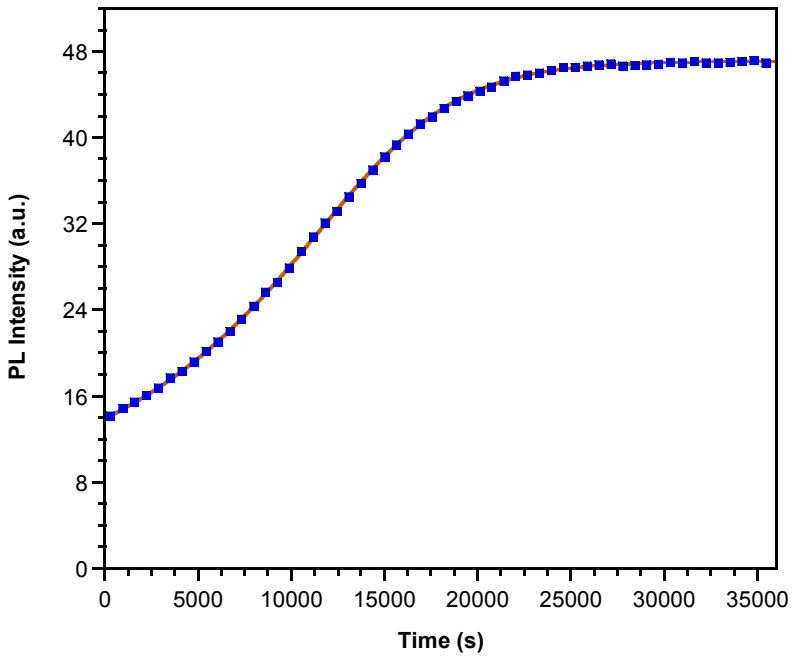

Figure 7. Luminescence recovery at 620 nm for $[Ru(bpy)_3]Cl_2$/TME/MeOH photooxygenation system, including data fit to Eq. 13 (solid line). Every 10th data point shown for clarity. λ_{ex} = 405 nm.

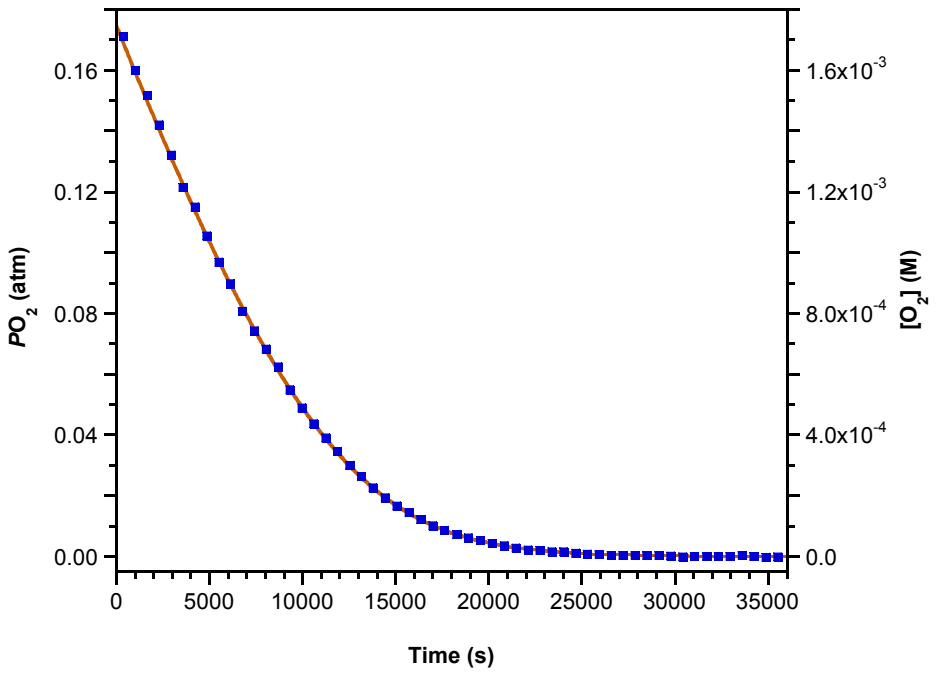

Figure 8. $[O_2]$ profile for $[Ru(bpy)_3]Cl_2$/TME/MeOH photooxygenation system, obtained from from Eq. 14 (■), Eq. 10 (solid line). Every 10th data point shown for clarity. λ_{ex} = 405 nm.

Data collection for the Ru(II)/TME/MeOH photooxygenation system were also performed in triplicate over the course of three days with actinometry conducted prior to data collection. Each data set was fit to the kinetic model shown in Equation 13 using both 0.175 atm and 1.69 x 10^{-3} M values for $[O_2]_{0,}$ parameters fit along with corresponding values for ϕ_{obs} are summarized in Table 5. A plot of the corresponding $[O_2]_t$ data is shown in Figure 8. Photooxygenations carried out using the Ru(II)/TME/MeOH and the Ru(II)/DMSO systems show very similar luminescent responses and provide excellent correlation to the kinetic model for both I_t and $[O_2]_t$ even with changes to the solvent and substrate. The values fit for both k_{obs} and K_{sv} are comparable across the three runs, and average values for k_{obs} (2.107(5) x 10^{-5} ± 4 % atm s^{-1}) and K_{sv} (13.46(9) ± 6 % atm^{-1}) have a variance less than 6 %. Quantum efficiencies of 14.0 % ± 1 % were consistently obtained for Ir(III)/DMSO photooxygenation system irradiated at 405 nm.

Table 5. Fitting Parameters[a] and Quantum Yield Determination for Ru(II)/TME/MeOH Photooxygenation System

Run	R^2	k_{obs} (atm s^{-1})	K_{sv} (atm^{-1})	I_0	base	ϕ_{obs} (%)
1	0.999994	2.187(2) x 10^{-5}	13.70(4)	47.12(1)	-0.01(6)	13.77
2	0.999983	2.113(4) x 10^{-5}	12.53(6)	50.63(2)	-26.4(10)	13.4
3	0.999996	2.021(2) x 10^{-5}	14.16(6)	147.65(2)[b]	-14.2(9)	13.50
Run	R^2	k_{obs} (M s^{-1})	K_{sv} (M^{-1})	I_0	base	ϕ_{obs} (%)
1	0.999994	2.115(2) x 10^{-7}	1416(4)	47.12(1)	0.002(51)	13.77
2	0.999983	2.046(4) x 10^{-7}	1292(6)	50.63(2)	-2.01(10)	13.84
3	0.999996	1.954(2) x 10^{-7}	1466(3)	147.65(2)[b]	1.08(12)	13.50

[a]Data were fit to Eq. 13 using both 0.175 atm and 1.69 x 10^{-3} M for initial values of O_2. [b]Higher intensity as result of increased spectrometer averaging not source intensity.

Adjusting the quantum efficiencies for the use of air-saturated rather than O_2-saturated solutions in determination of ϕ_{obs} increases the values by a factor of 4.8 and 5.7 to give ϕ'_{obs} = 19 and 78 % for the Ir(III)/DMSO and Ru(II)/TME/MeOH photooxygenation systems respectively. The adjusted value of ϕ'_{obs} = 78 % is then in good agreement with the value determined for the same photooxygenation system by Demas et al. monitored by O_2 uptake and shows extension of our analytical technique and analysis to additional photooxygenation systems. Although there are large differences in the solvent, sensitizer and the nature and concentration of the substrate, differences in the ϕ'_{obs} for the Ir(III)/DMSO and Ru(II)/TME/MeOH photooxygenation systems emphasize the differences in reactivity of DMSO and TME with $^1O_2$. A more accurate comparison would be to run a photooxygenation using Ru(II)/DMSO/MeOH system.

Conclusion. Photooxygenation of the common organic solvent DMSO upon reaction with $^1O_2$ results in the formation of the oxidized photoproduct $DMSO_2$. Identity of the photoproduct was confirmed through analysis of No-D ^1H NMR spectra collected before and after irradiation of O_2 sparged solutions of proteo-DMSO containing 1.74 x 10^{-3} M concentrations of triplet sensitizer. An increase of a sharp singlet at 2.95 ppm for the photooxygenated product represented the sole change observed in the ^1H NMR before and after irradiation, indicating the photoreaction was clean and free of side products. Significant conversions of the initial DMSO solution to the photooxygenated product were accomplished using the phosphorescent neutral Ir(III) bis-cyclometalate, $Ir(ppy)_2(cbz)$, and the nonphosphorescent organic chromophore, Methylene Blue, as triplet sensitizers. The triplet-sensitized photooxygenation showed no evidence for reaction in the absence of sensitizer, irradiation, or O_2.

In a sealed reaction vessel with no head space irradiation of air-saturated sensitizer solutions result in the depletion of O_2 from the solution as a result of the photooxygenation chemistry. For sensitizer solutions containing triplet sensitizer oxygen consumption is coupled with a luminescence increase as described by the Stern-Volmer relationship. Phosphorescent excited states can then be used to monitor O_2 consumption from the system through the observed luminescence recovery, serving as sensitizer for the generation of $^1O_2$, and luminescent probe for $[O_2]$. Based on these observations we have presented here a versatile, sensitive, and reproducible analytical technique to monitor the photooxygenation of various organic substrates in solution via steady-state luminescence spectroscopy.

The luminescence recovery was monitored for the irradiation of air-saturated DMSO sensitizer solutions containing phosphorescent $Ir(ppy)_2(cbz)$ and $[Ru(bpy)_3]Cl_2$ transition metal species. Experimental PL intensity versus time data were collected and fit to the kinetic model (Eq. 13) derived from the photooxygenation scheme shown in Scheme 1 with excellent correlation, giving validation to the model. Luminescent responses from the Ir(III) and Ru(II)/DMSO photooxygenation systems varied greatly from one another and showed a strong dependence on sensitizer photophysics. Extraction of $[O_2]$ versus time data may also be obtained through transformation of the corrected PL intensities using Eq. 10 and 11. A plot of $[O_2]$ versus time appears to show the decrease in $[O_2]$ to be linear at early times. Further analysis of the $[O_2]$ concentration data reveals that a mixed-order kinetic term is necessary for accurate description of the kinetic response.

Modeling of the photooxygenation chemistry was also extended to the previously investigated $[Ru(bpy)_3]Cl_2$/TME/MeOH combination of sensitizer/substrate/solvent. Corrections for the use of air-saturated rather than O_2-saturated sensitizer solutions in our investigation provided an observed quantum efficiency ϕ'_{obs} = 78 % which is in good agreement with value of 86 % reported previously for the same sensitizer/substrate/solvent combination. Determination of the observed quantum efficiency for the $Ir(ppy)_2(cbz)$/DMSO photooxygenation system was also carried out, giving a value for ϕ_{obs} = 4 %. Correction for differences in $[O_2]$ between air and pure O_2 gives an adjusted value of ϕ'_{obs} = 19 %. The large differences in the values of the observed quantum efficiencies are suggestive of the DMSO and TME substrate reactivity towards $^1O_2$ induced photooxygenation. Comparison of data sets which maintain use of a

consistent sensitizer, solvent, and source intensity, varying only the substrate and its concentration should provide meaningful information about the relative differences in substrate reactivity towards $^1O_2$ by comparison of k_{obs}. We feel analysis of triplet-sensitized photooxygenations with the steady-state luminescence technique presented here provides a powerful new methodology for investigation of these types of photoreactions.

─ Chapter Three ─

Effect of Axially Projected Oligothiophene Pendants and Nitro-Functionalized Diimine Ligands on the Lowest Excited State in Cationic Ir(III) bis-Cyclometalates.

Reprinted in part with permission from:
Schwartz, K. R.; Chitta, R.; Bohnsack, J. N.; Ceckanowicz, D. J.; Miró, P.; Cramer, C. J.; Mann, K. R. *Inorg. Chem.* **2012,** *51,* 5082.

Overview. The novel terthiophene (3T) oligomer **6** and a series of cationic Ir(III) bis-cyclometalates $[Ir(C^N)_2(N^N)]PF_6$ **9**–**12** were prepared. The synthesis, characterization, electrochemical, and photophysical properties are reported. The cyclometalating ligands (C^N) are 2–phenylpyridinato (ppy) or the 3T oligomer (3T–ppy), asymmetrically capped in the 5 and 5″ positions with the ppy and mesityl groups. The diimine ligands (N^N) are 2,2′–bipyridine (bpy) or 4–NO_2–bipyridine (4–NO_2–bpy). Hybrid metal-organic complexes **11** and **12** bear 3T–pendants ligated through the ppy cap, **10** and **12** contain NO_2 functionalized diimines, whereas **9** contains neither. Structural characterization of **10** by single crystal X-ray diffraction confirms the presence of the NO_2 substituent and pseudo-octahedral coordination geometry about the Ir(III) ion. Cyclic voltammetry highlights the large electron withdrawing effect of the NO_2 substituent, providing an 850 mV shift towards lower potentials for the first diimine centered reduction of **10** and **12**. Strong overlap of the intense $\pi \rightarrow \pi^*$ absorptions of the 3T–pendants with Ir(III) charge transfer bands is evident in complexes of **11** and **12**, precluding the possibility for selective excitation of either chromophore. Photoexcitation (λ_{ex} = 400 nm) of the series affords strong luminescence from the 3T oligomer **6** and the unsubstituted **9**, with ϕ_{em} = 0.11. In stark contrast the NO_2 and 3T functionalized complexes **10**–**12** display near total quenching of luminescence. Computations of the ground and excited-state electronic structure using density functional theory (DFT) and time-dependent density functional theory (TD-DFT) indicate that both the NO_2 and 3T substituents play an important role in excited-state deactivation of complexes **10**–**12**.

Introduction. Over the past several decades the properties of electro and photoredox active transition metal species have been extensively investigated. Most notable among this class of molecules are the Ru(II) polypyridyls, the most successful inorganic sensitizers for dye-sensitized solar cell (DSSC) applications.[1] The isostructural Ir(III) cyclometalates, have also found use in a variety of applications ranging from biolabelling agents[2] and oxygen sensors[3] to electron transfer arrays[4], photocatalytic hydrogen production[5], and light-harvesting materials.[6] Perhaps the true strength of Ir(III) cyclometalates is found as phosphorescent materials in organic light-emitting diodes (OLEDs) [6a, 7] and most recently for the fabrication of electroluminescent devices known as light-emitting electrochemical cells (LECs).[8]

The desirable photophysical properties of Ir(III) cyclometalates, such as high emission quantum yields, favorable excited-state lifetimes, photostability, and spectral tuning through ligand modification have been exploited for the fabrication of OLEDs as well as LECs.[4d, 7e, 9] LECs utilize ionic luminescent materials in the active layer, bringing charged transition metal species to the forefront. This is to the advantage of the field as the synthetic steps required to yield cationic Ir(III) bis-cyclometalates are relatively straightforward and isomer free compared their neutral tris-cyclometalated congeners.[2a, 4h, 7e, 9e, 9n, 10]

Taking into consideration the many favorable attributes of cationic Ir(III) bis-cyclometalates, their use in devices for light-to-energy or energy-to-light does not come without challenges, such as minimizing concentration-based quenching (triplet-triplet annihilation) and enhancing spectral coverage of these phosphorescent materials. These obstacles have been approached using several strategies. Aggregation can be discouraged

and charge transport enhanced by adjusting the amount of phosphorescent dopant found in the supportive hole transporting matrix[11] or by employing a single layer of a sterically encumbered phosphorescent material.[8a, 8g, 8h, 8j, 12] Previous work from others, as well as our own research lab, has been concerned with the synthesis, photophysical and electrochemical properties of various Ru(II) and Os(II) polypyridyls functionalized with oligothiophenes. These studies highlight the importance of organic chromophores in the construction of photoredox active dyads.[13] We expect enhanced spectral coverage to be provided by strongly absorbing oligothiophene chromophores and the possibility of hole transfer after selective hole generation at the metal chromophore, enhancing charge separation. With these considerations in mind we have designed a metal-organic hybrid motif consisting of a cationic Ir(III) bis-cyclometalate possessing axially projected steric bulk in the form of π–conjugated, hole transporting, photoredox active oligothiophene chromophores. The interplay of the metal and organic chromophores in the excited state makes this motif an interesting candidate for light-to-energy or energy-to-light devices. To our knowledge this is the first example of a cationic Ir(III) bis-cyclometalate to utilize axially projected photoredox active pendants in this manner.

Herein we present the synthesis, characterization, and studies of the photophysical and electrochemical properties of a series of cationic Ir(III) bis-cyclometalates of the type $[Ir(C^N)_2(N^N)]PF_6$ (C^N = cyclometalating ligand, N^N = diimine ligand) as shown in Figure 1. Two control complexes ($[Ir(ppy)_2(bpy)]PF_6$ (**9**) and $[Ir(ppy)_2(4–NO_2–bpy)]PF_6$ (**10**)) were synthesized to aid in understanding the photophysical and electrochemical properties of the series. These complexes provide a reference for the systematic introduction of the functionalized terthiophene (3T) pendants and electron withdrawing

NO_2 substituents found in complexes $[Ir(3T–ppy)_2(bpy)]PF_6$ (**11**) and $[Ir(3T–ppy)_2(4–NO_2–bpy)]PF_6$ (**12**) respectively. The 3T–pendants, selected for their well documented spectroscopic and electrochemical properties,[14] were functionalized with *n*–Bu chains and capped with mesityl groups to increase solubility and decrease aggregation. The 3T–pendants were placed *para* to the heteroatom of the pyridyl moiety to maximize axial projection (Figure 1); functionalization at this location has not been well studied for this class of compounds.[6a, 9k, 15] Finally, the NO_2 substituent in complexes **10** and **12** is predicted to lower the energy gap of the MLCT transition, acting as a trap for the lowest triplet excited state. This stabilization should also make reduction of the diimine facile and enhance charge separation.[4h, 7e, 9d, 9f, 9j, 9l, 9p, 16]

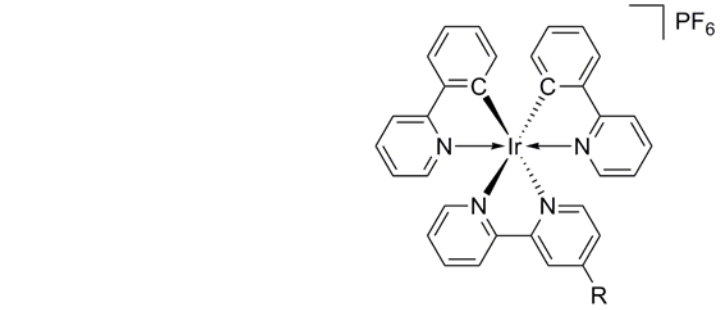

9 R = H [Ir(ppy)$_2$(bpy)]PF$_6$

10 R = NO_2 [Ir(ppy)$_2$(4-NO_2-bpy)]PF$_6$

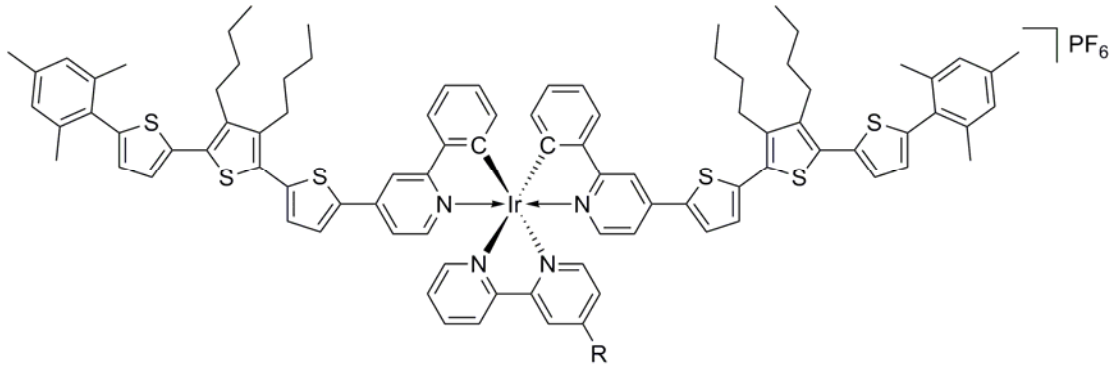

11 R = H [Ir(3T-ppy)$_2$(bpy)]PF$_6$

12 R = NO_2 [Ir(3T-ppy)(bpy)]PF$_6$

Figure 1. Molecular structures of cationic Ir(III) bis-cyclometalates. Control complexes **9**, **10**, and 3T**–** pendant complexes **11**, **12**.

Experimental Details.

Saftey Note. *CAUTION! Appropriate safety measures should be followed when using the organolithium and organostannane reagents described here due to their pyrophoric and toxic natures, respectively.*

General Considerations. NMR spectra were recorded on a Varian Unity or Varian Inova 300 MHz instrument. High-resolution mass spectrometry was performed on a Bruker BioTOF II mass spectrometer, Hewlett-Packard Series II Model 5890 gas chromatograph/Finnigan MAT 95 mass spectrometer, or Bruker Biflex III MALDI-TOF. All solvents and reagents used for synthetic procedures were purchased from commercially available sources and used without further purification. The following chemicals were used as provided: $IrCl_3 \cdot 3H_2O$ (Johnson Matthey), 2–phenylpyridine (Hppy) (Aldrich), 2,2′–bipyridine (bpy) (TCI Amercia), $NaPF_6$ (Aldrich).

Compounds 2,2′–bipyridine–N–oxide,[17] 4–nitro–2,2′–bipyridine–*N*–oxide,[18] and 3′,4′–dibutyl–2,2′:5′,2″–terthiophene (3′,4′–*n*–Bu–3T)[19] were synthesized according to the reported literature procedures. The cyclometalated Ir(III) dichloro-bridged dimers, $[Ir(ppy)_2(\mu\text{–}Cl)]_2$ (**7**) and $[Ir(3T\text{–}ppy)_2(\mu\text{–}Cl)]_2$ (**8**) were prepared using the method of Watts from $IrCl_3 \cdot 3H_2O$ in a mixture of 2–methoxyethanol and water with slight modification.[20] A series $Ir[(C^N)(N^N)]^+$ (**9–12**) complexes was prepared by cleavage of the corresponding dimers with an appropriate diimine ligand and subsequent metathesis to PF_6^- salts as previously described with slight modifications.[2a] Details for all procedural modifications are provided below.

4–Nitro–2,2′–bipyridine (1): Compound **1** was synthesized according to the literature procedure with slight modifications.[21] PCl_3 (16.1 mL, 25.3 g, 0.185 mol) was

added by syringe to a three neck round bottom flask containing 4–nitro–2,2′–bipyridine–*N*–oxide (1.0 g, 4.6 mmol) and the reaction mixture was refluxed (85 °C) under an inert gas atmosphere for 24 h. The reaction mixture was allowed to cool, then poured onto ice and stirred for 30 min. The reaction mixture was brought to a pH of ~11 through the dropwise addition of aq. NaOH, followed by extraction into $CHCl_3$. The organic extract was dried over Na_2SO_4 and evaporated to give **1** as a white solid. Yield: 97 %. ^{1}H NMR (300 MHz, CD_2Cl_2): δ 9.13 (dd, 1H, *J* = 2.4, 0.6 Hz), 8.95 (dd, 1H, *J* = 5.4, 0.6 Hz), 8.73 (ddd, 1H, *J* = 4.8, 1.8, 0.9 Hz), 8.48 (ddd, 1H, *J* = 7.8, 1.2, 0.9 Hz), 8.01 (dd, 1H, *J* = 5.1, 2.1 Hz), 7.89 (ddd, 1H, *J* = 7.8, 7.8, 1.8 Hz), 7.42 (ddd, 1H, *J* = 7.5, 4.5, 1.2 Hz).

4–Bromo–2–phenylpyridine (2): Compound **2** was synthesized according to the literature procedures with slight modifications.[22] A solution of 4–bromopyridine (10.0 g, 0.0516 mol) in dry THF (200 mL) was cooled to −78 °C to which a solution of phenylmagnesium chloride (2 M) in THF (65 mL) was added dropwise at −78 °C and allowed to stir for 15 min. Phenylchloroformate (8.00 mL, 10 g, 0.064 mol) in THF (20 mL) was then added dropwise over 10 min at −78 °C after which the reaction mixture was allowed to warm to r.t. The reaction mixture was cooled to 0 °C and quenched with 20 % NH_4Cl followed by stirring at 0 °C for 2 h and extraction into diethylether. The combined extracts were washed with H_2O, 20 % HCl and H_2O. The organic layer was dried over Na_2SO_4 and evaporated under vacuum to yield a pale yellow material. The residue was dissolved in dry toluene (200 mL) and *o*–chloronil (15.86 g, 0.06451 mol) dissolved in glacial acetic acid (120 mL) was added dropwise, the resultant red solution was stirred at r.t. for 36 h. The solution was made basic using aq. 10 % NaOH, filtered through Celite and washed with H_2O. The organic layer was extracted three times using

aq. 10 % HCl. The aqueous layers were made basic with NaOH and extracted with CH_2Cl_2. The combined organic layers were dried over Na_2SO_4 and the solvent was removed under vacuum to give the crude compound as a red oil. Purification of the crude compound by column chromatography (silica gel, hexanes:ethylacetate 98:2–95:5 v/v) yielded **2** as a pale yellow oil. Yield: 79 %. ^{1}H NMR (300 MHz, $CDCl_3$): δ 8.52 (d, 1H, *J* = 5.1 Hz), 7.99–7.96 (m, 2H), 7.91 (d, 1H, *J* = 1.8 Hz), 7.53–7.45 (m, 3H), 7.41 (dd, 1H, *J* = 5.4, 1.8 Hz).

5–Bromo–3′,4′–dibutyl–2,2′:5′,2″–terthiophene (3): Compound **3** was synthesized according to the literature procedure with slight modifications.[23] 3′,4′–*n*–Bu–3T (3.98 g, 0.0110 mol), was added to a round bottom flask and pumped/purged with Ar (3 times). DMF (25 mL) was added to the flask and the resulting solution purged for 15 min, then cooled to 0 °C. A solution of *N*–bromosuccinimide (1.96 g, 0.0111 mol) in DMF (6 mL) was then added dropwise over 45 min. The reaction mixture was stirred for 3 h at 0 °C, warmed to r.t. and allowed to stir an additional 21 h, followed by the addition of water (20 mL) and CH_2Cl_2 (15 mL). The resulting organic phase was separated and the aqueous phase extracted with CH_2Cl_2 (3 x 15 mL). The combined organic extracts were washed with H_2O (3 x 15 mL) and brine (1 x 20 mL), and then dried over $MgSO_4$. The solvent was removed via rotary evaporation to yield the crude product as a brown-yellow oil. The crude product was purified via column chromatography (silica gel, hexanes) to yield **3** as a yellow oil. Yield: 79 %. ^{1}H NMR (300 MHz, CD_2Cl_2): δ 7.35 (dd, 1H, *J* = 5.1 Hz, 1.2 Hz), 7.14 (dd, 1H, *J* = 3.6 Hz, 1.2 Hz), 7.08 (dd, 1H, *J* = 5.1 Hz, 3.6 Hz), 7.04 (d, 1H, *J* = 3.9 Hz), 6.90 (d, 1H, *J* = 3.9 Hz), 2.73–2.65 (m, 4H), 1.58–1.38 (m, 8H), 0.97–0.90 (m, 6H).

5–Mesityl–3′,4′–dibutyl–2,2′:5′,2″–terthiophene (4): 3 (2.50 g, 5.69 mmol), 2,4,6–trimethylphenyl boronic acid (1.12 g, 6.83 mmol), tetrakis(triphenylphosphine)palladium(0) (0.53 g, 0.46 mmol), and K_2CO_3 (2.36 g, 0.0171 mol) were added to a round bottom flask and pumped/purged with Ar (3x). A mixture of dimethoxyethane and H_2O (v/v, 35:11.6 mL) was degassed and added to the flask via cannulation. The reaction mixture was refluxed for 24 h then cooled to r.t., after which H_2O (20 mL) and hexanes (50 mL) were added. The resulting aqueous phase was extracted with hexanes (3 x 75 mL). The combined organic extracts were washed with water (3 x 100 mL), and then dried over Na_2SO_4. The solvent was removed via rotary evaporation to yield the crude product as a brown oily solid. The crude product was purified via column chromatography (alumina, hexanes) to yield **4** as a yellow oil. Yield: 82 %. ^{1}H NMR (300 MHz, CD_2Cl_2): δ 7.34 (dd, 1H, *J* = 5.4 Hz, 1.2 Hz), 7.16 (dd, 1H, *J* = 3.9 Hz, 1.2 Hz), 7.14 (d, 1H, *J* = 3.6 Hz), 7.08 (1H, dd, *J* = 5.4 Hz, 3.6 Hz), 6.95 (s, 2H), 6.76 (d, 1H, *J* = 3.6 Hz), 2.79–2.70 (m, 4H), 2.31 (s, 3H), 2.17 (s, 6H), 1.60–1.50 (m, 4H), 1.48–1.43 (m, 4H), 0.98–0.90 (m, 6H). HRMS (GC-MS EI) $[M\cdot]^+$: calcd for $C_{23}H_{34}S_3$ 478.1823, found 478.1790

5–((Tributyl)stannyl)–5″–mesityl–3′,4′–dibutyl–2,2′:5′,2″–terthiophene (5): 4 (2.10 g, 4.39 mmol) was added to an oven dried Schlenk flask and pumped/purged with Ar. THF (30 mL) was added and the solution was cooled to −78 °C with a dry ice/isopropanol bath. *n*–butyllithium (2.40 mL, 4.82 mmol) was added dropwise over 45 min, and the solution was stirred for an additional 30 min at −78 °C, followed by the addition of tributyltin chloride (1.50 mL, 5.27 mmol). The solution was warmed to r.t. and stirred for 1 h, followed by the addition of H_2O (10 mL) and hexanes (10 mL). The

resulting organic phase was separated and the aqueous phase extracted with hexanes (3 x 20 mL). The combined organic extracts were washed with H_2O (2 x 50 mL) and a saturated solution of aq. $NaHCO_3$ (2 x 50 mL), and then dried over $MgSO_4$. The solvent was removed via rotary evaporation to yield **5** as a yellow-brown oil Yield: 82 %. The material as isolated was considered a reaction intermediate that was pure enough for use without purification. ^{1}H NMR (300 MHz, CD_2Cl_2): δ 7.27 (d, 1H, *J* = 3.3 Hz), 7.13 (d, 2H, *J* = 3.6 Hz), 6.95 (s, 2H), 6.75 (d, 1H, *J* = 3.6 Hz) 2.78–2.71 (m, 4H), 2.31 (s, 3H), 2.17 (s, 6H), 1.63–1.30 (m, 20H), 1.17–1.11 (m, 6H), 1.0–0.90 (m, 15H).

4–(3′,4′–Dibutyl–5′′–mesityl–2,2′:5′,2′′–terthiophen–5–yl)–2–phenylpyridine (H3T–ppy, 6): 5 (1.08 g, 1.40 mmol), **2** (0.30 g, 1.3 mmol), and tetrakis(triphenylphosphine)palladium(0) (0.08 g, 0.07 mmol) were added to an oven dried Schlenk flask and pumped/purged with Ar. DMF (25 mL) was degassed and added to the flask via cannulation and the reaction mixture was heated to 100 °C for 48 h. The solution was cooled to r.t., transferred to a separatory funnel followed by the addition of H_2O (50 mL) and ethyl acetate (50 mL). The resulting organic phase was separated and the aqueous phase extracted with ethyl acetate (4 x 50 mL). The combined organic extracts were washed with water (4 x 100 mL) and a saturated solution of aq. $NaHCO_3$ (1 x 75 mL), and then dried over Na_2SO_4. The solvent was removed via rotary evaporation to yield the crude product as a red-brown oil. The crude material was purified via column chromatography (silica gel, CH_2Cl_2:hexanes 75:25 to 100 CH_2Cl_2) to yield **6** as a thick red oil. Yield: 78 %. ^{1}H NMR (300 MHz, CD_2Cl_2) δ 8.66 (dd, 1H, *J* = 5.4 Hz, 0.6 Hz), 8.07 (ddd, 1H, *J* = 5.7 Hz, 3.0 Hz, 1.5 Hz), 7.94 (dd, 1H, *J* = 1.8 Hz, 0.9 Hz): 7.59 (d, 1H, *J* = 3.9 Hz), 7.48 (m, 5H), 7.22 (d, 1H, *J* = 3.9 Hz), 7.17 (d, 1H, *J* = 3.6 Hz), 6.95 (s,

2H) 6.77 (d, 1H, *J* = 3.6 Hz) 2.82–2.74 (m, 4H), 2.31 (s, 3H), 2.17 (s, 6H), 1.61–1.42 (m, 8H), 1.00–0.94 (m, 6H). HRMS (ESI-TOF) $[M + H]^+$: calcd for $C_{40}H_{42}NS_3$ 632.2474, found 632.2464.

$[Ir(3T–ppy)_2Cl]_2$ (8): A solution of **6** (0.30 g, 0.48 mmol) in 2–methoxyethanol (15 mL) was added to a flask containing $IrCl_3 \cdot 3H_2O$ (0.08 g, 0.2 mmol) and H_2O (5 mL). The reaction mixture was allowed to reflux under an inert gas atmosphere for 24 h. After cooling to r.t. a red precipitate was collected by filtration. The reaction solid was dried by suction and dissolved off the frit with CH_2Cl_2 then concentrated by rotary evaporation. Precipitation was induced by addition of diethyl ether under a stream of N_2. The solid was filtered and washed with diethyl ether. Compound **8** was obtained as a brick red solid in a crude yield of 70 % and used without further purification. ^{1}H NMR (300 MHz, CD_2Cl_2): δ 9.28 (d, 4H, *J* = 6.3 Hz), 8.15 (s, 4H), 7.70 (d, 4H, *J* = 7.5 Hz), 7.59 (d, 4H, *J* = 3.9 Hz), 7.25 (d, 4H, *J* = 3.9 Hz), 7.14 (d, 4H, *J* = 3.6 Hz), 7.02 (dd, 4H, *J* = 6.3, 1.8 Hz), 6.94 (s, 8H), 6.89 (t, 4H, *J* = 7.5 Hz), 6.73 (d, 4H, *J* = 3.6 Hz) 6.68 (t, 4H, *J* = 7.5 Hz), 6.12 (d, 4H, *J* = 7.8 Hz), 2.71 (q, 16H, *J* = 7.2 Hz), 2.32 (s, 12H), 2.16 (s, 24H), 1.46 (m, 32H), 0.989 (t, 12H, *J* = 6.6 Hz), 0.910 (t, 12H, *J* = 7.2 Hz). MS (MALDI-TOF) $[M–C_{80}H_{80}Cl_2IrN_2S_6]^+$: calcd for $C_{80}H_{80}IrN_2S_6$ 1453.427, found 1453.427.

$[Ir(ppy)_2(bpy)]PF_6$ (9): $[Ir(ppy)_2Cl]_2$ (0.17 g, 0.16 mmol), and 2,2′–bipyridine (0.053 g, 0.34 mmol) were refluxed under an inert gas atmosphere in a 1:1 mixture of CH_2Cl_2:CH_3OH for 6 h. The reaction mixture was allowed to cool to r.t. and then concentrated by rotary evaporation. Diethyl ether was added to induce precipitation followed by filtration and washing with diethyl ether. Solid was then dissolved in CH_3OH. Addition of $NaPF_6$ (0.31 g) to the solution while stirring resulted in a bright

yellow precipitate that was filtered and washed with H_2O and diethyl ether then dried in vacuo giving compound **9** as a yellow solid. Yield: 92 %. ^{1}H NMR (300 MHz, CD_2Cl_2): δ 8.49 (d, 2H, *J* = 8.4 Hz), 8.13 (ddd, 2H, *J* = 7.5, 7.5, 1.5 Hz), 8.03 (ddd, 2H, *J* = 5.4, 1.5, 0.6 Hz), 7.97 (d, 2H, *J* = 7.8 Hz), 7.80 (dd, 2H, *J* = 7.5, 1.5 Hz), 7.76 (ddd, 2H, *J* = 9.0, 7.5, 0.9 Hz), 7.49 (ddd, 2H, *J* = 5.4, 1.5, 0.9 Hz), 7.46 (dd, 2H, *J* = 5.4, 1.2 Hz), 7.08 (ddd, 2H, *J* = 7.5, 7.5, 1.5 Hz) 6.93 (ddd, 2H, *J* = 7.5, 6.0, 1.5 Hz), 6.94 (ddd, 2H, *J* = 7.5, 7.5, 1.2 Hz), 6.31 (ddd, 2H, *J* = 7.5, 1.2, 0.6 Hz). HRMS (ESI-TOF) $[M]^+$: calcd for $C_{32}H_{24}IrN_4$ 657.1625, found 657.1638.

[Ir(ppy)$_2$(4–NO$_2$–bpy)]PF$_6$ (10): The synthesis of complex **10** was conducted in a manner similar to that of complex **9** with the exception of amounts used, $[Ir(ppy)_2Cl]_2$ (0.09 g, 0.09 mmol), and **1** (0.04 g, 0.2 mmol). Compound **10** was obtained as a brown-red solid. Yield: 79 %. ^{1}H NMR (300 MHz, CD_2Cl_2): δ 9.09 (d, 1H, *J* = 2.1 Hz), 8.61 (d, 1H, *J* = 8.4 Hz), 8.33 (d, 1H, *J* = 6.3 Hz), 8.21 (ddd, 1H, *J* = 8.1, 8.1, 1.8 Hz), 8.11 (dd, 1H, *J* = 5.7, 2.1 Hz), 8.08 (d, 1H, *J* = 5.4 Hz), 7.97 (d, 2H, *J* = 8.1 Hz), 7.81 (ddd, 2H, *J* = 7.5, 7.5, 1.5 Hz), 7.76 (d, 2H, *J* = 7.8 Hz) 7.58 (ddd, 1H, *J* = 7.8, 5.4, 1.2 Hz), 7.54 (d, 1H, *J* = 6.0 Hz), 7.47 (d, 1H, *J* = 5.4 Hz), 7.03 (m, 6H), 6.32 (d, 1H, *J* = 7.2 Hz), 6.45 (d, 1H, *J* = 7.8 Hz). HRMS (ESI-TOF) $[M]^+$: calcd for $C_{32}H_{23}IrN_5O_2$ 702.1476, found 702.1474.

[Ir(3T–ppy)$_2$(bpy)]PF$_6$ (11): $[Ir(3T–ppy)_2Cl]_2$ (0.15 g, 0.050 mmol), and 2,2′–bipyridine (0.02 g, 0.1 mmol) were refluxed under an inert gas atmosphere in a 2:1 mixture of CH_2Cl_2:CH_3OH for 6 h. The reaction mixture was allowed to cool to r.t. and the solvent was removed by rotary evaporation. The sticky residue was sonicated in diethyl ether to give a solid that was filtered and washed with diethyl ether. The solid was

dissolved in CH_3OH and filtered before the addition of $NaPF_6$ (0.12 g) to the stirred solution. Concentration of the solution resulted in a precipitate that was collected by filtration and washed with H_2O then dried in vacuo to give compound **11** as an orange-brown solid. Yield: 51 %. ^{1}H NMR (300 MHz, CD_2Cl_2): δ 8.52 (d, 2H, *J* = 8.1 Hz), 8.15 (ddd, 2H, *J* = 7.5, 7.5, 1.2 Hz), 8.08 (d, 4H, *J* = 6.0 Hz), 7.84 (d, 2H, *J* = 7.2 Hz), 7.62 (d, 2H, *J* = 3.9 Hz), 7.50 (t, 2H, *J* = 6.6 Hz), 7.44 (d, 2H, *J* = 6.3 Hz), 7.24 (d, 2H, *J* = 3.9 Hz), 7.17 (d, 2H, *J* = 3.6 Hz) 7.17 (d, 2H, *J* = 8.4 Hz), 7.12 (d, 2H, *J* = 8.4 Hz), 7.00 (ddd, 2H, *J* = 8.4, 8.4, 1.8 Hz), 6.95 (s, 4H), 6.78 (d, 2H, *J* = 3.6 Hz), 6.49 (d, 2H, *J* = 7.5 Hz), 2.78 (q, 8H, *J* = 8.4 Hz), 2.31 (s, 6H), 2.17 (s, 12H), 1.51 (m, 16H), 0.979 (t, 6H, *J* = 7.2 Hz), 0.937 (t, 6H, *J* = 7.2 Hz). HRMS (ESI-TOF) $[M]^+$: calcd for $C_{90}H_{88}IrN_4S_6$ 1609.4957, found 1609.4914.

$[Ir(3T–ppy)_2(4–NO_2–bpy)]PF_6$ (12): The synthesis of complex **12** was conducted in a manner similar to that of complex **11** with the exception of amounts used, $[Ir(3T–ppy)_2Cl]_2$ (0.09 g, 0.03 mmol), and **1** (0.01 g, 0.06 mmol). Compound **12** was obtained as an orange-brown solid. Yield: 51 %. ^{1}H NMR (300 MHz, CD_2Cl_2): δ 9.12 (d, 1H, *J* = 2.1 Hz), 8.64 (d, 1H, *J* = 8.1), 8.38 (d, 1H, *J* = 5.7 Hz), 8.23 (ddd, 1H, *J* = 8.1, 8.1, 1.5 Hz), 8.14 (ddd, 1H, *J* = 6.0, 6.0, 2.4 Hz), 8.09 (s, 4H), 7.86 (d, 2H, *J* = 6.9 Hz), 7.63 (d, 2H, *J* = 3.9 Hz), 7.60 (d, 1H, *J* = 6.3 Hz) 7.48 (d, 1H, *J* = 6.3 Hz) 7.41 (d, 1H, *J* = 6.3 Hz), 7.24 (dd, 2H, *J* = 4.8, 0.9 Hz), 7.17 (d, 2H, *J* = 3.6 Hz), 7.15(m, 3H), 7.03 (q, 2H, *J* = 6.6 Hz), 6.95 (s, 4H), 6.78 (d, 2H, *J* = 3.6 Hz), 6.50 (d, 1H, *J* = 7.2 Hz), 6.46 (d, 1H, *J* = 7.5 Hz) 2.79 (q, 8H, *J* = 8.4 Hz), 2.31 (s, 6H), 2.17 (s, 12H), 1.50 (m, 16H) 0.977 (t, 6H, *J* = 7.2 Hz), 0.936 (t, 6H, *J* = 7.2). HRMS (ESI-TOF) $[M]^+$: calcd for $C_{90}H_{87}IrN_5O_2S_6$ 1654.4808, found 1654.4813.

Electrochemical Measurements. Electrochemical experiments were performed with a BAS 100B electrochemical analyzer using a standard three electrode setup consisting of a glassy-carbon working electrode, a platinum auxiliary electrode, and a Ag/AgCl reference electrode containing 1.0 M KCl. Supporting electrolyte tetrabutylammonium hexafluorophosphate ($TBAPF_6$, Sigma-Aldrich) was recrystallized from ethanol, dried and stored in a desiccator prior to use. All compounds studied by electrochemical analysis were prepared as 0.5 mM solutions in acetonitrile, dried over an activated alumina column and deaerated, containing 0.1 M $TBAPF_6$. Potentials are reported vs. aqueous Ag/AgCl and are not corrected for the junction potential. The $E°'$ values for the ferrocenium/ferrocene couple for concentrations similar to those used in this study were +0.40 V for acetonitrile solutions at a glassy carbon electrode. A thorough description of the experimental setup and conditions used here has been described previously by our group.[24]

X–ray Structural Determination. The data for the structural determination were collected in the X–ray Crystallographic Lab in the LeClair-Dow Instrumentation Facility (Department of Chemistry, University of Minnesota). A single crystal of compound **10** was secured to a glass capillary and mounted on a Siemens SMART platform CCD diffractometer for a data collection at 173(2) K using a graphite monochromator and Mo Kα radiation (λ = 0.71073 Å). An initial set of cell constants was calculated from 51 reflections harvested from three sets of 20 frames such that orthogonal wedges of reciprocal space were surveyed. Final cell constants were determined from a minimum of 4023 strong reflections from the actual data collection. Data were collected to the extent of 1.5 hemispheres to a resolution of 0.77 Å. Four major sections of frames were

collected with 0.30º steps in ω. The intensity data were corrected for absorption and decay using *SADABS*.[25] The space group *Pnma* was determined based on systematic absences and intensity statistics. A direct-methods solution provided the positions of most nonhydrogen atoms. Full-matrix least squares/difference Fourier cycles were performed to locate the remaining nonhydrogen atoms. All nonhydrogen atoms were refined with anisotropic displacement parameters, and all hydrogen atoms were placed in ideal positions and refined as riding atoms with relative isotropic displacement parameters. All calculations were performed using the *SHELXTL* suite of programs.[26]

Optical Spectroscopy. Absorption spectra of the 3T oligomer and cationic Ir(III) bis-cyclometalates were collected for acetonitrile solutions using a 1.0 cm pathlength cell with a Cary 14 spectrophotometer running the *OLIS globalworks* software suite. Photoluminescence experiments were obtained using an excitation wavelength of 400 nm in acetonitrile using a front face geometry, with optical densities of solutions >2.0. Data was collected on a Spex Fluorolog 1680 0.2 m double spectrofluorimeter, equipped with a Hamamatsu R928 photomultiplier tube, running *Datamax* software. Solutions of the cationic Ir(III) bis-cyclometalates were deaerated for 15 minutes prior to collection using an argon purge. All spectra were corrected for the wavelength dependence of the detector. Luminescence quantum yields (ϕ_{em}) were measured relative to Coumarin 485 (C485) in acetonitrile solutions ($\phi_{em} = 0.28$), estimated uncertainties in ϕ_{em} measurements is ± 20 % or better.

Computational Details. All geometries were fully optimized using density functional theory (DFT) with the M06-L functional.[27] The 6-31G(d,p) basis set[28] was used for all nonmetal atoms and the Stuttgart/Dresden (SDD) basis set[29] relativistic

effective core potential was used for the Ir(III) metal centers. The *n*–Bu groups found in the 3′ and 4′ positions of the terthiophene pendants were replaced with hydrogen atoms for all computations. No symmetry restrictions were imposed while determining the fully optimized ground state geometries. Integral evaluation made use of the grid defined as ultrafine in the *Gaussian 09* program.[30] The nature of all stationary points was verified by analytic computation of vibrational frequencies.[31] Solvent effects for acetonitrile were modeled with SMD.[32] To obtain the vertical excitation energies of the three lowest singlet and triplet excited states of the studied complexes time-dependent DFT (TD-DFT)[33] calculations were performed using the M06-2X functional[34] at the M06-L optimized ground-state (S_0) geometry. Acetonitrile nonequlibrium solvatochromic effects were evaluated via a linear response formalism using SMD cavities.[33a]

Results and Discussion.

Synthesis of Ligands and Complexes. Synthesis of the 3T oligomer **6**, its corresponding Ir(III) complexes **11–12**, and the Ir(III) control complexes **9–10** are outlined in Scheme 1. The diimine ligand 4–nitro–2,2′–bipyridine (**1**)[21], precursor 4–bromo–2–phenylpyridine (**2**)[22] and 5–bromo–3′,4′–dibutyl–2,2′:5′,2″–terthiophene (**3**)[23] were synthesized with slight modifications to previously reported literature procedures. Compound **3** was reacted with mesitylboronic acid ((Mes)B(OH)$_2$) under Suzuki coupling conditions to obtain the monomesityl-capped terthiophene **4** in good yield (82 %). The monostannylated terthiophene **5** was prepared in quantitative yield by reaction of the monolithiated derivative of **4**, generated in situ, with tributyltin chloride. Compound **5** was then coupled to **2** using standard Stille coupling conditions to obtain the desired cyclometalating 3T oligomer **6** in good yield (78 %).

The desired series of complexes **9–12** were synthesized via conventional synthetic procedures for cationic Ir(III) bis-cyclometalates, with control complexes **9–10** (79–92 %), and the 3T–pendant complexes **11–12** (51 %), isolated in good to moderate yields. The μ–chloro–bridged dimers [Ir(C^N)$_2$(μ–Cl)]$_2$ **7** and **8**, were prepared using the method described by Watts et al., substituting 2–ethoxyethanol for 2–methoxyethanol.[20] Dimers **7** and **8** were cleaved with the appropriate diimine ligand in a 1:1 mixture of refluxing CH_2Cl_2/MeOH for **7** or 2:1 for **8** generating the monomeric [Ir(C^N)$_2$(N^N)]$^+$ species as Cl^- salts. These salts were subsequently metathesized by treatment with $NaPF_6$ to give PF_6^- as the counterion.[2a] Complexes **9–12** were characterized by ^{1}H NMR spectroscopy as well as HR–ESI mass spectrometry. Ir(III) complexes **9–12** display ^{1}H NMR spectra consistent with a C,C–*cis* / N,N–*trans* coordination mode for the

Scheme 1. Synthesis of 3T Oligomer and cationic Ir(III) bis-Cyclometalates

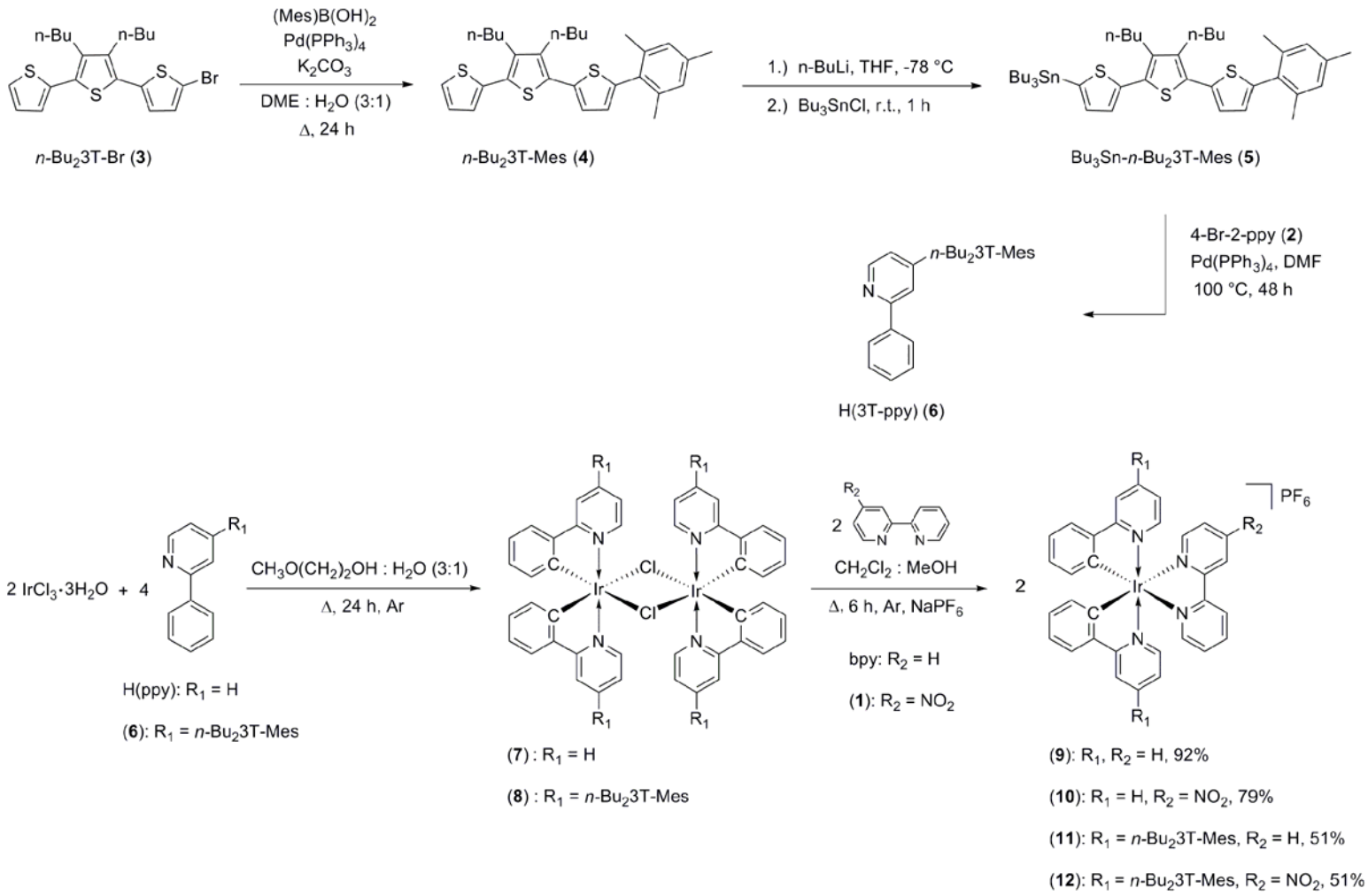

cyclometalating ligands. As expected for molecules of C_2 symmetry, **9** and **11** show a single resonance for each set of aromatic ^{1}H signals, 12 total for **9**, and 15 total for **11**. Complexes **10** and **12** display more complicated ^{1}H NMR spectra as introduction of the NO_2 substituent results in a loss of symmetry. The number of ^{1}H signals observed for the aromatic region is increased, 15 total for **10**, and 19 total for **12**. In the case of **10** further confirmation of structural assignment was provided by single crystal X–ray crystallography.

X–ray Crystallography. Single crystals of **10** were grown by slow evaporation from a CH_2Cl_2 solution. Relevant crystallographic data for **10** is shown in Table 1, a list of selected bond lengths and angles (experimental and calculated) can be found in Table 2. The structure obtained for **10** displays two ppy cyclometalating ligands in the C,C–*cis* / N,N–*trans* or "*mer* like" arrangement about a pseudo-octahedrally coordinated Ir(III) ion (Figure 2). The 4–NO_2–bpy diimine ligand occupies the remaining two coordination sites with both N atoms *trans* to the carbanions of the ppy ligands. Ir(III) ligand bond lengths for the diimine and cyclometalating ligands are in good agreement with distances found for similar $[Ir(C\hat{}N)_2(N\hat{}N)]^+$ species.[2b, 7e, 9p, 16b, 35] As is typically observed within cyclometalating ligands the Ir–C bonds (~2.02 Å) are slightly shorter than those of the Ir–N bonds (~2.04 Å), while the Ir–N bonds (~2.14 Å) to the diimine ligand are longer than those observed for the cyclometalating ligands (Table 1). Lengthening of the Ir–$N_{(N\hat{}N)}$ is regularly observed in these complexes due to the strong *trans*-influence of the cyclometalated carbanions.[2b, 7e, 9p, 16b, 35]

A search of the Cambridge Crystallographic Database (CSD)[36] finds only five transition metal complexes which contain a NO_2 functionalized bipyridine ligand,

Table 1. Crystallographic Data and Refinement Parameters for $[Ir(ppy)_2(4–NO_2–bpy)]PF_6$

empirical formula	$C_{32}\ H_{23}\ F_6\ Ir\ N_5\ O_2\ P$
crystal color, morphology	red–orange, plate
crystal system	Orthorhombic
space group	*Pnma*
a, Å	21.287(4)
b, Å	26.420(5)
c, Å	13.113(3)
α, deg	90
β, deg	90
γ, deg	90
Volume (*V*), $Å^3$	7375(2)
Z	8
formula weight, g mol^{-1}	731.76
density (calculated), g cm^{-3}	1.525
temperature, K	173(2)
absorption coefficient (*μ*), mm^{-1}	3.728
F(000)	3296
θ range, deg	1.54 to 27.51
index ranges	$-27 \le h \le 27$
	$-34 \le k \le 34$
	$-17 \le l \le 16$
reflections collected	75379
independent reflections	8645 [R_{int} = 0.1145]
weighting factors,[a] *a, b*	0.0493, 11.7270
max, min transmission	0.9126, 0.3316
data/restraints/parameters	8645/3/446
R_1, wR_2 [$I > 2\sigma(I)$]	0.0548, 0.1038
R_1, wR_2 (all data)	0.1095, 0.1181
GOF	1.052
largest diff. peak, hole e$Å^{-3}$	1.037, −0.788

[a] $w = [\sigma^2(F_o^2) + (aP)^2 + (bP)]^{-1}$, where $P = (F_o^2 + 2F_c^2)/3$.

with that of **10** representing the first Ir(III) species to be characterized crystallographically.[37] Surprisingly the presence of a NO_2 substituent on the diimine ligand appears to have no observable effect on the Ir1–N4 or the Ir1–C11 distances. The average N–O bond length found for atoms O1, O2 and N5 is 1.220(11) Å, which compares well with the average values attained from the CSD[36] (1.213(12) Å) and the DFT optimized ground state geometry (1.229 Å). The NO_2 substituent was nearly coplanar with the bpy ligand, with a small torsion angle of 10.6(4)°, as measured from the O2–N5–C25–C24 unit. A slight twist in the NO_2 substituent is commonly observed for transition metal complexes with NO_2 functionalized phenanthroline and bipyridine ligands in the coordination sphere.[37b, 38]

Table 2. Selected Bond Lengths and Angles for $[Ir(ppy)_2(4–NO_2–bpy)]PF_6$ (**10**)

	Bond Length (Å)			Bond Angle (°)	
Atoms	Experimental	Calculated	Atoms	Experimental	Calculated
Ir1 – N1	2.043(5)	2.087	N1 – Ir1 – C22	80.7(2)	79.8
Ir1 – N2	2.038(5)	2.089	N2 – Ir1 – C11	79.6(3)	79.7
Ir1 – N3	2.137(5)	2.217	N3 – Ir1 – N4	76.5(2)	74.2
Ir1 – N4	2.139(5)	2.209	O1 – N5 – O2	124.7(7)	125.1
Ir1 – C11	2.031(6)	2.018			
Ir1 – C22	2.013(7)	2.020			
N5 – O1	1.240(8)	1.229			
N5 – O2	1.199(8)	1.229			

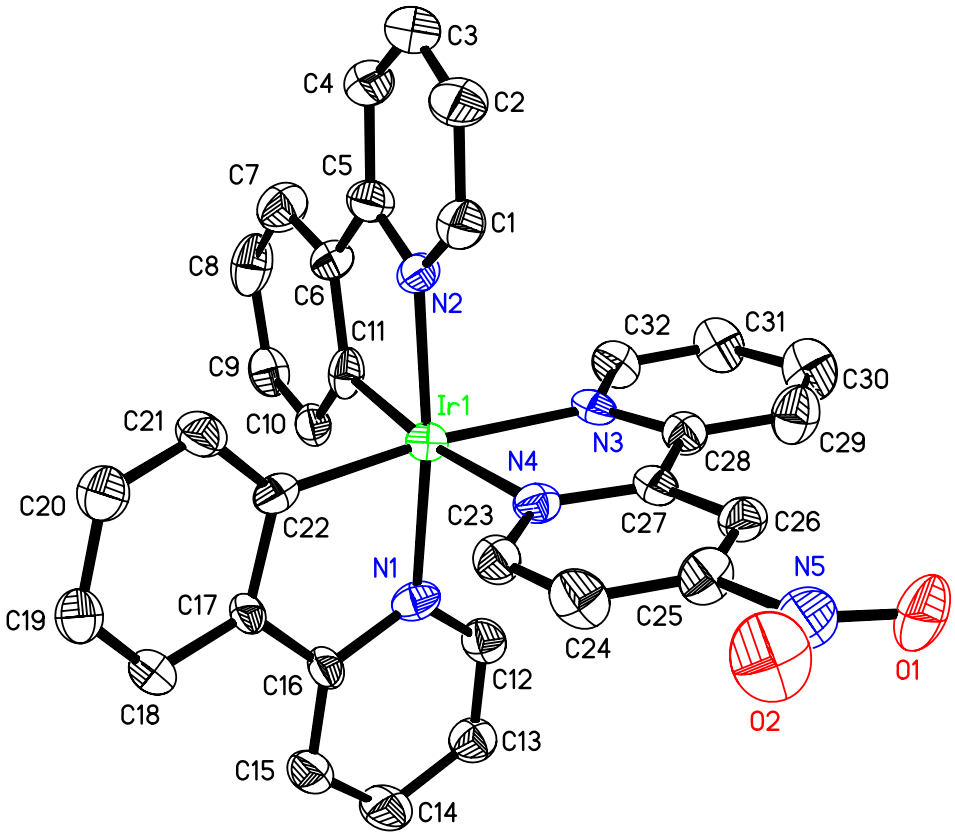

Figure 2. Thermal ellipsoid plot of $[Ir(ppy)_2(4–NO_2–bpy)]PF_6$ (**10**). Major component of disordered NO_2 substituent is shown. Hydrogen atoms, and PF_6^- counterion have been removed for clarity.

Frontier Orbital Analysis. Theoretical calculations were performed in support of experiment to assess the optimized ground state geometry and electronic structure of both the control (**9–10**) and 3T–pendant (**11–12**) complexes. Calculations at the DFT level of theory allowed for the investigation of the stepwise addition of 3T–pendants and NO_2 substituents. Contour plots representing the frontier orbitals for the series (**9–12**) can be found in Figure 3. Control complexes **9** and **10** exhibit electron density assigned to the HOMO localized over the Ir(III) ion and the phenyl ring of the cyclometalating ligands. The HOMO is virtually unchanged on addition of the NO_2 substituent. The LUMO is found to reside almost exclusively on the π–system of the diimine ligand (bpy/4–NO_2–bpy) in **9** and **10**, greatly stabilized by the NO_2 substituent.

Addition of 3T–pendants to complexes **11** and **12** does little to affect the energy or nature of the molecular orbital (MO) localized on the Ir(III)–$(Ph^{-}_{C\wedge N})_2$ moiety, assigned as the HOMO−2 in the 3T–pendant complexes (Figure 3). In both complexes **11** and **12** calculations show a higher lying pair of degenerate MOs representing the HOMO and HOMO−1 delocalized over the 3T π–system. The small contribution of electron density to the HOMO or HOMO−1 from the cyclometalating ligand cap indicates poor interaction between the 3T–pendant and the Ir(III) ion in the ground state.

Analysis of the lowest unoccupied orbitals for the series (**9–12**) shows a MO of similar composition localized on the diimine ligand. These MOs are assigned as the LUMO in **9** and the LUMO+2 in **11**, while the diimine based MOs on the NO_2 functionalized compounds are greatly stabilized, leading to their assignment as LUMO in both **10** and **12**. For the 3T–pendant complexes **11** and **12**, calculations show a pair of

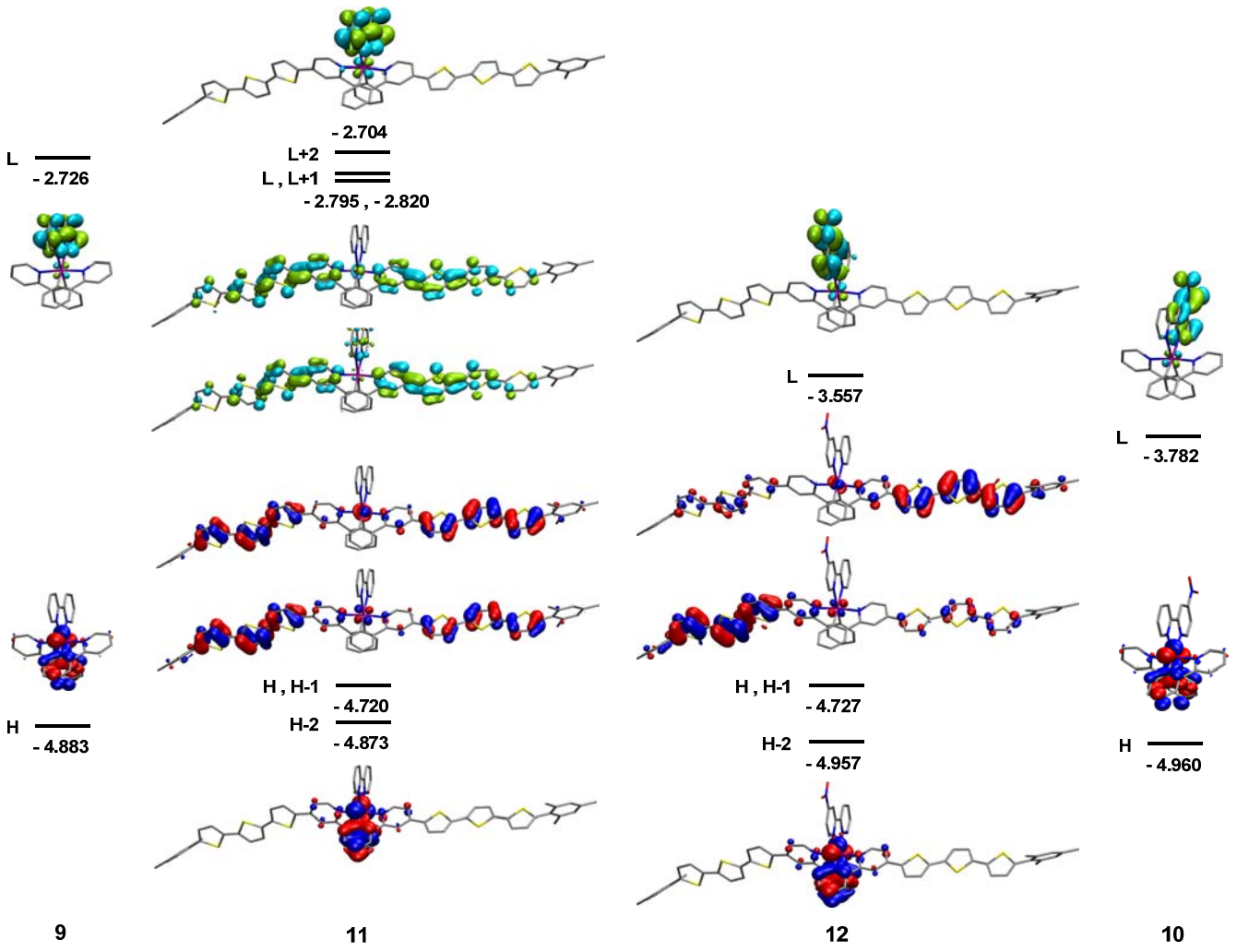

Figure 3. Contour plots of frontier orbitals (0.002 a.u.) for control complexes (**9–10**) and 3T–pendant complexes (**11**–**12**) in the ground state. Occupied orbitals are shown in blue/red, virtual orbitals are in cyan/green. Hydrogen atoms omitted for clarity.

nearly degenerate MOs delocalized over the 3T–pendant and pyridyl ring of each cyclometalating ligand. In the case of **11**, these orbitals (LUMO/LUMO+1) lie close in energy to the diimine based MO, while in complex **12** these orbitals (LUMO+1/LUMO+2) are significantly higher in energy (-2.833 eV, not shown) than the NO_2 stabilized diimine MO.

Table 3. Photophysical[a] and Electrochemical[b] Properties of 3T Oligomer (**6**) and Cationic Ir(III) Complexes (**9**–**12**)

				$E_{1/2(ox)}$, V		$E_{1/2(red)}$, V
Compound	λ_{abs}, nm	λ_{em}, nm[c]	ϕ_{em}[d]	Ir(IV)/Ir(III)[e]	$3T^{\cdot+}$/3T	bpy/$bpy^{\cdot-}$
6	252, 378	498	0.11	—	1.04	—
9	255, 265, 312, 344375, 415, 470	603	0.11	1.29	—	− 1.37
10	252, 266, 305, 381400, 530	599	0.005	1.35	—	− 0.52
11	263, 300, 421	579, 756	0.001	1.36	1.10	− 1.25
12	263, 308, 418	592	0.0003	1.38	1.10	− 0.40

[a]Spectra recorded in ACN solutions. [b]Potentials measured vs Ag/AgCl 1.0 M KCl at room temperature in dry degassed 0.1 M $TBAPF_6$ ACN solution, scan rate 100 mV/s. [c]Deaerated solutions at 298 K, λ_{ex} = 400 nm. [d]Determined relative to Coumarin 485 in ACN (ϕ_{em} = 0.28). [e]Redox couple also conatains significant contribution from the cyclometalating ligands.

Electrochemistry of the Control Complexes. The electrochemical properties of the cationic Ir(III) bis-cyclometalates (**9** − **12**) investigated here are in agreement with the DFT simulations discussed above. Results of the electrochemical investigation in acetonitrile (ACN) for control complexes **9** and **10** are given in Table 3 and Figure 4. Both complexes **9** and **10** displayed electrochemical behavior typical of $[Ir(C^N)_2(N^N)]^+$ type complexes.[4g, 7e, 8j, 9d, 9n, 10] Quasi-reversible single electron processes within the solvent window were observed for **9** and **10**, centered at 1.29 and

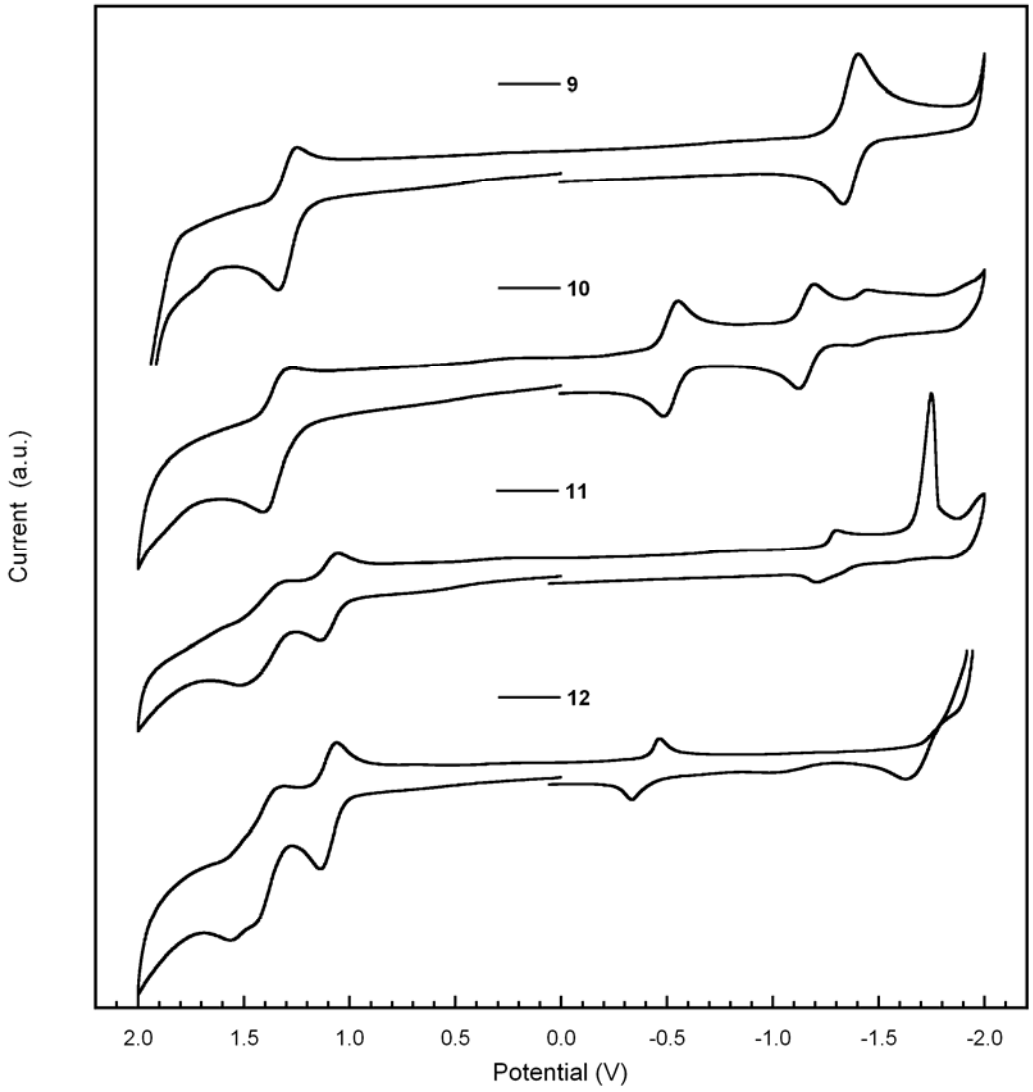

Figure 4. Cyclic voltammograms in ACN for control complexes **9**, **10** and 3T−pendant complexes **11**, **12**. Anodic currents are positive and plotted downward. Scan rate of 100 mV s^{-1}.

1.35 V respectively. Addition of the NO_2 substituent causes a nominal positive shift (60 mV) in the oxidation of **10** relative to **9**, consistent with the minimal disturbance in their HOMO energies, as predicted by DFT. A single reduction centered at −1.37 V for complex **9**, is replaced by two reductions for complex **10**, centered at −0.52 and −1.16 V. A third reduction at −1.42 V may be due to the successive reduction of the doubly reduced species. These reductive processes are assigned to ligand based reductions of the diimine ligand found in **9** and **10**.

The most notable difference between the electrochemistry of the control complexes is the large positive shift (850 mV) in the first reduction of **10** relative to **9**. Significant perturbation of the first reduction potential and LUMO energy of **10** clearly demonstrates the strong electron withdrawing character of the NO_2 substituent. A positive shift in the location of the first reductive process is well documented for similar complexes coordinating NO_2 substituted ligands, although the terminus of the electron has been a topic of debate.[9d, 39] Recent work to determine the reduction site of 4–NO_2–bpy (**1**) and its Pt(II) coordination complex Pt(4–NO_2–bpy)Cl_2 was conducted by Murray et al. with a combination of theoretical calculations, cyclic voltammetry, as well as UV/vis, NIR, and EPR spectroelectrochemistry.[40] Their results indicate that after electrochemical reduction or photoexcitation (MLCT, $d\pi_{Pt(II)} \rightarrow \pi^*_{N\text{^}N}$) the major component of electron density is localized on the NO_2 substituted pyridyl ring in both the bound and unbound ligand. We adopt their assignment for the first reduction in complex **10** as the one-electron reduction of the NO_2 substituted pyridyl ring of the coordinated 4–NO_2–bpy ligand. It is likely that the reduction at more negative potentials in **10** is the

addition of the second electron to the unsubstituted pyridyl ring, slightly stabilized by induction.

Electrochemistry of the 3T Oligomer and 3T–Pendant Complexes. The electrochemical properties of the 3T oligomer **6** and its corresponding Ir(III) complexes **11** and **12** were also examined in ACN by cyclic voltammetry (Table 3, Figure 4). No reductions were observed for the 3T oligomer within the solvent window, as expected for similar aryl capped terthiophene species,[14b, 14e, 14g] but the oligomer did exhibit rich oxidation chemistry, undergoing two reversible, and one quasi-reversible oxidation processes. The first 3T oligomer oxidation is centered at 1.04 V, and is assigned to the formation of the 3T radical cation.[13e, 14b, 14c, 14e, 14f] Further oxidation produces a dicationic species (1.39 V).

As observed for complexes **9** and **10**, each of the 3T–pendant complexes undergoes a quasi-reversible reduction located at −1.25 and −0.40 V respectively for **11** and **12**. Generation of more highly reduced species at more negative potentials during electrochemical experiments conducted with **11** and **12** gave evidence for precipitation on the electrode surface. These additional reductions were not assigned. A noteworthy similarity in the electrochemical data is the 850 mV positive shift observed for the first reduction of the diimine ligand in the NO_2 functionalized **10** and **12**, relative to complexes **9** and **11**. The similarity in the reduction chemistry of the 3T–pendant complexes is fully supported by computational results, which present diimine MOs nearly identical to those of the analogous control complexes.

The 3T–pendant complexes **11** and **12** revealed three oxidation processes rather than the single process observed for the control complexes **9** and **10** (Table 3). In the 3T–

pendant complexes the first quasi-reversible oxidation at 1.10 V is assigned to the isopotential one-electron oxidation of both 3T–pendants to form the respective 3T radical cations. This process is nearly unchanged in potential from the analogous process in the free 3T oligomer, suggesting the ground states of the 3T–pendant complexes and 3T oligomer are comparable. The second process at ~ 1.37 V is assigned to the oxidation of the Ir(III)–$(Ph^{-}_{C\wedge N})_2$ moiety, only slightly shifted from the values observed for the same process in control complexes (Table 3). The third oxidation process located at ~ 1.54 V is attributed to a second oxidation of the 3T–pendant to form the dicationic terthiophene species.[13e, 14b, 14e, 24] This process is not reversible on the CV time scale and occurs at potentials close to the second oxidation making it difficult to resolve electrochemically. Ordering of the first two oxidative processes are in accord with the composition of the HOMO/HOMO–1, and HOMO–2 predicted by DFT calculations.

Electronic Spectroscopy and Excited State Analysis. UV-vis absorption spectra collected in ACN for cationic Ir(III) bis-cyclometalates **9**–**12**, and the free 3T oligomer **6**, are shown in Figure 5. Corresponding photophysical and spectral data have been summarized in Table 3. To assist with the interpretation of excited state properties, TD-DFT calculations were performed for all molecules in the series (**9**–**12**) on their fully optimized ground-state geometries. An energy level diagram representing the three lowest singlet and triplet excited states of complexes **11** and **12** is shown in Figure 6 and a detailed assignment of states can be found in Table 4. The free 3T oligomer exhibits a relatively simple electronic spectrum with only two strongly absorbing features. The high energy band, located at 252 nm, is assigned to the $\pi \rightarrow \pi^*$ transition localized on the

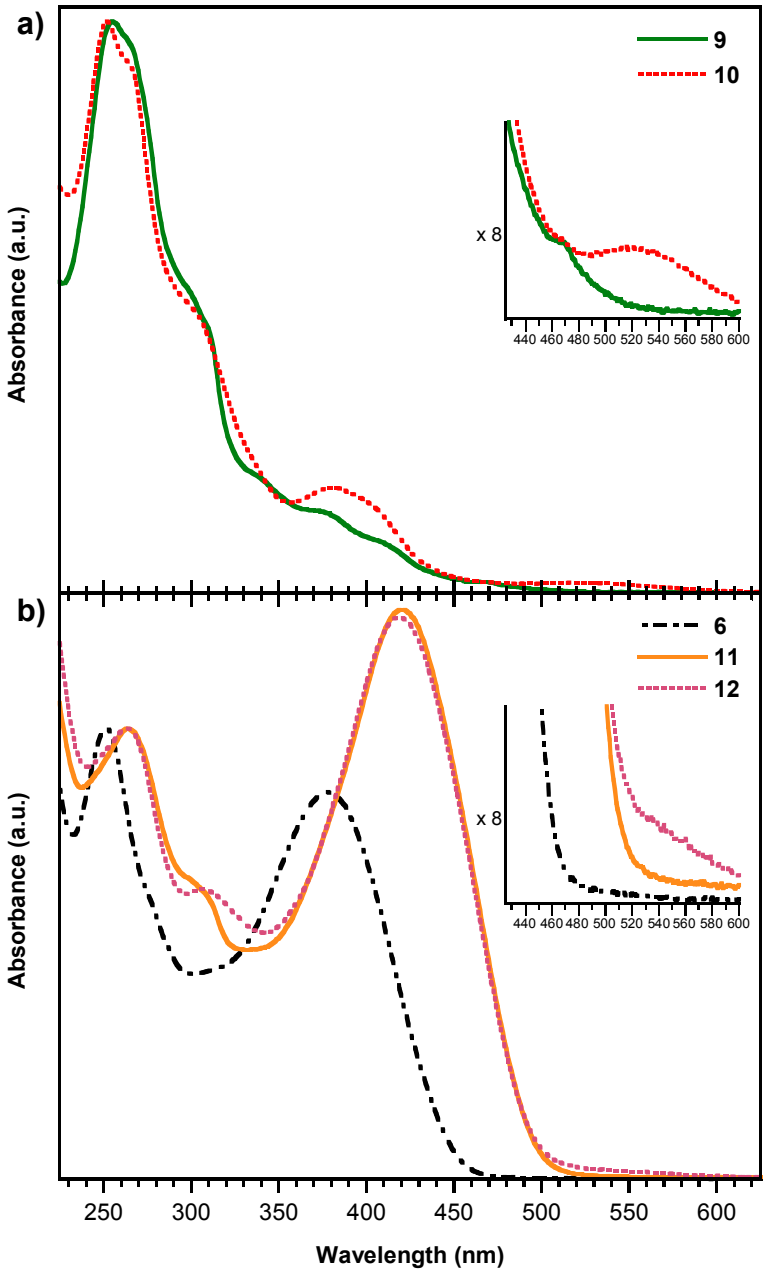

Figure 5. Normalized UV-vis absorption spectra in ACN solutions at room temperature of (a) control complexes **9** and **10**, (b) 3T oligomer **6** and 3T-pendant complexes **11** and **12**. Insets depict long wavelength absorbance of **10** and **12**.

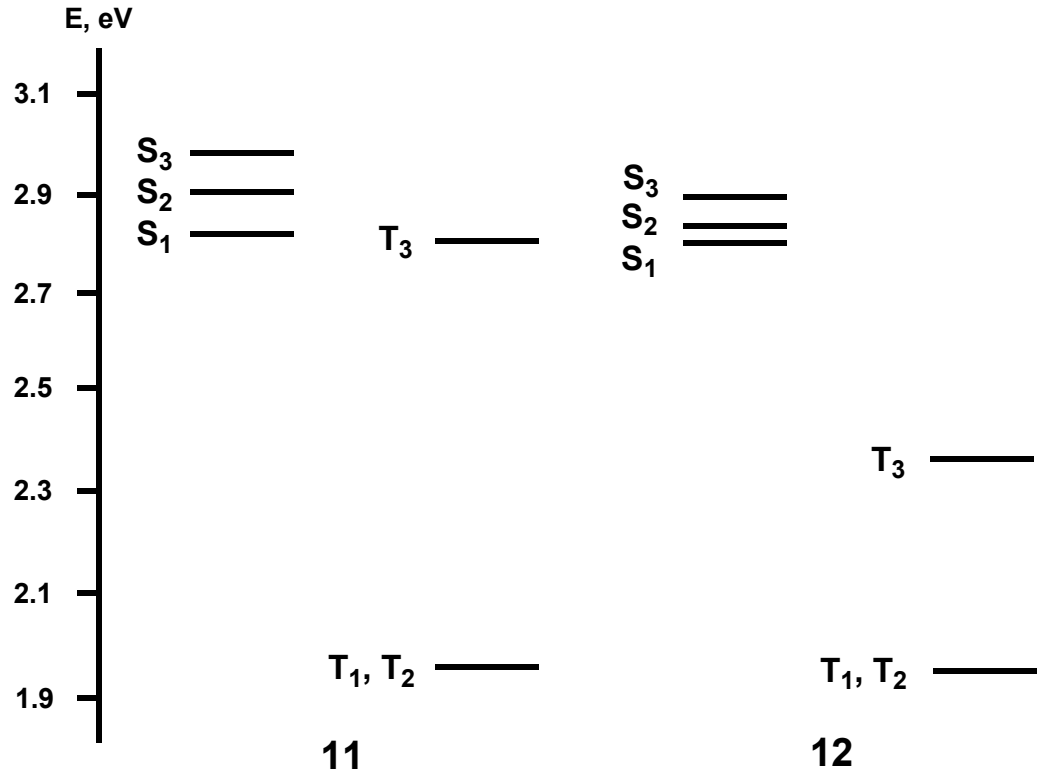

Figure 6. Energy level diagram for the lowest excited states in the 3T–pendant complexes **11** and **12**.

Table 4. TD-DFT Predicted Energies and Transitions for the Three Lowest Singlet and Triplet Excited States of 3T-Pendant Complexes **11** and **12**.

	State	E_{calcd} (eV)	λ_{calcd} (nm)	Excitation (%)	Character
11					
	S_3	2.93	423	HOMO–2 → LUMO (54)	π–π*/MLCT
	S_2	2.86	434	HOMO → LUMO+1 (48)	π–π*
				HOMO–1 → LUMO (47)	
	S_1	2.78	446	HOMO → LUMO (47)	π–π*
				HOMO–1 → LUMO+1 (46)	
	T_3	2.77	448	HOMO–3 → LUMO+1 (29)	π–π*/MLCT
				HOMO → LUMO+3 (27)	
	T_2	1.96	633	HOMO–1 → LUMO (39)	π–π*
				HOMO → LUMO (34)	
	T_1	1.96	633	HOMO → LUMO+1 (38)	π–π*
				HOMO–1 → LUMO+1 (35)	
12					
	S_3	2.85	435	HOMO–2 → LUMO (65)	MLCT/LLCT
	S_2	2.80	443	HOMO–1 → LUMO+2 (40)	π–π*
				HOMO → LUMO+1 (33)	
	S_1	2.77	448	HOMO → LUMO+1 (47)	π–π*
				HOMO–1 → LUMO+2 (40)	
	T_3	2.36	525	HOMO–39 → LUMO (57)[a]	π–π*
	T_2	1.95	636	HOMO–1 → LUMO+2 (53)	π–π*
	T_1	1.95	636	HOMO → LUMO+1 (53)	π–π*

[a] TD-DFT predicts a rather unusual transition from the MO HOMO–39 → LUMO, the transition is localized to the NO_2–bpy ligand.

ppy cap of **6**. The broad, intense absorption at lower energy (378 nm) is identified as the $\pi \rightarrow \pi^*$ transition characteristic of π–conjugated thiophene oligomers.

Control complexes **9** and **10** presented absorption spectra representative of comparable cationic Ir(III) bis-cyclometalates.[2a, 4h, 7e, 9b, 9e, 9n, 10a, 41] Vertical excitations to the lowest energy singlet state S_1 in the control complexes are described as a mixed ^{1}LLCT/^{1}MLCT transition by TD-DFT, computed to occur at 326 (**9**) and 388 (**10**) nm. Experiment shows intense absorption bands and shoulders present at high energy (320–350 nm), assigned to ^{1}LC transitions ($\pi \rightarrow \pi^*$) on the cyclometalating and diimine ligands. At lower energy a series of weak absorption shoulders (340–440 nm) followed by a set of very weak absorptions (450–470 nm) can be found. The bands located between 340–440 nm are assigned to ^{1}LLCT/^{1}MLCT transitions ($\pi_{ph}- \rightarrow \pi^*_{N\hat{}N}/d\pi_{Ir(III)} \rightarrow \pi^*_{N\hat{}N}$), while those found at wavelengths longer than 450 nm likely result from transitions to the corresponding triplet states. The exact ordering of these bands is not known for complexes **9** and **10**. The long wavelength absorption band centered at 530 nm for complex **10** is likely due to transitions terminating on the significantly stabilized MO of the NO_2 substituted diimine ligand (see inset Figure 5).

Interpretation of the electronic spectra for the 3T–pendant complexes **11** and **12** becomes increasingly more complicated than for either the 3T oligomer or the control complexes. Vertical excitations to the lowest energy singlet state S_1 in the 3T–pendant complexes are described as a $^1\pi \rightarrow \pi^*$ transition by TD-DFT. Calculated values for excitation of the S_1 state are 446 (**11**) and 448 (**12**) nm. Experimentally the ultraviolet region of complexes **11** and **12** display the same intense high energy absorptions as **9** and **10**, consistent with the ^{1}LC transitions ($\pi \rightarrow \pi^*$) on the cyclometalating and diimine

ligands. The remaining portions of the spectra are dominated by the characteristic $^1\pi \rightarrow \pi^*$ transition of the 3T–pendants, as observed in the 3T oligomer. The absorbance of this band is also increased (~ x1.5) due to the existence of two 3T–pendants within the same molecule. Presence of the NO_2 substituent on the diimine ligand of **12** yields a long wavelength absorption near 540 nm analogous to the band observed in **10**. The NO_2 substitution appears to have no effect on the overall position of the absorption bands corresponding to the 3T–pendants. The broad absorptions attributed to the 3T–pendants in complexes **11** and **12** overlap substantially with the position of the charge transfer bands observed in the control complexes. Observation and assignment of those bands expected to be present beneath the 3T–pendant absorptions would require additional experiments and data treatment beyond the scope of this study.

A noteworthy red shift (~ 40 nm) in the absorption of the 3T–pendants $^1\pi \rightarrow \pi^*$ transition is observed upon complexation of **6** to the Ir(III) ion in both **11** and **12**. Behavior such as this has been consistently observed for coordination of ligands functionalized with oligothiophene pendants to transition metal centers,[13h] rationalized as stabilization of the oligothiophene excited state resulting from increased conjugation with the aryl caps along with the metal cations inductive effect.[24b] We believe this reasoning can be applied as the likely cause of the red shift described here for complexes **11** and **12**.

Aside from complex **9**, whose luminescence has been previously reported,[2a, 9b, 9e, 9n, 10b, 41a, 41e] the remaining cationic Ir(III) bis-cyclometalates display extremely weak luminescence at room temperature. Quantum efficiencies obtained for the NO_2 and 3T functionalized compounds are 2–3 orders of magnitude smaller than that of control complex **9**. In the case of the 3T–pendant complexes accurate measurement of quantum

efficiencies or time dependent decay dynamics using our experimental configuration were not possible due to extremely low luminescence intensities.

The experimentally observed luminescence of control complexes **9** and **10** (Table 3, Figure 7) is described by TD-DFT as an excitation to the lowest triplet excited state T_1 with ^{3}LLCT/^{3}MLCT character, computed to arise at 381 (**9**) and 524 (**10**) nm. For the nonluminescent 3T–pendant complexes TD-DFT predicts excitations to the 3T centered T_1 and T_2 states (Figure 6), a degenerate pair of low lying triplet states, $^3\pi \rightarrow \pi^*$ in character. Calculations place the energy of these degenerate triplet states 1.96 eV above the ground. This value is in excellent agreement with the values measured and computed for the lowest triplet excited state of the unfunctionalized 3T oligomer, ranging from 1.76–1.92 eV.[42]

A partial decrease in emission intensity has been observed for Ir(III) complexes similar to **10** coordinating electron withdrawing diimine ligands bearing COOH or COOR substituents.[4h, 7e, 9p] In cases where the strong electron withdrawing NO_2 substituent is used, near total quenching of charge transfer phosphorescence is reported for Ru(II), Re(I), Pt(II), and Ir(III) species.[9d, 39a, 43] Strong involvement of the NO_2 substituent with the excited state and its vibrational modes are believed to be the major deactivation pathway of radiative decay in **10**.[39a] There is also evidence in NO_2 aromatics for excited-state deactivation due to structural reorganization, involving intramolecular twisting of the NO_2 substituent out of the aromatic ring plane.[44] The weak emission measured for **10** is in nearly the same location as that of control complex **9** (Table 3, Figure 7). Electrochemical measurements and analysis of absorption band energies for **10** suggest excitation of the ^{1}LLCT/^{1}MLCT state and subsequent decay from the

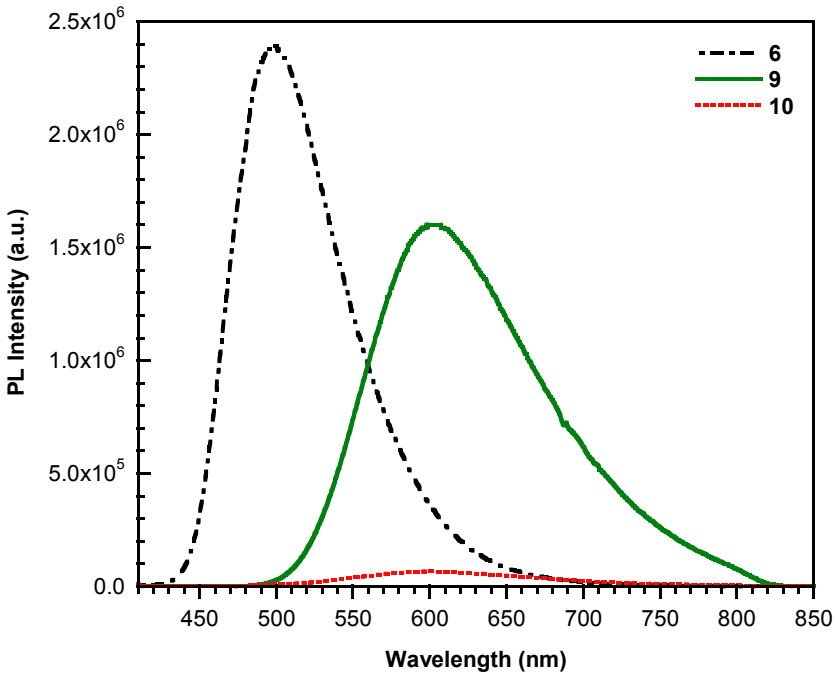

Figure 7. Luminescence spectra of 3T oligomer **6** and control complexes **9** and **10** in deaerated ACN solutions at 298 K. $\lambda_{ex} = 400$ nm.

^{3}LLCT/^{3}MLCT after rapid intersystem crossing to occur at much lower energies than observed. Considering the position and the extremely low quantum yield we cannot be certain of the origin of luminescence from **10**; for example, the luminescence may originate from an alternate triplet state on the diimine ligand. In any event, efficient deactivation of excitation energy likely occurs through a triplet state partially localized on the NO_2 substituent.

Discussion. Electrochemistry and DFT calculations for the first oxidation and reduction processes in complexes **9** and **10** correlate with the relative positioning of the HOMO and LUMO, respectively. From the electrochemical and theoretical results, it is reasonable to infer that the HOMO in complex **10** is relatively undisturbed by the NO_2 substituent. Conversely, the very large shift in the reduction potential and computed energy of the LUMO for **10** suggests significant stabilization of this MO, as has been previously reported.[9d, 39-40] These results emphasize the ability to independently modify the energy of HOMO and LUMO. Specific functionalization of the cyclometalating and diimine ligands then allows for the potential to create a low lying trap state for triplet energy.

Introduction of 3T–pendants into the system provides additional photoredox chromophores with MOs that may produce dramatic changes in the excited-state dynamics. Relative to both the control complexes and the 3T oligomer an overall positive shift for the oxidation of the 3T–pendants and the Ir(III)–$(Ph^{-}{}_{C\wedge N})_2$ moiety in complexes **11** and **12** is apparent, but minimal. The minimal disturbance in the oxidation potential of the 3T–pendants is indicative of minor electronic involvement between the 3T and Ir(III) chromophores in the ground state. Further evidence of the weak interaction is found in the contour plots of the HOMO/HOMO−1 for complexes **11** and **12**. This type of weak electronic coupling is commonly observed in metal-oligothiophene systems, attributed to decreased conjugation between the ligated aryl caps and their oligothiophene pendants.[24b, 45] This suggests that coordination of the ligand containing the 3T oligomer is unlikely to be a significant contributor to the changes in the electrochemical processes observed at positive potentials. Rather, this shift to positive potentials is likely a

consequence of the increased positive charge imparted on the complexes through sequential oxidation.

The 3T–pendants have a more pronounced effect on the excited states of complexes **11** and **12**. The absence of strong luminescence from the 3T–pendant complex **11** is striking as both the free 3T oligomer **6** and the control compound **9** display strong fluorescence and phosphorescence respectively, both with $\phi_{em} = 0.11$. For uncoordinated oligothiophene chromophores fluorescence from the initial photoexcited $^1\pi$–π^* state is observed, with intersystem crossing to the lowest energy nonemissive $^3\pi$–π^* state representing the major nonradiative pathway.[42a] It has also been shown that asymmetric capping of 3T oligomers in the 5 or 5″ position with electron withdrawing substituents enhances the rate of nonradiative decay (k_{nr}) in polar solvents by imparting a charge transfer character from the 3T–backbone to the polarized caps, deactivating fluorescence from the $^1\pi$–π^* state.[14d] In complex **11** the presence of a positively charged Ir(III) ion coordinated to the ppy cap of the 3T oligomer serves as electron withdrawing moiety in the excited state, as indicated by the significant contribution from the pyridyl ring of the cyclometalating ligands in the contour plot of the LUMO/LUMO+1.

On the basis of TD-DFT results and the disparity between the extinction coefficients of the 3T and Ir(III) chromophore, photoexcitation of the 3T–pendant complexes efficiently populates the 3T $^1\pi$–π^* state, although contributions of a charge-transfer character cannot be mutually excluded. We suggest that following photoexcitation, the $^1\pi$–π^* state rapidly undergoes intersystem crossing to the lowest energy excited triplet state facilitated by the strong spin-orbit coupling of the Ir(III) ion. TD-DFT finds the lowest energy excited state to be the 3T based $^3\pi$–π^* state, where the

excitation energy is left to decay nonradiatively.[8a, 46] Existence of the dark $^3\pi$–π^* states below the potentially emissive Ir(III) based triplet states found in the control complexes further supports deactivation of potential radiative decay pathways. This relative positioning of excited triplet states has been observed in other metal-oligothiophene systems, resulting in quenching of oligomer fluorescence and metal centered phosphorescence, supporting the quenching observed here.[13a, 13b, 13j, 46a]

The 3T/NO_2 functionalized compound **12** is similar to **11** and its photophysical behavior can be rationalized using the arguments outlined above for both complexes **10** and **11**. In summary, attempts to design a trap for the lowest triplet excited state through functionalization of the diimine ligand with a NO_2 substituent did not lower the energy of the diimine MO (Figure 7, T_3 for **12**) enough to shift the resulting ^{3}LLCT/^{3}MLCT state below the 3T $^3\pi$–π^* state. As a result it is no surprise that neither fluorescence nor phosphorescence is observed in the 3T–pendant complexes.

Conclusions. We have carried out electrochemical and photophysical investigations that include theoretical calculations on a series of cationic Ir(III) bis-cyclometalated complexes (**9**–**12**) incorporating 3T–pendants and the potent electron withdrawing NO_2 substituent. Differences arising from the systematic introduction of 3T–pendants and the NO_2 substituent are illustrated dramatically in the cyclic voltammetry experiments. The potentials for the one-electron oxidative processes of the 3T–pendants and the Ir(III)–$(Ph^{-}_{C\wedge N})_2$ moiety are unaffected by each other but the one-electron reductive process of the diimine ligand is greatly affected by addition of the NO_2 substituent. These trends are confirmed by DFT calculations that show almost no disturbance in the Ir(III)–$(Ph^{-}_{C\wedge N})_2$ based MO upon addition of 3T–pendants, while considerable stabilization of the diimine based MO is evident upon addition of a NO_2 substituent. Both electrochemical and DFT results suggest that the series should be capable of providing a low lying trap state localized on the NO_2 functionalized diimine ligand.

The excited-state properties of the series and the supportive TD-DFT calculations tell a different story. Examination of the absorption spectra of 3T–pendant complexes (**11** and **12**) shows complete overlap of the bands originating from both the metal and organic chromophores ruling out selective excitation. Aside from control complex **9** and the uncomplexed 3T oligomer **6**, NO_2 functionalized complex **10** is weakly luminescent and no luminescence is observed upon photoexcitation of 3T–pendant complexes at 400 nm in room temperature ACN solutions. TD-DFT calculations suggest that the absence of luminescence from the 3T–pendant complexes results because the lowest triplet excited

state is found on the 3T–pendants rather than on the diimine ligand, regardless of the NO_2 substituent.

The systems studied here have merit as potential light-harvesting materials that have been improved through the addition of the strongly absorbing 3T–pendants as secondary chromophores to increase spectral efficacy; however, further tuning of the system energetics will be necessary to direct the excitation energy to a triplet state capable of charge injection. This latter adjustment has proven somewhat difficult to achieve as cationic Ir(III) bis-cyclometalates have higher energy triplet excited states than their Ru(II) polypyridyl counterparts. The use of UV-absorbing pendant chromophores is then required to raise the triplet state energy of the pendant to prevent energy funneling into a noneffective lowest energy state. This strategy is not particularly beneficial for light-harvesting in the visible region, but use of longer wavelength absorbers such as the 3T oligomers used in this study may still provide worth in light-generating devices such as LECs.

─ Bibliography ─

Chapter One:

(1) (a) Farrer, N. J.; Salassa, L.; Sadler, P. J., *Dalton Trans.* **2009**, 10690. (b) Fukuzumi, S.; Ohkubo, K.; Zheng, X.; Chen, Y.; Pandey, R. K.; Zhan, R.; Kadish, K. M., *J. Phys. Chem. B* **2008,** *112*, 2738. (c) Gianferrara, T.; Bergamo, A.; Bratsos, I.; Milani, B.; Spagnul, C.; Sava, G.; Alessio, E., *J. Med. Chem.* **2010,** *53*, 4678. (d) Lai, C.-W.; Wang, Y.-H.; Lai, C.-H.; Yang, M.-J.; Chen, C.-Y.; Chou, P.-T.; Chan, C.-S.; Chi, Y.; Chen, Y.-C.; Hsiao, J.-K., *Small* **2008,** *4*, 218. (e) Liu, Y.; Hammitt, R.; Lutterman, D. A.; Joyce, L. E.; Thummel, R. P.; Turro, C., *Inorg. Chem.* **2009,** *48*, 375.

(2) (a) Goodrich, L. E.; Paulat, F.; Praneeth, V. K. K.; Lehnert, N., *Inorg. Chem.* **2010,** *49*, 6293. (b) Schopfer, M. P.; Wang, J.; Karlin, K. D., *Inorg. Chem.* **2010,** *49*, 6267. (c) Tonzetich, Z. J.; McQuade, L. E.; Lippard, S. J., *Inorg. Chem.* **2010,** *49*, 6338.

(3) (a) Fontaine, P. P.; Yonke, B. L.; Zavalij, P. Y.; Sita, L. R., *J. Am. Chem. Soc.* **2010,** *132*, 12273. (b) Fryzuk, M. D.; Johnson, S. A., *Coord. Chem. Rev.* **2000,** *200-202*, 379. (c) Gilbertson, J. D.; Szymczak, N. K.; Tyler, D. R., *J. Am. Chem. Soc.* **2005,** *127*, 10184. (d) Laplaza, C. E.; Cummins, C. C., *Science* **1995,** *268*, 861. (e) Lee, Y.; Mankad, N. P.; Peters, J. C., *Nature Chem.* **2010,** *2*, 558. (f) MacKay, B. A.; Fryzuk, M. D., *Chem. Rev.* **2004,** *104*, 385. (g) Pool, J. A.; Lobkovsky, E.; Chirik, P. J., *Nature* **2004,** *427*, 527. (h) Yandulov, D. V.; Schrock, R. R., *Science* **2003,** *301*, 76.

(4) (a) Blakemore, J. D.; Schley, N. D.; Balcells, D.; Hull, J. F.; Olack, G. W.; Incarvito, C. D.; Eisenstein, O.; Brudvig, G. W.; Crabtree, R. H., *J. Am. Chem. Soc.* **2010,** *132*, 16017. (b) Concepcion, J. J.; Jurss, J. W.; Templeton, J. L.; Meyer, T. J., *J. Am. Chem. Soc.* **2008,** *130*, 16462. (c) Gagliardi, C. J.; Westlake, B. C.; Kent, C. A.; Paul, J. J.; Papanikolas, J. M.; Meyer, T. J., *Coord. Chem. Rev.* **2010,** *254*, 2459. (d) McDaniel, N. D.; Coughlin, F. J.; Tinker, L. L.; Bernhard, S., *J. Am. Chem. Soc.* **2008,** *130*, 210. (e) Wasylenko, D. J.; Ganesamoorthy, C.; Koivisto, B. D.; Henderson, M. A.; Berlinguette, C. P., *Inorg. Chem.* **2010,** *49*, 2202. (f) Yin, Q.; Tan, J. M.; Besson, C.; Geletii, Y. V.; Musaev, D. G.; Kuznetsov, A. E.; Luo, Z.; Hardcastle, K. I.; Hill, C. L., *Science* **2010,** *328*, 342. (g) Zong, R.; Thummel, R. P., *J. Am. Chem. Soc.* **2005,** *127*, 12802.

(5) (a) Federsel, C.; Jackstell, R.; Beller, M., *Angew. Chem., Int. Ed.* **2010,** *49*, 6254. (b) Himeda, Y., *Eur. J. Inorg. Chem.* **2007,** *2007*, 3927. (c) Sadique, A. R.; Brennessel, W. W.; Holland, P. L., *Inorg. Chem.* **2008,** *47*, 784. (d) Silvia, J. S.; Cummins, C. C., *J. Am. Chem. Soc.* **2010,** *132*, 2169. (e) van der Boom, M. E., *Angew. Chem., Int. Ed.* **2009,** *48*, 28.

(6) (a) Chen, B.; Ma, S.; Hurtado, E. J.; Lobkovsky, E. B.; Zhou, H.-C., *Inorg. Chem.* **2007,** *46*, 8490. (b) Demessence, A.; D'Alessandro, D. M.; Foo, M. L.; Long, J. R., *J. Am. Chem. Soc.* **2009,** *131*, 8784. (c) Keskin, S.; van Heest, T. M.; Sholl, D. S., *ChemSusChem* **2010,** *3*, 879. (d) Millward, A. R.; Yaghi, O. M., *J. Am. Chem. Soc.*

2005, *127*, 17998. (e) Phan, A.; Doonan, C. J.; Uribe-Romo, F. J.; Knobler, C. B.; O'Keeffe, M.; Yaghi, O. M., *Acc. Chem. Res.* **2009,** *43*, 58.

(7) (a) Amao, Y.; Nakamura, N., *Sens. Actuators, B* **2004,** *100*, 347. (b) Amao, Y.; Nakamura, N., *Sens. Actuators, B* **2005,** *107*, 861. (c) Darwish, T. A.; Evans, R. A.; James, M.; Malic, N.; Triani, G.; Hanley, T. L., *J. Am. Chem. Soc.* **2010,** *132*, 10748. (d) DeGrandpre, M. D., *Anal. Chem.* **1993,** *65*, 331. (e) Fernández-Sánchez, J. F.; Cannas, R.; Spichiger, S.; Steiger, R.; Spichiger-Keller, U. E., *Sens. Actuators, B* **2007,** *128*, 145. (f) Mills, A.; Lepre, A.; Wild, L., *Sens. Actuators, B* **1997,** *39*, 419. (g) Mills, A.; Skinner, G. A., *Analyst* **2010,** *135*, 1912. (h) Nakamura, N.; Amao, Y., *Anal. Bioanal. Chem.* **2003,** *376*, 642.

(8) (a) Ali, R.; Lang, T.; Saleh, S. M.; Meier, R. J.; Wolfbeis, O. S., *Anal. Chem.* **2011,** *83*, 2846. (b) Borisov, S. M.; Krause, C.; Arain, S.; Wolfbeis, O. S., *Adv. Mater.* **2006,** *18*, 1511. (c) Burke, C. S.; Markey, A.; Nooney, R. I.; Byrne, P.; McDonagh, C., *Sens. Actuators, B* **2006,** *119*, 288. (d) Cajlakovic, M.; Bizzarri, A.; Ribitsch, V., *Anal. Chim. Acta* **2006,** *573-574*, 57. (e) Ertekin, K.; Alp, S., *Sens. Actuators, B* **2006,** *115*, 672. (f) Liu, Y.; Tang, Y.; Barashkov, N. N.; Irgibaeva, I. S.; Lam, J. W. Y.; Hu, R.; Birimzhanova, D.; Yu, Y.; Tang, B. Z., *J. Am. Chem. Soc.* **2010,** *132*, 13951. (g) Nakamura, N.; Amao, Y., *Sens. Actuators, B* **2003,** *92*, 98. (h) Oter, O.; Ertekin, K.; Topkaya, D.; Alp, S., *Anal. Bioanal. Chem.* **2006,** *386*, 1225. (i) Stich, M. I. J.; Fischer, L. H.; Wolfbeis, O. S., *Chem. Soc. Rev.* **2010,** *39*, 3102.

(9) (a) Hampe, E. M.; Rudkevich, D. M., *Tetrahedron* **2003,** *59*, 9619. (b) Herman, P.; Murtaza, Z.; Lakowicz, J. R., *Anal. Biochem.* **1999,** *272*, 87. (c) Masuda, K.; Ito, Y.; Horiguchi, M.; Fujita, H., *Tetrahedron* **2005,** *61*, 213.

(10) (a) Charbonniere, L. J.; Ziessel, R. F.; Sams, C. A.; Harriman, A., *Inorg. Chem.* **2003,** *42*, 3466. (b) de Silva, A. P.; Gunaratne, H. Q. N.; Gunnlaugsson, T.; Huxley, A. J. M.; McCoy, C. P.; Rademacher, J. T.; Rice, T. E., *Chem. Rev* **1997,** *97*, 1515. (c) de Silva, A. P.; Gunaratne, H. Q. N.; McCoy, C. P., *Chem. Commun.* **1996**, 2399. (d) de Silva, S. A.; Zavaleta, A.; Baron, D. E.; Allam, O.; Isidor, E. V.; Kashimura, N.; Percarpio, J. M., *Tetrahedron Lett.* **1997,** *38*, 2237. (e) Wong, K. H.; Chan, M. C. W.; Che, C. M., *Chem.-Eur. J.* **1999,** *5*, 2845.

(11) (a) Bottomley, F., *Q. Rev. Chem. Soc.* **1970,** *24*, 617. (b) Dilworth, J. R., *Coord. Chem. Rev.* **1976,** *21*, 29. (c) Heaton, B. T.; Jacob, C.; Page, P., *Coord. Chem. Rev.* **1996,** *154*, 193.

(12) Sprouse, S.; King, K. A.; Spellane, P. J.; Watts, R. J., *J. Am. Chem. Soc.* **1984,** *106*, 6647.

(13) (a) McGee, K. A.; Mann, K. R., *Inorg. Chem.* **2007,** *46*, 7800. (b) Schmid, B.; Garces, F. O.; Watts, R. J., *Inorg. Chem.* **1994,** *33*, 9.

(14) (a) Blessing, R. H., *Acta Crystallogr., Sect. A* **1995,** *51*, 33. (b) Sheldrick, G. *SADABS*, v.2.03; Bruker AXS: Madison, WI, 2002.

(15) *SHELXTL*, v.6.1; Bruker AXS: Madison, WI, 2001.

(16) King, K. A.; Spellane, P. J.; Watts, R. J., *J. Am. Chem. Soc.* **1985,** *107*, 1431.

(17) McGee, K. A.; Veltkamp, D. J.; Marquardt, B. J.; Mann, K. R., *J. Am. Chem. Soc.* **2007,** *129*, 15092.

(18) Nazeeruddin, M. K.; Humphry-Baker, R.; Berner, D.; Rivier, S.; Zuppiroli, L.; Graetzel, M., *J. Am. Chem. Soc.* **2003,** *125*, 8790.

(19) Chin, C. S.; Eum, M.-S.; yi Kim, S.; Kim, C.; Kang, S. K., *Eur. J. Inorg. Chem.* **2007,** *2007*, 372.

(20) Appearance of a new resonance for the released hydrazino ligand is not observed due to rapid exchange with residual H_2O in DMSO-d_6.

(21) Seino, H.; Saito, A.; Kajitani, H.; Mizobe, Y., *Organometallics* **2008,** *27*, 1275.

(22) Allen, F. H., *Acta. Crystallogr., Sect. B.* **2002,** *58*, 380.

(22) Schmidt, E. W. *Hydrazine and Its Derivatives: Preperation, Properties, Applications;* John Wiley & Sons: New York, 1984.

(24) Bergs, R.; Suenkel, K.; Robl, C.; Beck, W., *J. Organomet. Chem.* **1997,** *533*, 247.

(25) (a) Colombo, M. G.; Brunold, T. C.; Riedener, T.; Guedel, H. U.; Fortsch, M.; Buergi, H.-B., *Inorg. Chem.* **1994,** *33*, 545. (b) Garces, F. O.; King, K. A.; Watts, R. J., *Inorg. Chem.* **1988,** *27*, 3464. (c) Hay, P. J., *J. Phys. Chem. A* **2002,** *106*, 1634. (d) Lamansky, S.; Djurovich, P.; Murphy, D.; Abdel-Razzaq, F.; Kwong, R.; Tsyba, I.; Bortz, M.; Mui, B.; Bau, R.; Thompson, M. E., *Inorg. Chem.* **2001,** *40*, 1704. (e) Ohsawa, Y.; Sprouse, S.; King, K. A.; DeArmond, M. K.; Hanck, K. W.; Watts, R. J., *J. Phys. Chem.* **1987,** *91*, 1047.

(26) Flamigni, L.; Barbieri, A.; Sabatini, C.; Ventura, B.; Barigelletti, F., *Top. Curr. Chem.* **2007,** *281*, 143.

Chapter Two:

(1) (a) Eisenberg, R.; Gray, H. B. *Inorg. Chem.* **2008,** *47*, 1697. (b) Ivers-Tiffée, E.; Härdtl, K. H.; Menesklou, W.; Riegel, J. *Electrochim. Acta* **2001,** *47*, 807. (c) Kasting, J. F.; Siefert, J. L. *Science* **2002,** *296*, 1066. (d) Keith, J. A.; Jerkiewicz, G.; Jacob, T. *ChemPhysChem* **2010,** *11*, 2779. (e) Komatsu, T.; Ohmichi, N.; Nakagawa, A.; Zunszain, P. A.; Curry, S.; Tsuchida, E. *J. Am. Chem. Soc.* **2005,** *127*, 15933. (f) McEvoy, J. P.; Gascon, J. A.; Batista, V. S.; Brudvig, G. W. *Photochem. Photobiol. Sci.* **2005,** *4*, 940. (g) Que, J. L. *J. Chem. Soc., Dalton Trans.* **1997**, 3933. (h) Van Der Giezen, M.; Lenton, T. M. *J. Eukaryotic. Microbiol.* **2012,** *59*, 111.

(2) (a) Carbonare, M. D.; Pathak, M. A. *J. Photochem. Photobiol., B* **1992,** *14*, 105. (b) Halliwell, B. *Plant Physiol.* **2006,** *141*, 312. (c) Min, D. B.; Boff, J. M. *Comprehensive Reviews in Food Science and Food Safety* **2002,** *1*, 58. (d) Pospíšil, P. *Biochim. Biophys. Acta* **2009,** *1787*, 1151. (e) Triantaphylidès, C.; Krischke, M.; Hoeberichts, F. A.; Ksas, B.; Gresser, G.; Havaux, M.; Van Breusegem, F.; Mueller, M. J. *Plant Physiol.* **2008,** *148*, 960. (f) Wang, S. Y.; Jiao, H. *J. Agric. Food Chem.* **2000,** *48*, 5677.

(3) (a) DeRosa, M. C.; Crutchley, R. J. *Coord. Chem. Rev.* **2002,** *233*, 351. (b) Schmidt, R. *Photochem. Photobiol.* **2006,** *82*, 1161. (c) Schweitzer, C.; Schmidt, R. *Chem. Rev.* **2003,** *103*, 1685.

(4) (a) Lévesque, F.; Seeberger, P. H. *Org. Lett.* **2011,** *13*, 5008. (b) Yavorskyy, A.; Shvydkiv, O.; Limburg, C.; Nolan, K.; Delaure, Y. M. C.; Oelgemoller, M. *Green Chem.* **2012,** *14*, 888. (c) Kyriakopoulos, J.; Tzirakis, M. D.; Panagiotou, G. D.; Alberti, M. N.; Triantafyllidis, K. S.; Giannakaki, S.; Bourikas, K.; Kordulis, C.; Orfanopoulos, M.; Lycourghiotis, A. *Appl. Catal., B* **2012,** *117–118*, 36.

(5) (a) Castano, A. P.; Mroz, P.; Hamblin, M. R. *Nature Rev. Cancer* **2006,** *6*, 535. (b) Dolmans, D. E. J. G. J.; Fukumura, D.; Jain, R. K. *Nature Rev. Cancer* **2003,** *3*, 380. (c) Kelkar, S. S.; Reineke, T. M. *Bioconjugate Chem.* **2011,** *22*, 1879. (d) Nyokong, T. *Pure Appl. Chem.* **2011,** *83*, 1763.

(6) (a) al Housari, F.; Vione, D.; Chiron, S.; Barbati, S. *Photochem. Photobiol. Sci.* **2010,** *9*, 78. (b) Dalrymple, R. e. M.; Carfagno, A. K.; Sharpless, C. M. *Environ. Sci. Technol.* **2010,** *44*, 5824. (c) Halladja, S.; ter Halle, A.; Aguer, J.-P.; Boulkamh, A.; Richard, C. *Environ. Sci. Technol.* **2007,** *41*, 6066. (d) Latch, D. E.; McNeill, K. *Science* **2006,** *311*, 1743. (e) Sharpless, C. M. *Environ. Sci. Technol.* **2012,** *46*, 4466.

(7) (a) Cló, E.; Snyder, J. W.; Ogilby, P. R.; Gothelf, K. V. *ChemBioChem* **2007,** *8*, 475. (b) Verma, S.; Watt, G. M.; Mai, Z.; Hasan, T. *Photochem. Photobiol.* **2007,** *83*, 996. (c) Natarajan, A.; Kaanumalle, L. S.; Jockusch, S.; Gibb, C. L. D.; Gibb, B. C.; Turro, N. J.; Ramamurthy, V. *J. Am. Chem. Soc.* **2007,** *129*, 4132.

(8) (a) Alberti, M. N.; Orfanopoulos, M. *Chem. Eur. J.* **2010,** *16*, 9414. (b) Araki, Y.; Dobrowolski, D. C.; Goyne, T. E.; Hanson, D. C.; Jiang, Z. Q.; Lee, K. J.; Foote, C. S. *J. Am. Chem. Soc.* **1984,** *106*, 4570. (c) Clennan, E. L.; Pace, A. *Tetrahedron* **2005,** *61*, 6665. (d) Feng, K.; Zhang, R.-Y.; Wu, L.-Z.; Tu, B.; Peng, M.-L.; Zhang, L.-P.; Zhao, D.; Tung, C.-H. *J. Am. Chem. Soc.* **2006,** *128*, 14685. (e) Gollnick, K.; Griesbeck, A. *Tetrahedron Lett.* **1984,** *25*, 725. (f) Prein, M.; Adam, W. *Angew. Chem. Int. Ed. Engl.* **1996,** *35*, 477. (g) Shailaja, J.; Sivaguru, J.; Robbins, R. J.; Ramamurthy, V.; Sunoj, R. B.; Chandrasekhar, J. *Tetrahedron* **2000,** *56*, 6927. (h) Singleton, D. A.; Hang, C.; Szymanski, M. J.; Meyer, M. P.; Leach, A. G.; Kuwata, K. T.; Chen, J. S.; Greer, A.; Foote, C. S.; Houk, K. N. *J. Am. Chem. Soc.* **2003,** *125*, 1319.

(9) (a) Baciocchi, E.; Giacco, T. D.; Elisei, F.; Gerini, M. F.; Guerra, M.; Lapi, A.; Liberali, P. *J. Am. Chem. Soc.* **2003,** *125*, 16444. (b) Clennan, E. L. *Acc. Chem. Res.* **2001,** *34*, 875. (c) Clennan, E. L.; Greer, A. *J. Org. Chem.* **1996,** *61*, 4793. (d) Foote, C. S.; Peters, J. W. *J. Am. Chem. Soc.* **1971,** *93*, 3795. (e) Jensen, F.; Greer, A.; Clennan, E. L. *J. Am. Chem. Soc.* **1998,** *120*, 4439. (f) Nahm, K.; Li, Y.; Evanseck, J. D.; Houk, K. N.; Foote, C. S. *J. Am. Chem. Soc.* **1993,** *115*, 4879. (g) Robert-Banchereau, E.; Lacombe, S.; Ollivier, J. *Tetrahedron* **1997,** *53*, 2087. (h) Toutchkine, A.; Clennan, E. L. *J. Org. Chem.* **1999,** *64*, 5620.

(10) (a) Li, X.-H.; Wu, L.-Z.; Zhang, L.-P.; Tung, C.-H.; Che, C.-M. *Chem. Commun.* **2001**, 2280. (b) Marisa, C.; Ilaria, D. S.; Marotta, R.; Roberto, A.; Vincenzo, C. *J Photochem. Photobiol., A* **2010,** *210*, 69.

(11) (a) Caspi, V.; Malkin, S.; Marder, J. B. *Photochem. Photobiol.* **2000,** *71*, 441. (b) Gollnick, K.; Schnatterer, A. *Photochem. Photobiol.* **1986,** *43*, 365. (c) Tanielian, C.; Mechin, R.; Seghrouchni, R.; Schweitzer, C. *Photochem. Photobiol.* **2000,** *71*, 12.

(12) (a) Bilski, P.; Daub, M. E.; Chignell, C. F. Direct detection of singlet oxygen via its phosphorescence from cellular and fungal cultures. In *Methods in Enzymology;* Academic Press: 2002; Vol. Volume 352, pp 41-52. (b) Criado, S.; Marioli, J. M.; Allegretti, P. E.; Furlong, J.; Rodríguez Nieto, F. J.; Mártire, D. O.; García, N. A. *J. Photochem. Photobiol., B* **2001,** *65*, 74. (c) Nonell, S.; Braslavsky, S. E. Time-resolved singlet oxygen detection. In *Methods in Enzymology;* Lester Packer, H. S., Ed.; Academic Press: 2000; Vol. Volume 319, pp 37-49.

(13) Bilski, P.; Chignell, C. F. *J. Biochem. Biophys. Methods* **1996,** *33*, 73.

(14) (a) Amao, Y.; Okura, I.; Miyashita, T. *Bull. Chem. Soc. Jpn.* **2000,** *73*, 2663. (b) Borisov, S. M.; Vasylevska, A. S.; Krause, C.; Wolfbeis, O. S. *Adv. Funct. Mater.* **2006,** *16*, 1536. (c) Chu, B. W.-K.; Yam, V. W.-W. *Langmuir* **2006,** *22*, 7437. (d) Demas, J. N.; DeGraff, B. A.; Coleman, P. B. *Anal. Chem.* **1999,** *71*, 793A. (e) Douglas, P.; Eaton, K. *Sens. Actuators, B* **2002,** *82*, 200. (f) García-Fresnadillo, D.;

Marazuela, M. D.; Moreno-Bondi, M. C.; Orellana, G. *Langmuir* **1999,** *15*, 6451. (g) Kneas, K. A.; Demas, J. N.; Nguyen, B.; Lockhart, A.; Xu, W.; DeGraff, B. A. *Anal. Chem.* **2002,** *74*, 1111.

(15) (a) McGee, K. A.; Mann, K. R. *J. Am. Chem. Soc.* **2009,** *131*, 1896. (b) McGee, K. A.; Marquardt, B. J.; Mann, K. R. *Inorg. Chem.* **2008,** *47*, 9143. (c) McGee, K. A.; Veltkamp, D. J.; Marquardt, B. J.; Mann, K. R. *J. Am. Chem. Soc.* **2007,** *129*, 15092. (d) Smith, C. S.; Branham, C. W.; Marquardt, B. J.; Mann, K. R. *J. Am. Chem. Soc.* **2010,** *132*, 14079. (e) Smith, C. S.; Mann, K. R. *Chem. Mater.* **2009,** *21*, 5042.

(16) (a) Akasaka, T.; Misawa, Y.; Goto, M.; Ando, W. *Tetrahedron* **1989,** *45*, 6657. (b) Mali, S. L.; Vaidya, V.; Pitliya, R. L.; Vaidya, V. K.; Ameta, S. C. *Asian J. Chem.* **1994,** *6*, 796.

(17) Schwartz, K. R.; Mann, K. R. *Inorg. Chem.* **2011,** *50*, 12477.

(18) (a) Borisov, S. M.; Klimant, I. *Anal. Chem.* **2007,** *79*, 7501. (b) DeRosa, M. C.; Mosher, P. J.; Yap, G. P. A.; Focsaneanu, K. S.; Crutchley, R. J.; Evans, C. E. B. *Inorg. Chem.* **2003,** *42*, 4864. (c) Di Marco, G.; Lanza, M.; Mamo, A.; Stefio, I.; Di Pietro, C.; Romeo, G.; Campagna, S. *Anal. Chem.* **1998,** *70*, 5019. (d) Djurovich, P. I.; Murphy, D.; Thompson, M. E.; Hernandez, B.; Gao, R.; Hunt, P. L.; Selke, M. *Dalton Trans.* **2007**, 3763. (e) Fernández-Sánchez, J. F.; Roth, T.; Cannas, R.; Nazeeruddin, M. K.; Spichiger, S.; Graetzel, M.; Spichiger-Keller, U. E. *Talanta* **2007,** *71*, 242. (f) Köse, M. E.; Crutchley, R. J.; DeRosa, M. C.; Ananthakrishnan, N.; Reynolds, J. R.; Schanze, K. S. *Langmuir* **2005,** *21*, 8255.

(19) Demas, J. N.; McBride, R. P.; Harris, E. W. *J. Phys. Chem.* **1976,** *80*, 2248.

(20) (a) Fischer, E. *EPA Newsletter* **1984,** *21*, 33. (b) Montaliti, M.; Alberto, C.; Prodi, L.; Gandolfi, M. T. Chemical Actinometry. In *Handbook of Photochemistry;* Third ed.; CRC Press, Taylor & Francis Group: Boca Raton, 2006; pp 601-616.

(21) Johnson, R. C. *J. Chem. Educ.* **1970,** *47*, 702.

(22) Hatchard, C. G.; Parker, C. A. *Proc. Roy. Soc. Lond. A* **1956,** *235*, 518.

(23) Hoye, T. R.; Eklov, B. M.; Ryba, T. D.; Voloshin, M.; Yao, L. J. *Org. Lett.* **2004,** *6*, 953.

(24) Demas, J. N.; Diemente, D.; Harris, E. W. *J. Am. Chem. Soc.* **1973,** *95*, 6864.

(25) (a) Akasaka, T.; Ando, W. *J. Chem. Soc., Chem. Commun.* **1983**, 1203. (b) Ishiguro, K.; Hayashi, M.; Sawaki, Y. *J. Am. Chem. Soc.* **1996,** *118*, 7265. (c) Sofikiti, N.; Rabalakos, C.; Stratakis, M. *Tetrahedron Lett.* **2004,** *45*, 1335.

(26) (a) Brimblecombe, P.; Shooter, D. *Mar. Chem.* **1986,** *19*, 343. (b) Gu, C.-L.; Foote, C. S.; Kacher, M. L. *J. Am. Chem. Soc.* **1981,** *103*, 5949.

(27) Pretsch, E.; Bühlmann, P.; Affolter, C. *Structure Determination of Organic Compounds - Tables of Spectral Data;* 3rd ed.; Springer - Verlag: Berlin Heidelberg, 2000.

(28) Salignac, B.; Grundler, P. V.; Cayemittes, S.; Frey, U.; Scopelliti, R.; Merbach, A. E.; Hedinger, R.; Hegetschweiler, K.; Alberto, R.; Prinz, U.; Raabe, G.; Kölle, U.; Hall, S. *Inorg. Chem.* **2003,** *42*, 3516.

(29) Clennan, E. L.; Dobrowolski, P.; Greer, A. *J. Am. Chem. Soc.* **1995,** *117*, 9800.

(30) Franco, C.; Olmsted III, J. *Talanta* **1990,** *37*, 905.

(31) Dymond, J. H. *J. Phys. Chem.* **1967,** *71*, 1829.

(32) (a) Goličnik, M. *Biochem. Mol. Biol. Educ.* **2011,** *39*, 117. (b) Schnell, S.; Mendoza, C. *J. Theor. Biol.* **1997,** *187*, 207.

(33) Dad'ová, J.; Svobodová, E.; Sikorski, M.; König, B.; Cibulka, R. *ChemCatChem* **2012,** *4*, 620.

(34) Korínek, M.; Dědic, R.; Molnár, A.; Svoboda, A.; Hála, J. *J. Mol. Struct.* **2005,** *744*, 727.

Chapter Three:

(1) (a) Asbury, J. B.; Ellingson, R. J.; Ghosh, H. N.; Ferrere, S.; Nozik, A. J.; Lian, T. *J. Phys. Chem. B* **1999,** *103*, 3110. (b) Bisquert, J.; Cahen, D.; Hodes, G.; Ruehle, S.; Zaban, A. *J. Phys. Chem. B* **2004,** *108*, 8106. (c) Figgemeier, E.; Hagfeldt, A. *Int. J. Photoenergy* **2004,** *6*, 127. (d) Gao, F.; Wang, Y.; Shi, D.; Zhang, J.; Wang, M.; Jing, X.; Humphry-Baker, R.; Wang, P.; Zakeeruddin, S. M.; Gratzel, M. *J. Am. Chem. Soc.* **2008,** *130*, 10720. (e) Gratzel, M. *J. Photochem. Photobiol.* **2004,** *164*, 3. (f) Hagfeldt, A.; Graetzel, M. *Acc. Chem. Res.* **2000,** *33*, 269. (g) Heimer, T. A.; Heilweil, E. J.; Bignozzi, C. A.; Meyer, G. J. *J. Phys. Chem. A* **2000,** *104*, 4256. (h) Kamat, P. V.; Haria, M.; Hotchandani, S. *J. Phys. Chem. B* **2004,** *108*, 5166. (i) Nazeeruddin, M. K.; De Angelis, F.; Fantacci, S.; Selloni, A.; Viscardi, G.; Liska, P.; Ito, S.; Takeru, B.; Graetzel, M. *J. Am. Chem. Soc.* **2005,** *127*, 16835. (j) Nazeeruddin, M. K.; Zakeeruddin, S. M.; Lagref, J. J.; Liska, P.; Comte, P.; Barolo, C.; Viscardi, G.; Schenk, K.; Graetzel, M. *Coord. Chem. Rev.* **2004,** *248*, 1317. (k) O'Regan, B.; Graetzel, M. *Nature* **1991,** *353*, 737. (l) Yum, J.-H.; Chen, P.; Gratzel, M.; Nazeruddin, M. K. *ChemSusChem* **2008,** *1*, 699.

(2) (a) Lo, K. K.-W.; Chan, J. S.-W.; Lui, L.-H.; Chung, C.-K. *Organometallics* **2004,** *23*, 3108. (b) Lo, K. K.-W.; Hui, W.-K.; Chung, C.-K.; Tsang, K. H.-K.; Lee, T. K.-M.; Li, C.-K.; Lau, J. S.-Y.; Ng, D. C.-M. *Coord. Chem. Rev.* **2006,** *250*, 1724. (c) Lo, K. K.-W.; Tsang, K. H.-K.; Sze, K.-S.; Chung, C.-K.; Lee, T. K.-M.; Zhang, K. Y.; Hui, W.-K.; Li, C.-K.; Lau, J. S.-Y.; Ng, D. C.-M.; Zhu, N. *Coord. Chem. Rev.* **2007,** *251*, 2292. (d) Shao, F.; Elias, B.; Lu, W.; Barton, J. K. *Inorg. Chem.* **2007,** *46*, 10187. (e) Zhang, K. Y.; Lo, K. K.-W. *Inorg. Chem.* **2009,** *48*, 6011.

(3) (a) Borisov, S. M.; Klimant, I. *Anal. Chem.* **2007,** *79*, 7501. (b) Di Marco, G.; Lanza, M.; Mamo, A.; Stefio, I.; Di Pietro, C.; Romeo, G.; Campagna, S. *Anal. Chem.* **1998,** *70*, 5019. (c) Fernandez-Sanchez, J. F.; Roth, T.; Cannas, R.; Nazeeruddin, M. K.; Spichiger, S.; Graetzel, M.; Spichiger-Keller, U. E. *Talanta* **2007,** *71*, 242. (d) Koese, M. E.; Crutchley, R. J.; DeRosa, M. C.; Ananthakrishnan, N.; Reynolds, J. R.; Schanze, K. S. *Langmuir* **2005,** *21*, 8255. (e) Mak, C. S. K.; Pentlehner, D.; Stich, M.; Wolfbeis, O. S.; Chan, W. K.; Yersin, H. *Chem. Mater.* **2009,** *21*, 2173. (f) Marin-Suarezdel Toro, M.; Fernandez-Sanchez, J. F.; Baranoff, E.; Nazeeruddin, M. K.; Graetzel, M.; Fernandez-Gutierrez, A. *Talanta* **2010,** *82*, 620. (g) Xie, Z.; Ma, L.; de Krafft, K. E.; Jin, A.; Lin, W. *J. Am. Chem. Soc.* **2010,** *132*, 922.

(4) (a) Baranoff, E.; Barigelletti, F.; Bonnet, S.; Collin, J.-P.; Flamigni, L.; Mobian, P.; Sauvage, J.-P. *Struct. Bonding* **2007,** *123*, 41. (b) Baranoff, E.; Dixon, I. M.; Collin, J.-P.; Sauvage, J.-P.; Ventura, B.; Flamigni, L. *Inorg. Chem.* **2004,** *43*, 3057. (c) Baranoff, E.; Griffiths, K.; Collin, J.-P.; Sauvage, J.-P.; Ventura, B.; Flamigni, L. *New J. Chem.* **2004,** *28*, 1091. (d) Flamigni, L.; Barbieri, A.; Sabatini, C.; Ventura, B.; Barigelletti, F. *Top. Curr. Chem.* **2007,** *281*, 143. (e) Flamigni, L.; Collin, J.-P.; Sauvage, J.-P. *Acc. Chem. Res.* **2008,** *41*, 857. (f) Flamigni, L.; Ventura, B.; Baranoff, E.; Collin, J.-P.; Sauvage, J.-P. *Eur. J. Inorg. Chem.* **2007**, 5189. (g) Geiss, B.;

Lambert, C. *Chem. Commun.* **2009**, 1670. (h) Hanss, D.; Freys, J. C.; Bernardinelli, G.; Wenger, O. S. *Eur. J. Inorg. Chem.* **2009**, 4850.

(5) (a) Cline, E. D.; Adamson, S. E.; Bernhard, S. *Inorg. Chem.* **2008,** *47*, 10378. (b) Fukuzumi, S. *Eur. J. Inorg. Chem.* **2008**, 1351. (c) Fukuzumi, S.; Kobayashi, T.; Suenobu, T. *J. Am. Chem. Soc.* **2010,** *132*, 1496. (d) Goldsmith, J. I.; Hudson, W. R.; Lowry, M. S.; Anderson, T. H.; Bernhard, S. *J. Am. Chem. Soc.* **2005,** *127*, 7502. (e) Lowry, M. S.; Goldsmith, J. I.; Slinker, J. D.; Rohl, R.; Pascal, R. A., Jr.; Malliaras, G. G.; Bernhard, S. *Chem. Mater.* **2005,** *17*, 5712.

(6) (a) Baranoff, E.; Yum, J.-H.; Graetzel, M.; Nazeeruddin, M. K. *J. Organomet. Chem.* **2009,** *694*, 2661. (b) Baranoff, E.; Yum, J.-H.; Jung, I.; Vulcano, R.; Gratzel, M.; Nazeeruddin, M. K. *Chem. Asian. J.* **2010,** *5*, 496. (c) Huang, J.; Yu, J.; Guan, Z.; Jiang, Y. *Appl. Phys. Lett.* **2010,** *97*, 143301. (d) Mayo, E. I.; Kilsa, K.; Tirrell, T.; Djurovich, P. I.; Tamayo, A.; Thompson, M. E.; Lewis, N. S.; Gray, H. B. *Photochem. Photobiol. Sci.* **2006,** *5*, 871. (e) Ning, Z.; Zhang, Q.; Wu, W.; Tian, H. *J. Organomet. Chem.* **2009,** *694*, 2705.

(7) (a) Bolink, H. J.; Coronado, E.; Garcia Santamaria, S.; Sessolo, M.; Evans, N.; Klein, C.; Baranoff, E.; Kalyanasundaram, K.; Graetzel, M.; Nazeeruddin, M. K. *Chem. Commun.* **2007**, 3276. (b) Bolink, H. J.; De Angelis, F.; Baranoff, E.; Klein, C.; Fantacci, S.; Coronado, E.; Sessolo, M.; Kalyanasundaram, K.; Graetzel, M.; Nazeeruddin, M. K. *Chem. Commun.* **2009**, 4672. (c) Bulovic, V.; Gu, G.; Burrows, P. E.; Forrest, S. R.; Thompson, M. E. *Nature* **1996,** *380*, 29. (d) Chou, P.-T.; Chi, Y. *Chem. Eur. J.* **2007,** *13*, 380. (e) Tamayo, A. B.; Garon, S.; Sajoto, T.; Djurovich, P. I.; Tsyba, I. M.; Bau, R.; Thompson, M. E. *Inorg. Chem.* **2005,** *44*, 8723. (f) Wong, W.-Y.; Ho, C.-L. *Coord. Chem. Rev.* **2009,** *253*, 1709. (g) You, Y.; Park, S. Y. *Dalton Trans.* **2009**, 1267.

(8) (a) Costa, R. D.; Fernández, G.; Sánchez, L.; Martín, N.; Ortí, E.; Bolink, H. J. *Chem. Eur. J.* **2010,** *16*, 9855. (b) Costa, R. D.; Ortí, E.; Bolink, H. J.; Graber, S.; Housecroft, C. E.; Constable, E. C. *Adv. Funct. Mater.* **2010,** *20*, 1511. (c) Costa, R. D.; Ortí, E.; Bolink, H. J.; Graber, S.; Schaffner, S.; Neuburger, M.; Housecroft, C. E.; Constable, E. C. *Adv. Funct. Mater.* **2009,** *19*, 3456. (d) Graber, S.; Doyle, K.; Neuburger, M.; Housecroft, C. E.; Constable, E. C.; Costa, R. D.; Orti, E.; Repetto, D.; Bolink, H. J. *J. Am. Chem. Soc.* **2008,** *130*, 14944. (e) Liu, S.-J.; Zhao, Q.; Fan, Q.-L.; Huang, W. *Eur. J. Inorg. Chem.* **2008,** *2008*, 2177. (f) Rodriguez-Redondo, J. L.; Costa, R. D.; Orti, E.; Sastre-Santos, A.; Bolink, H. J.; Fernandez-Lazaro, F. *Dalton Trans.* **2009**, 9787. (g) Rothe, C.; Chiang, C.-J.; Jankus, V.; Abdullah, K.; Zeng, X.; Jitchati, R.; Batsanov, A. S.; Bryce, M. R.; Monkman, A. P. *Adv. Funct. Mater.* **2009,** *19*, 2038. (h) Shan, G.-G.; Zhu, D.-X.; Li, H.-B.; Li, P.; Su, Z.-M.; Liao, Y. *Dalton Trans.* **2011,** *40*, 2947. (i) Su, H.-C.; Chen, H.-F.; Wu, C.-C.; Wong, K.-T. *Chem. Asian. J.* **2008,** *3*, 1922. (j) Zeng, X.; Tavasli, M.; Perepichka, I. F.; Batsanov, A. S.; Bryce, M. R.; Chiang, C.-J.; Rothe, C.; Monkman, A. P. *Chem. Eur. J.* **2008,** *14*, 933.

(9) (a) Colombo, M. G.; Brunold, T. C.; Riedener, T.; Guedel, H. U.; Fortsch, M.; Buergi, H.-B. *Inorg. Chem.* **1994,** *33*, 545. (b) Colombo, M. G.; Hauser, A.; Guedel, H. U. *Inorg. Chem.* **1993,** *32*, 3088. (c) Dedeian, K.; Djurovich, P. I.; Garces, F. O.; Carlson, G.; Watts, R. J. *Inorg. Chem.* **1991,** *30*, 1685. (d) Dragonetti, C.; Falciola, L.; Mussini, P.; Righetto, S.; Roberto, D.; Ugo, R.; Valore, a. A.; De Angelis, F.; Fantacci, S.; Sgamellotti, A.; Ramon, M.; Muccini, M. *Inorg. Chem.* **2007,** *46*, 8533. (e) Garces, F. O.; King, K. A.; Watts, R. J. *Inorg. Chem.* **1988,** *27*, 3464. (f) Hay, P. J. *J. Phys. Chem. A* **2002,** *106*, 1634. (g) King, K. A.; Spellane, P. J.; Watts, R. J. *J. Am. Chem. Soc.* **1985,** *107*, 1431. (h) Lamansky, S.; Djurovich, P.; Murphy, D.; Abdel-Razzaq, F.; Lee, H. E.; Adachi, C.; Burrows, P. E.; Forrest, S. R.; Thompson, M. E. *J. Am. Chem. Soc.* **2001,** *123*, 4304. (i) Li, X.-N.; Wu, Z.-J.; Zhang, H.-J.; Liu, X.-J.; Zhou, L.; Li, Z.-F.; Si, Z.-J. *Phys. Chem. Chem. Phys.* **2009,** *11*, 6051. (j) Lowry, M. S.; Bernhard, S. *Chem. Eur. J.* **2006,** *12*, 7970. (k) Lowry, M. S.; Hudson, W. R.; Pascal, R. A., Jr.; Bernhard, S. *J. Am. Chem. Soc.* **2004,** *126*, 14129. (l) Nazeeruddin, M. K.; Gratzel, M. *Struct. Bonding* **2007,** *123*, 113. (m) Nazeeruddin, M. K.; Humphry-Baker, R.; Berner, D.; Rivier, S.; Zuppiroli, L.; Graetzel, M. *J. Am. Chem. Soc.* **2003,** *125*, 8790. (n) Ohsawa, Y.; Sprouse, S.; King, K. A.; DeArmond, M. K.; Hanck, K. W.; Watts, R. J. *J. Phys. Chem.* **1987,** *91*, 1047. (o) Tamayo, A. B.; Alleyne, B. D.; Djurovich, P. I.; Lamansky, S.; Tsyba, I.; Ho, N. N.; Bau, R.; Thompson, M. E. *J. Am. Chem. Soc.* **2003,** *125*, 7377. (p) Waern, J. B.; Desmarets, C.; Chamoreau, L.-M.; Amouri, H.; Barbieri, A.; Sabatini, C.; Ventura, B.; Barigelletti, F. *Inorg. Chem.* **2008,** *47*, 3340.

(10) (a) Bandini, M.; Bianchi, M.; Valenti, G.; Piccinelli, F.; Paolucci, F.; Monari, M.; Umani-Ronchi, A.; Marcaccio, M. *Inorg. Chem.* **2010,** *49*, 1439. (b) King, K. A.; Watts, R. J. *J. Am. Chem. Soc.* **1987,** *109*, 1589. (c) Ladouceur, S. b.; Fortin, D.; Zysman-Colman, E. *Inorg. Chem.* **2010,** *49*, 5625.

(11) (a) Baldo, M. A.; Lamansky, S.; Burrows, P. E.; Thompson, M. E.; Forrest, S. R. *Appl. Phys. Lett.* **1999,** *75*, 4. (b) Baldo, M. A.; O'Brien, D. F.; You, Y.; Shoustikov, A.; Sibley, S.; Thompson, M. E.; Forrest, S. R. *Nature* **1998,** *395*, 151. (c) Chen, X.; Liao, J.-L.; Liang, Y.; Ahmed, M. O.; Tseng, H.-E.; Chen, S.-A. *J. Am. Chem. Soc.* **2003,** *125*, 636. (d) D'Andrade, B. W.; Baldo, M. A.; Adachi, C.; Brooks, J.; Thompson, M. E.; Forrest, S. R. *Appl. Phys. Lett.* **2001,** *79*, 1045. (e) Sandee, A. J.; Williams, C. K.; Evans, N. R.; Davies, J. E.; Boothby, C. E.; Köhler, A.; Friend, R. H.; Holmes, A. B. *J. Am. Chem. Soc.* **2004,** *126*, 7041. (f) Schulz, G. L.; Chen, X.; Chen, S.-A.; Holdcroft, S. *Macromolecules* **2006,** *39*, 9157. (g) Wang, L.; Lei, G.; Qiu, Y. *J. Appl. Phys.* **2005,** *97*, 114503. (h) Yan, Q.; Yue, K.; Yu, C.; Zhao, D. *Macromolecules* **2010,** *43*, 8479.

(12) (a) Ding, J.; Lü, J.; Cheng, Y.; Xie, Z.; Wang, L.; Jing, X.; Wang, F. *Adv. Funct. Mater.* **2008,** *18*, 2754. (b) Qin, T.; Ding, J.; Wang, L.; Baumgarten, M.; Zhou, G.; Müllen, K. *J. Am. Chem. Soc.* **2009,** *131*, 14329.

(13) (a) Bair, J. S.; Harrison, R. G. *J. Org. Chem.* **2007,** *72*, 6653. (b) Barbieri, A.; Ventura, B.; Flamigni, L.; Barigelletti, F.; Fuhrmann, G.; Bäuerle, P.; Goeb, S.; Ziessel, R. *Inorg. Chem.* **2005,** *44*, 8033. (c) Hjelm, J.; Handel, R. W.; Hagfeldt, A.; Constable, E. C.; Housecroft, C. E.; Forster, R. J. *Inorg. Chem.* **2005,** *44*, 1073. (d) Moorlag, C.; Wolf, M. O. *Polym. Prepr.* **2007,** *48*, 543. (e) Pappenfus, T. M.; Mann, K. R. *Inorg. Chem.* **2001,** *40*, 6301. (f) Sauvage, F.; Fischer, M. K. R.; Mishra, A.; Zakeeruddin, S. M.; Nazeeruddin, M. K.; Baeuerle, P.; Graetzel, M. *ChemSusChem* **2009,** *2*, 761. (g) Steen, R. O.; Nurkkala, L. J.; Angus-Dunne, S. J.; Schmitt, C. X.; Constable, E. C.; Riley, M. J.; Bernhardt, P. V.; Dunne, S. J. *Eur. J. Inorg. Chem.* **2008,** *2008*, 1784. (h) Stott, T. L.; Wolf, M. O. *Coord. Chem. Rev.* **2003,** *246*, 89. (i) Yin, J.-F.; Chen, J.-G.; Lu, Z.-Z.; Ho, K.-C.; Lin, H.-C.; Lu, K.-L. *Chem. Mater.* **2010,** *22*, 4392. (j) Ziessel, R.; Bauerle, P.; Ammann, M.; Barbieri, A.; Barigelletti, F. *Chem. Commun.* **2005**, 802.

(14) (a) Beek, W. J. E.; Janssen, R. A. J. *Adv. Funct. Mater.* **2002,** *12*, 519. (b) Casado, J.; Pappenfus, T. M.; Miller, L. L.; Mann, K. R.; Orti, E.; Viruela, P. M.; Pou-Amerigo, R.; Hernandez, V.; Lopez Navarrete, J. T. *J. Am. Chem. Soc.* **2003,** *125*, 2524. (c) Facchetti, A.; Yoon, M.-H.; Stern, C. L.; Hutchison, G. R.; Ratner, M. A.; Marks, T. J. *J. Am. Chem. Soc.* **2004,** *126*, 13480. (d) Huss, A. S.; Pappenfus, T.; Bohnsack, J.; Burand, M.; Mann, K. R.; Blank, D. A. *J. Phys. Chem. A* **2009,** *113*, 10202. (e) Pappenfus, T. M.; Burand, M. W.; Janzen, D. E.; Mann, K. R. *Org. Lett.* **2003,** *5*, 1535. (f) Roncali, J. *Acc. Chem. Res.* **2009,** *42*, 1719. (g) Tian, H.; Shi, J.; He, B.; Hu, N.; Dong, S.; Yan, D.; Zhang, J.; Geng, Y.; Wang, F. *Adv. Funct. Mater.* **2007,** *17*, 1940. (h) Won, Y. S.; Yang, Y. S.; Kim, J. H.; Ryu, J.-H.; Kim, K. K.; Park, S. S. *Energy Fuels* **2010,** *24*, 3676. (i) Xia, P. F.; Feng, X. J.; Lu, J.; Tsang, S.-W.; Movileanu, R.; Tao, Y.; Wong, M. S. *Adv. Mater.* **2008,** *20*, 4810.

(15) Araya, J. C.; Gajardo, J.; Moya, S. A.; Aguirre, P.; Toupet, L.; Williams, J. A. G.; Escadeillas, M.; Le Bozec, H.; Guerchais, V. *New J. Chem* **2010,** *34*, 21.

(16) (a) Bolink, H. J.; Coronado, E.; Costa, R. D.; Lardies, N.; Orti, E. *Inorg. Chem.* **2008,** *47*, 9149. (b) He, L.; Duan, L.; Qiao, J.; Wang, R.; Wei, P.; Wang, L.; Qiu, Y. *Adv. Funct. Mater.* **2008,** *18*, 2123. (c) Zhao, Q.; Liu, S.; Shi, M.; Wang, C.; Yu, M.; Li, L.; Li, F.; Yi, T.; Huang, C. *Inorg. Chem.* **2006,** *45*, 6152.

(17) Demnitz, F. W. J.; D'heni, M. B. *Org. Prep. Proced. Int.* **1998,** *30*, 467.

(18) Zhu, S. S.; Kingsborough, R. P.; Swager, T. M. *J. Mater. Chem.* **1999,** *9*, 2123.

(19) Wang, C.; Benz, M. E.; LeGoff, E.; Schindler, J. L.; Allbritton-Thomas, J.; Kannewurf, C. R.; Kanatzidis, M. G. *Chem. Mater.* **1994,** *6*, 401.

(20) Sprouse, S.; King, K. A.; Spellane, P. J.; Watts, R. J. *J. Am. Chem. Soc.* **1984,** *106*, 6647.

(21) Wenkert, D.; Woodward, R. B. *J. Org. Chem.* **1983,** *48*, 283.

(22) Comins, D. L.; Mantlo, N. B. *J. Org. Chem.* **1985,** *50*, 4410.

(23) Araki, K.; Endo, H.; Masuda, G.; Ogawa, T. *Chem. Eur. J.* **2004,** *10*, 3331.

(24) (a) Graf, D. D.; Mann, K. R. *Inorg. Chem.* **1997,** *36*, 150. (b) Graf, D. D.; Mann, K. R. *Inorg. Chem.* **1997,** *36*, 141.

(25) (a) Blessing, R. H. *Acta Crystallogr., Sect. A* **1995,** *51*, 33. (b) Sheldrick, G. *SADABS*, v.2.03; Bruker AXS: Madison, WI, 2002.

(26) *SHELXTL*, v.6.1; Bruker AXS: Madison, WI, 2001.

(27) Zhao, Y.; Truhlar, D. G. *J. Chem. Phys.* **2006,** *125*, 194101.

(28) Hehre, W. J.; Radom, L.; Schleyer, P. v. R.; Pople, J. A. *Ab Initio Molecular Orbital Theory;* John Wiley & Sons: New York, 1986.

(29) Andrae, D.; Häußermann, U.; Dolg, M.; Stoll, H.; Preuß, H. *Theoretica Chimica Acta* **1990,** *77*, 123.

(30) Frisch, M. J.; Trucks, G. W.; Shchlegel, H. B.; Scuseria, G. E.; Robb, M. A.; Cheeseman, J. R.; Scalmani, G.; Barone, V.; Mennucci, B.; Petersson, G. A.; Nakatsuji, H.; Caricato, M.; Li, X.; Hratchian, H. P.; Izmaylov, A. F.; Bloino, J.; Zheng, G.; Sonnenberg, J. L.; Hada, M.; Ehara, M.; Toyota, K.; Fukuda, R.; Hasegawa, J.; Ishida, M.; Nakajima, T.; Honda, Y.; Kitao, O.; Nakai, H.; Vreven, T.; Montgomery, J., J. A.; Peralta, J. E.; Ogliaro, F.; Bearpark, M.; Heyd, J. J.; Brothers, E.; Kudin, K. N.; Staroverov, V. N.; Kobayashi, R.; Normand, J.; Raghavachari, K.; Rendell, A.; Burant, J. C.; Iyengar, S. S.; Tomasi, J.; Cossi, M.; Rega, N.; Millam, N. J.; Klene, M.; Knox, J. E.; Cross, J. B.; Bakken, V.; Adamo, C.; Jaramillo, J.; Gomperts, R.; Stratmann, R. E.; Yazyev, O.; Austin, A. J.; Cammi, R.; Pomelli, C.; Ochterski, J. W.; Martin, R. L.; Morokuma, K.; Zakrzewski, V. G.; Voth, G. A.; Salvador, P.; Dannenberg, J. J.; Dapprich, S.; Daniels, A. D.; Farkas, Ö.; Foresman, J. B.; Ortiz, J. V.; Cioslowski, J.; Fox, D. J. *Gaussian 09*, Gaussian, Inc.: Wallingford, CT, 2009.

(31) Cramer, C. J. *Essentials of Computational Chemistry: Theories and Models;* Second ed.; John Wiley & Sons, Ltd: Chichester, U.K., 2004.

(32) Marenich, A. V.; Cramer, C. J.; Truhlar, D. G. *J. Phys. Chem. B* **2009,** *113*, 6378.

(33) (a) Runge, E.; Gross, E. K. U. *Phys. Rev. Lett.* **1984,** *52*, 997. (b) Cammi, R.; Mennucci, B.; Tomasi, J. *J. Phys. Chem. A* **2000,** *104*, 5631.

(34) Zhao, Y.; Truhlar, D. G. *Acc. Chem. Res.* **2008,** *41*, 157.

(35) (a) Jiang, W.; Gao, Y.; Sun, Y.; Ding, F.; Xu, Y.; Bian, Z.; Li, F.; Bian, J.; Huang, C. *Inorg. Chem.* **2010,** *49*, 3252. (b) Zhao, Q.; Liu, S.; Shi, M.; Li, F.; Jing, H.; Yi, T.; Huang, C. *Organometallics* **2007,** *26*, 5922.

(36) Allen, F. H. *Acta Crystallogr., Sect. B* **2002,** *B58*, 380.

(37) (a) Chen, C.-T.; Lin, T.-Y. J.; Chen, C.-H.; Lin, K.-J. *J. Chin. Chem. Soc.* **2000,** *47*, 197. (b) Kinnunen, T.-J. J.; Haukka, M.; Nousiainen, M.; Patrikka, A.; Pakkanen, T. A. *J. Chem. Soc., Dalton Trans.* **2001**, 2649.

(38) (a) Busby, M.; Gabrielsson, A.; Matousek, P.; Towrie, M.; Di Bilio, A. J.; Gray, H. B.; Vlček, A. *Inorg. Chem.* **2004,** *43*, 4994. (b) Bush, P. M.; Whitehead, J. P.; Pink, C. C.; Gramm, E. C.; Eglin, J. L.; Watton, S. P.; Pence, L. E. *Inorg. Chem.* **2001,** *40*, 1871. (c) Chen, X.-F.; Cheng, P.; Liu, X.; Zhao, B.; Liao, D.-Z.; Yan, S.-P.; Jiang, Z.-H. *Inorg. Chem.* **2001,** *40*, 2652. (d) Lam, S. C.-F.; Yam, V. W.-W.; Wong, K. M.-C.; Cheng, E. C.-C.; Zhu, N. *Organometallics* **2005,** *24*, 4298.

(39) (a) Basu, A.; Weiner, M. A.; Strekas, T. C.; Gafney, H. D. *Inorg. Chem.* **1982,** *21*, 1085. (b) Canivet, J.; Süss-Fink, G.; Štěpnička, P. *Eur. J. Inorg. Chem.* **2007,** *2007*, 4736. (c) Morotti, T.; Pizzotti, M.; Ugo, R.; Quici, S.; Bruschi, M.; Mussini, P.; Righetto, S. *Eur. J. Inorg. Chem.* **2006,** *2006*, 1743. (d) Stepnicka, P.; Ludvík, J.; Canivet, J.; Süss-Fink, G. *Inorg. Chim. Acta* **2006,** *359*, 2369.

(40) Murray, P.; Jack, L.; McInnes, E. J. L.; Yellowlees, L. J. *Dalton Trans.* **2010,** *39*, 4179.

(41) (a) Colombo, M.; Hauser, A.; Güdel, H. *Top. Curr. Chem.* **1994,** *171*, 143. (b) Colombo, M. G.; Guedel, H. U. *Inorg. Chem.* **1993,** *32*, 3081. (c) Dixon, I. M.; Collin, J.-P.; Sauvage, J.-P.; Flamigni, L.; Encinas, S.; Barigelletti, F. *Chem. Soc. Rev.* **2000,** *29*, 385. (d) Lafolet, F.; Welter, S.; Popovic, Z.; Cola, L. D. *J. Mater. Chem.* **2005,** *15*, 2820. (e) Wilde, A. P.; King, K. A.; Watts, R. J. *J. Phys. Chem.* **1991,** *95*, 629.

(42) (a) Rubio, M.; Merchán, M.; Ortí, E. *ChemPhysChem* **2005,** *6*, 1357. (b) Wasserberg, D.; Marsal, P.; Meskers, S. C. J.; Janssen, R. A. J.; Beljonne, D. *J. Phys. Chem. B* **2005,** *109*, 4410.

(43) (a) Hissler, M.; Connick, W. B.; Geiger, D. K.; McGarrah, J. E.; Lipa, D.; Lachicotte, R. J.; Eisenberg, R. *Inorg. Chem.* **2000,** *39*, 447. (b) Villegas, J. M.; Stoyanov, S. R.; Huang, W.; Rillema, D. P. *Inorg. Chem.* **2005,** *44*, 2297.

(44) (a) Crespo-Hernández, C. E.; Burdzinski, G.; Arce, R. *J. Phys. Chem. A* **2008,** *112*, 6313. (b) Farztdinov, V. M.; Schanz, R.; Kovalenko, S. A.; Ernsting, N. P. *J. Phys.*

Chem. A **2000,** *104*, 11486. (c) Kovalenko, S. A.; Schanz, R.; Farztdinov, V. M.; Hennig, H.; Ernsting, N. P. *Chem. Phys. Lett.* **2000,** *323*, 312. (d) Mohammed, O. F.; Vauthey, E. *J. Phys. Chem. A* **2008,** *112*, 3823. (e) Takezaki, M.; Hirota, N.; Terazima, M.; Sato, H.; Nakajima, T.; Kato, S. *J. Phys. Chem. A* **1997,** *101*, 5190.

(45) Laye, R. H.; Couchman, S. M.; Ward, M. D. *Inorg. Chem.* **2001,** *40*, 4089.

(46) (a) Kozhevnikov, D. N.; Kozhevnikov, V. N.; Shafikov, M. Z.; Prokhorov, A. M.; Bruce, D. W.; Gareth Williams, J. A. *Inorg. Chem.* **2011,** *50*, 3804. (b) Spaenig, F.; Olivier, J.-H.; Prusakova, V.; Retailleau, P.; Ziessel, R.; Castellano, F. N. *Inorg. Chem.* **2011,** *50*, 10859.

Appendix A

Structural Discussion of C, N Ring Flip In Single Crystal X-ray Crystallography

The possibility of ring flip disorder present within the cyclometalating ligand ppy for the structures obtained for Ir(III) bis-cyclometalates $[Ir(ppy)_2(N_2H_4)_2]OTf$, $Ir(ppy)_2(H_2NNHCOO)$, and $[Ir(ppy)_2(4\text{-}NO_2\text{-}bpy)]PF_6$ was modeled to ensure that the identities and absolute connectivity of the atoms bonded to the Ir(III) metal center were assigned properly. The identities of those C and N atoms in the ppy ligand bonded to the Ir(III) center were exchanged and the results inspected visually by examining the thermal ellipsoid plot. The outcome of this exercise clearly displayed a set of thermal ellipsoids too small and too large when exchanging N for C and C for N respectively. These results clearly illustrate the absence of any ring flip disorder and confirm the proper assignment of the C and N atoms in the ppy ligand confirming the C,C-*cis*/N,N-*trans* arrangement about the Ir(III) center for all single crystal structural determinations reported here.

Appendix B

Obtaining the Implicit and Explicit forms of the Integrated Rate Law for O_2 Consumption

Starting from the final expression for the rate law for $[O_2]$ consumption (Eq. 5, Ch. 2) a simple inversion of this expression provides Equation B1, which after separation of the variables dt and $d[O_2]$, and algebraic simplification, allows for the direct integration of the expression.

$$\frac{d[O_2]}{dt} = -k_{obs}\frac{K_{sv}[O_2]}{K_{sv}[O_2]+1} \tag{5}$$

Invert Equation 5 to provide Equation B1.

$$\frac{dt}{d[O_2]} = -\frac{1}{k_{obs}}\frac{K_{sv}[O_2]+1}{K_{sv}[O_2]} \tag{B1}$$

Separate dt and $d[O_2]$, then simplify.

$$\frac{dt}{d[O_2]} = -\frac{1}{k_{obs}}\left(\frac{1}{K_{sv}[O_2]}+\frac{K_{sv}[O_2]}{K_{sv}[O_2]}\right) \tag{B2}$$

$$\frac{dt}{d[O_2]} = -\frac{1}{k_{obs}}\left(\frac{1}{K_{sv}[O_2]}+1\right) \tag{B3}$$

$$-k_{obs}\,dt = d[O_2]\left(\frac{1}{K_{sv}[O_2]}+1\right) \tag{B4}$$

$$-k_{obs}\,dt = \frac{d[O_2]}{K_{sv}[O_2]} + d[O_2] \tag{B5}$$

Integrate Equation B5 and simplify.

$$-k_{obs}\int_{t_0}^{t} dt = \frac{1}{K_{sv}}\int_{[O_2]_0}^{[O_2]_t}\frac{d[O_2]}{[O_2]} + \int_{[O_2]_0}^{[O_2]_t} d[O_2] \tag{B6}$$

$$-k_{obs}\, t\Big|_{t_0}^{t} = \frac{1}{K_{sv}} \ln[O_2]\Big|_{[O_2]_0}^{[O_2]_t} + [O_2]\Big|_{[O_2]_0}^{[O_2]_t} \tag{B7}$$

$$-k_{obs}(t - t_0) = \frac{\ln[O_2]_t}{K_{sv}} - \frac{\ln[O_2]_0}{K_{sv}} + [O_2]_t - [O_2]_0 \tag{B8}$$

$$k_{obs}(t - t_0) = -\frac{\ln[O_2]_t}{K_{sv}} + \frac{\ln[O_2]_0}{K_{sv}} - [O_2]_t + [O_2]_0 \tag{B9}$$

$$k_{obs}(t - t_0) = \frac{1}{K_{sv}}(\ln[O_2]_0 - \ln[O_2]_t) + [O_2]_0 - [O_2]_t \tag{B10}$$

$$k_{obs}(t - t_0) = \frac{1}{K_{sv}} \ln\frac{[O_2]_0}{[O_2]_t} + [O_2]_0 - [O_2]_t \tag{B11}$$

$$k_{obs}(t - t_0) = \frac{\ln\frac{[O_2]_0}{[O_2]_t}}{K_{sv}} + [O_2]_0 - [O_2]_t \tag{B12}$$

Equation B13 represents the implicit form of the integrated rate law in a linear y = mx form shown below.

$$\frac{\ln\frac{[O_2]_0}{[O_2]_t}}{K_{sv}} + [O_2]_0 - [O_2]_t = k_{obs}(t - t_0) \tag{B13}$$

Further manipulation of Equation B13 provides the integrated rate law in a y = mx + b slope intercept form shown in Equation B16.

$$\left(\frac{\ln[O_2]_0}{K_{sv}} + [O_2]_0\right) - \left(\frac{\ln[O_2]_t}{K_{sv}} + [O_2]_t\right) = k_{obs}(t - t_0) \tag{B14}$$

$$-\left(\frac{\ln[O_2]_t}{K_{sv}} + [O_2]_t\right) = k_{obs}(t - t_0) - \left(\frac{\ln[O_2]_0}{K_{sv}} + [O_2]_0\right) \tag{B15}$$

$$\left(\frac{\ln[O_2]_t}{K_{sv}} + [O_2]_t\right) = -k_{obs}(t - t_0) + \left(\frac{\ln[O_2]_0}{K_{sv}} + [O_2]_0\right) \tag{B16}$$

Explicit solutions to the integrated rate law for both the time dependent oxygen concentration ($[O_2]_t$) and the time dependent PL intensity (I_t) can be obtained by further manipulating the form of the integrated rate law shown in Equation B16 into the $x = y\, e^y$ form shown in Equation B20 and applying the Lambert W function (W).

Multiply Equation 16 by K_{sv} on each side of the expression and simplify.

$$K_{sv}\left(\frac{\ln[O_2]_t}{K_{sv}} + [O_2]_t\right) = -K_{sv}\, k_{obs}(t - t_0) + K_{sv}\left(\frac{\ln[O_2]_0}{K_{sv}} + [O_2]_0\right) \quad \text{(B17)}$$

$$\ln[O_2]_t + K_{sv}[O_2]_t = -K_{sv}\, k_{obs}(t - t_0) + \ln[O_2]_0 + K_{sv}[O_2]_0 \quad \text{(B18)}$$

Add ln K_{sv} to each side of the expression then simplify.

$$\ln[O_2]_t + K_{sv}[O_2]_t + \ln K_{sv} = -K_{sv}\, k_{obs}(t - t_0) + \ln[O_2]_0 + K_{sv}[O_2]_0 + \ln K_{sv} \quad \text{(B19)}$$

$$\ln(K_{sv}[O_2]_t) + K_{sv}[O_2]_t = -K_{sv}\, k_{obs}(t - t_0) + \ln(K_{sv}[O_2]_0) + K_{sv}[O_2]_0 \quad \text{(B20)}$$

Exchange the right and left hand sides.

$$-K_{sv}\, k_{obs}(t - t_0) + \ln(K_{sv}[O_2]_0) + K_{sv}[O_2]_0 = \ln(K_{sv}[O_2]_t) + K_{sv}[O_2]_t \quad \text{(B21)}$$

Apply the exponential function and simplify to obtain the $x = y\, e^y$ form.

$$e^{(-K_{sv}\, k_{obs}(t - t_0) + \ln(K_{sv}[O_2]_0) + K_{sv}[O_2]_0)} = e^{(\ln(K_{sv}[O_2]_t) + K_{sv}[O_2]_t)} \quad \text{(B22)}$$

$$K_{sv}[O_2]_0\, e^{K_{sv}([O_2]_0 - k_{obs}(t - t_0))} = K_{sv}[O_2]_t\, e^{K_{sv}[O_2]_t} \quad \text{(B23)}$$

Application of the Lambert W function to the $x = y\, e^y$ form provides the $y = W(x)$ form shown below in Equation B24.

$$K_{sv}[O_2]_t = W(K_{sv}[O_2]_0\, e^{K_{sv}([O_2]_0 - k_{obs}(t - t_0))}) \quad \text{(B24)}$$

Equation B24 can be solved for $[O_2]_t$ to give Equation 25, providing one of two explicit solutions of interest.

$$[O_2]_t = \frac{W(K_{sv}[O_2]_0 e^{K_{sv}([O_2]_0 - k_{obs}(t-t_0))})}{K_{sv}} \quad \text{(B25)}$$

The second explicit solution of interest can be obtained by making a substitution for $[O_2]_t$ shown in Equation B26, based on the rearranged Stern-Volmer relationship.

$$[O_2]_t = \frac{\frac{I_0}{I_t} - 1}{K_{sv}} \quad \text{(B26)}$$

Substitute for $[O_2]_t$ in equation B24 and simplify

$$K_{sv}\frac{\frac{I_0}{I_t} - 1}{K_{sv}} = W(K_{sv}[O_2]_0 e^{K_{sv}([O_2]_0 - k_{obs}(t-t_0))}) \quad \text{(B27)}$$

$$\frac{I_0}{I_t} - 1 = W(K_{sv}[O_2]_0 e^{K_{sv}([O_2]_0 - k_{obs}(t-t_0))}) \quad \text{(B28)}$$

Solve for I_t.

$$I_t = \frac{I_0}{W(K_{sv}[O_2]_0 e^{K_{sv}([O_2]_0 - k_{obs}(t-t_0))}) + 1} \quad \text{(B29)}$$

Equation B29 represents the second explicit solution to the integrated rate law solved for the experimentally measurable variable PL intensity.